School of Science and Engineering

Investigation of Performance of Carbon and Glass Fibre Strengthened Concrete Beams with Different End Anchorages

Hiew Kee Hon

This thesis is presented for the Degree of
Master of Philosophy (Civil Engineering)

of

Curtin University

March 2012

Declaration

To the best of my knowledge and belief this thesis contains no material previously published by any other person except where due acknowledgment has been made.

This thesis contains no material that has been accepted for the award of any other degree or diploma in any university.

Signature: …….

Date: ……...

Contents

Acknowledgements

I wish to express my sincere appreciation to Dr Natalie Lloyd and Dr Ian Chandler for their assistance, support, invaluable guidance and encouragement during the course of this research. This thesis would not have been possible without their help.

I would also like to thank the entire crew of technicians at the School of Civil and Mechanical Engineering Heavy Testing Laboratory, Curtin University, for their invaluable help from the beginning of this research and for their support and advice in constructing and testing the specimens. I would also like to express my gratitude to my supplier who provided their innovative product for this research.

In closing, I would like to thank my family for their encouragement and love and support throughout the years. Without this I feel I would not have been able to complete this thesis.

List of Tables

List of Figures

List of Abbreviations

CF	Carbon fibre
CFRP	Carbon fibre reinforced polymer
EBR	External bonded reinforcement
FRP	Fibre-reinforced polymer
GFRP	Glass fibre reinforced polymer
LVDT	Linear variable differential transformer
MTS	Melbourne Testing Services
PFC	Parallel flange channel
RC	Reinforced concrete

List of Symbols

C_c	Concrete Compression Force
δ	Deflection
δ_{yield}	Deflection at Yield
δ_{ult}	Deflection at Ultimate
f'_{cm}	Compressive Strength of Concrete
f_{yv}	Tensile Strength of Steel
M_u	Moment Ultimate
T_{s1}	Tension of Top Steel
T_{s2}	Tension of Bottom Steel
T_{sfg}	Tension of Side Face GFRP
T_{ufg}	Tension of Under Face GFRP

Abstract

In this research, 12 reinforced concrete (RC) beams, comprising two beams as control beams, and 10 beams strengthened with fibre-reinforced polymer (FRP), were tested in a four-point bending configuration to determine the ability of externally bonded composite fabrics to improve the flexural capacity of a beam. The composite fabrics used were made of glass and carbon fibre. The fabrics were bonded to the RC beams using a two-part epoxy. These two fabrics were chosen to allow a variety of fabric strengths to be studied. The external bonded reinforcement (EBR) led to an average 240 per cent increase in flexural capacity. Different end anchorages and application configurations of the externally bonded glass and carbon fibres were evaluated to assess their effectiveness in minimising or preventing the debonding of these externally applied composite materials. The results indicate that the anchorages effectively prevented the debonding of the FRP laminates during flexural testing. Beams that were reinforced with glass fabric but without end anchorages failed, with tensile rupture of the FRP followed by debonding. Beams that were externally bonded with anchorages escaped debonding, instead suffering concrete crushing of the compression zone at mid-span as well as tensile rupture of the composite fabrics. However, the fibre reinforced composite concrete beams exhibited non-ductile failures, which suggests the need for further research to resolve these matters when designing the fibre post-strengthening system.

Keywords: Composite materials, FRP, anchorages, debonding, flexural, fibre strengthened, EBR

Chapter 1: Introduction

1.1 Statement of the Problem

The cracking of concrete due to weathering and changes in loading requirements is a major problem in concrete structures. When these structures are subjected to variations in the intensity of loads, the lifespan of the structure will gradually be reduced. Over the last decade, the strengthening of concrete structures has been a challenging and important task for engineers. New strong materials are being used to extend the lifespan of existing concrete structures. Fibre reinforced polymer (FRP) has recently become popular, as it performs extremely well when used to strengthen concrete structures. This was demonstrated in a study conducted by Toutanji and Ortiz (2001) in which externally bonded FRP sheets were used with reinforced concrete (RC) specimens to increase both the tensile strength and the stiffness of the structure. Furthermore, because FRP is more affordable than structural steel, it offers a cost-effective strengthening solution with many structural benefits. Hashemi, Maghsoudi and Rahgozar (2008), found that FRP's high resistance to electrochemical corrosion, its high strength-to-weight ratio, excellent fatigue resistance and non-magnetic and non-metallic properties makes it a viable alternative to bonding steel plates when repairing and rehabilitating RC structures. The authors also found that as a consequence, FRP could save both time and money in maintenance.

Past research has investigated ways to improve the performance of fibre-strengthened concrete beams. When RC elements failed, it was generally due to the yielding of the internal steel reinforcement, whereas FRP materials showed a linear elastic behaviour up until failure. In general, FRP has not achieved high strength when used as an external reinforcement because the strengthened elements have often exhibited failure in the concrete layer immediately below the adhesive, due to either peeling at the ends or cracking which spread from an existing crack in the high-moment zone of the beam (Achintha, Guan & Burgoyne 2010). This peeling or cracking mechanism is known as 'debonding'. The key issue then, is to resolve debonding as it occurs in FRP towards the end of the beam.

The failure mode depends on the behaviour of the bond at the concrete–FRP reinforcement interface, and failure generally occurs in the form of the detachment of a relatively thick concrete cover (Ceroni 2010). The location of the failure along the beam, and the thickness of the detached concrete cover largely depend on cracking patterns, internal steel reinforcement percentage, presence of steel fitment, loading scheme and interaction between shear and normal bond stresses along the interfaces (Yao and Teng 2007). Therefore, the ductility of an externally bonded reinforcement (EBR) strengthened RC member depends chiefly on the failure modes. End anchorage systems could be very useful for avoiding or delaying debonding and for achieving a relative increase in strength and ductility (Ceroni et al. 2008). There has been a variety of research assessing the flexural response of RC members externally strengthened with FRP laminates and sheets, and this research aimed to investigate performance at both serviceability and ultimate limit states. This research is discussed in Chapter 2.

1.2 Objectives of this Study

The objectives of this study are to:

1. evaluate the bending strength of carbon fibre and glass fibre strengthened RC beams loaded in flexure
2. investigate the efficiency of different end anchorage methods—transverse fabric and mechanical anchorage
3. assess the ductility of carbon fibre and glass fibre strengthened RC beams under flexural load, by recording and evaluating the load-deflection response of the beams.

1.3 Scope of Work

This research considers the behaviour of RC beams externally bonded with FRP. Twelve large-scale steel-RC beams were constructed and then strengthened with either glass fibre or carbon fibre. Anchorage configurations were also introduced to investigate the effect of the strengthening work. Different anchorage designs were used in order to determine the performance of each setup. Experiments and

numerical analyses were developed to assess the flexural and ductile behaviour of the beams.

1.4 Testing and Data Collection Methods

The flexural performance of these 12 RC beams was tested at the School of Civil and Mechanical Engineering Heavy Testing Laboratory, Curtin University. Ten of the 12 beams were externally applied with either carbon fibre reinforced polymer (CFRP) or glass fibre reinforced polymer (GFRP). The remaining two beams, which did not receive any application of either CFRP or GFRP, were used as control beams. Further details are discussed in Chapter 3. For the collection of experimental data during flexural testing, a linear variable differential transformer (LVDT) was used along with and close-range photogrammetry.

1.5 Organisation of Thesis

In Chapter 2, existing literature on the flexural behaviour and failure mechanisms of conventional beams is reviewed. This is followed by a review of the literature on the effects of FRP on the strength of RC beams. Finally, literature on the effects of using anchorage in conjunction with FRP strengthening is also reviewed. In Chapter 3, the experimental program, including equipment setup, from the initial stage to the testing stage is presented. Chapter 4 shows the results of the testing of all materials utilised in this research and presents the characteristics of each individual material. Chapter 5 presents the results of the flexural bending tests. All results and the behaviour of the specimens are discussed. Ductility measurements and related discussions are also presented. Chapter 6 provides the conclusion to this research. Chapter 7 gives recommendations for future studies.

Chapter 2: Literature Review

2.1 Introduction

Interface failure is a major problem arising from the use of RC elements externally strengthened with FRP; local behaviour at the interfaces can influence the global efficiency of the strengthened element. Generally, debonding occurs in the support material since the bond strength is related to the tensile strength of the concrete, which is lower than the adhesive, while bond stress distribution at the interfaces depends on the stiffness of adhesive and fibres. When strengthened RC elements bend, debonding of the external FRP reinforcement can occur at various locations. Surface cracks and irregularities can cause weak points for bond behaviour, but in many cases, debonding occurs at the end part of the external reinforcement, where a high concentration of normal and shear stress occurs, with subsequent propagation along the beam and detachment of the concrete cover (Chen and Teng 2001; fib 2001). When diagonal shear cracks intersect the external reinforcement near the end of the FRP due to a lack of internal steel fitment, debonding is initiated due to shear and normal interfacial stresses on the side of the diagonal crack. The crack propagates toward the plate end (Jansze 1997; Oehlers et al. 2004; Teng and Yao 2007), and failure generally occurs in the concrete that is adjacent to the adhesive - concrete interface. In general, such 'end debonding' failures can be avoided or delayed by using suitable anchorage systems (Ceroni 2010).

2.2 Debonding of FRP

The debonding of FRP is defined as a failing stage, where the FRP material and the bonding epoxy resin separate due to various factors such as excessive loading, poor surface preparation and improper installation of the FRP. Cracks or discontinuities of concrete generally increase or widen due to an increase in the magnitude of load during the process of loading. The extent of the debonding of FRP is influenced by crack width. Generally, cracks can be classified as flexural or shear. Shear cracks form at the bottom of the support, and propagate diagonally. Flexural cracks form at the tension face of the concrete beam and propagate vertically, perpendicular to the

tension side of the beam. With the beam continuing to sustain further loading, the internal forces change paths, causing shear cracks to form diagonally and horizontally. When the horizontal cracks reach the end of the longitudinal layer, the FRP layer eventually debonds and peels away.

According to Büyüköztürk and Yu (2006), flexural failures of critical sections, in FRP-strengthened RC members may occur, such as FRP rupture and crushing of compressive concrete, or debonding of the FRP plate from the RC beams. This latter type of flexural failure occurs with a loss in the composite action between the bonded FRP and the RC member. Debonding in FRP-strengthened RC members occurs in regions of high stress concentration, which are often associated with material discontinuities and the presence of cracks. The propagation path of debonding that is initiated from stress concentration, depends on the elasticity and strength properties of the repair and substrate materials, as well as their interface fracture properties. The term 'debonding failure' is often used to describe a significant decrease in member capacity due to the initiation or propagation of a major crack near the interface region. Theoretically, debonding can occur within a constituent element, or at the interface of the materials that form the strengthening system, favouring a propagation path with the least amount of energy. However, interface debonding is often encountered in cases of poor surface preparation. The majority of debonding failures have been reported as occurring in the concrete substrate. Nevertheless, depending on the geometric properties, material properties and the mechanical and environmental effects to which the interface region is subjected to, other types of debonding can also occur. Experimental results have shown that FRP debonding is a highly complex phenomenon that can involve failure propagation within the concrete substrate, within the adhesive, within the FRP laminate or at the interfaces of these layers (Au 2006; Büyüköztürk, Gunes and Karaca 2002; Büyüköztürk et al. 2003; Büyüköztürk et al. 2004; Büyüköztürk and Yu 2006; Gunes 2004; Smith and Teng 2001).

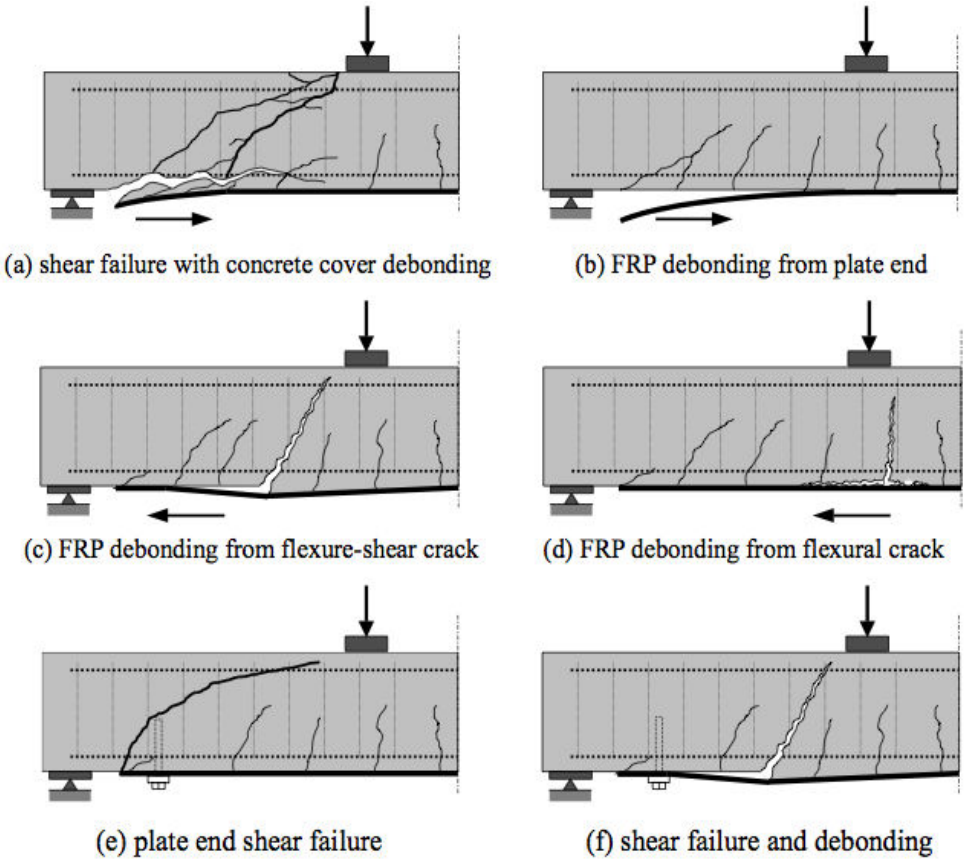

Figure 2.1: Debonding Mechanisms of FRP (taken from Gunes 2004)

Fundamental debonding mechanisms that may result in premature failure of FRP-strengthened beams with and without plate-end anchorages are shown in Figure 2.1 (Gunes 2004). They are (a) shear failure with concrete cover debonding, (b) FRP debonding from plate end, (c) FRP debonding from flexure-shear crack, (d) FRP debonding from flexural crack, (e) plate-end shear failure and (f) shear failure and debonding.

The mechanism of shear failure with the debonding of the concrete cover, as shown in Figure 2.1(a) is usually associated with high interfacial stresses, low concrete strength and/or extensive shear cracking. If the concrete strength and the shear capacity of the beam are sufficiently high, potential debonding failure is most likely to take place through FRP debonding, as shown in Figure 2.1(b), which initiates at the plate ends and propagates towards the centre of the beam. Depending on the material properties, FRP debonding may occur within the FRP plate, at the concrete–FRP interface or a few millimetres within the concrete. If the shear span of the strengthened beam is sufficiently long enough to enable proper bond development, or

the plate ends are anchored against shear failure and debonding, as shown in Figure 2.1(f), debonding may initiate at flexure-shear cracks and propagate towards the ends of the beam as in Figure 2.1(c). If the shear capacity of the beam is sufficiently high, debonding may also initiate from the flexural cracks as shown in Figure 2.1(d). However, this failure mechanism is very rare, especially in four-point bending tests (Büyüköztürk, Gunes and Karaca 2002). Propagation of debonding within the constant moment region does not change the stress distribution within the strengthened system. Thus, a conceptual interpretation suggests that debonding within the constant moment region is unlikely to happen. It is possible that high stress concentrations around flexural cracks promote debonding (Leung 2001). However, such stress concentrations diminish rapidly with propagation of debonding, resulting in a limited debonded area.

Shear failure in a flexurally strengthened beam with insufficient shear capacities becomes more distinct when plate-end anchorage methods are employed to prevent debonding failures. Plate-end anchor bolts can prevent debonding from the plate ends, in which case the beam may fail in shear outside the plated length, as shown in Figure 2.1(e). The loading levels at shear failure are approximately 60–65 per cent of the theoretical shear capacities of the beam. An alternative failure mode with beams strengthened in flexure using prestressed and non-prestressed FRP plates with or without plate-end anchor bolts was also observed, as shown in Figure 2.1(f). This failure mode was due to a large flexure-shear crack within the shear span of the beam, leading to debonding of the external FRP reinforcement and shear failure of the beam.

2.3 Anchorage

2.3.1 Introduction

As discussed in Section 2.2, debonding failure is a key aspect for consideration in the process of strengthening concrete structures with externally bonded FRP laminates. In most cases, the failure of RC elements strengthened with FRP laminates or sheets is caused by the detachment of the external reinforcement in the concrete tension face due to the low strength of concrete under tension. There are many practical applications for strengthening RC elements by means of externally bonded FRP

laminates and sheets (e.g. flexural and shear reinforcement of beams, confinement of columns and joints), but with each type of application, debonding failure can limit the strength of the reinforced member. Further, debonding causes a brittle failure that must be avoided when ductility is required for the structural behaviour, as in seismic upgrading (confinement of columns, strengthening of beam–column joints). In some cases, anchorage devices are essential to transfer the stress from one structural component to another, as occurs with internal steel reinforcement (from the column to the base foundation, from the beam to the column) or when the bond length at the end of the FRP laminate is limited by the geometrical configuration, for example, in the shear strengthening of the T-shaped sections.

There are national and international code provisions (fib TG 9.3) for the design of elements externally bonded with FRP, and there have been many experimental tests in this field of research. Experimental results and code suggestions indicate that performance improvement can be realised by introducing anchorage systems. However, the performance and benefits of the suggested possible solutions have not yet been quantified.

2.3.2 Anchorage Systems

A range of techniques can be used to fix the fibres to the end of the beam to prevent debonding. Different anchorage designs result in different debonding effects. The anchorage designs used for this research are discussed in Section 3.2.3 of Chapter 3. To understand more about the use of anchorage systems on FRP-strengthened structures, previous research that has been undertaken is discussed below.

To realise sufficient anchorage capacity for the shear reinforcement of T-beams or confinement of the column in configurations with wing walls, Jinno, Tsukagoshi and Yabe (2001) and Koayshi et al. (2001) proposed that the fibres should end in the form of a fan, as shown in Figure 2.2. The largest part of the fan is fully bonded to the FRP, while at the summit the fibres are braided to form a string that is inserted into a hole.

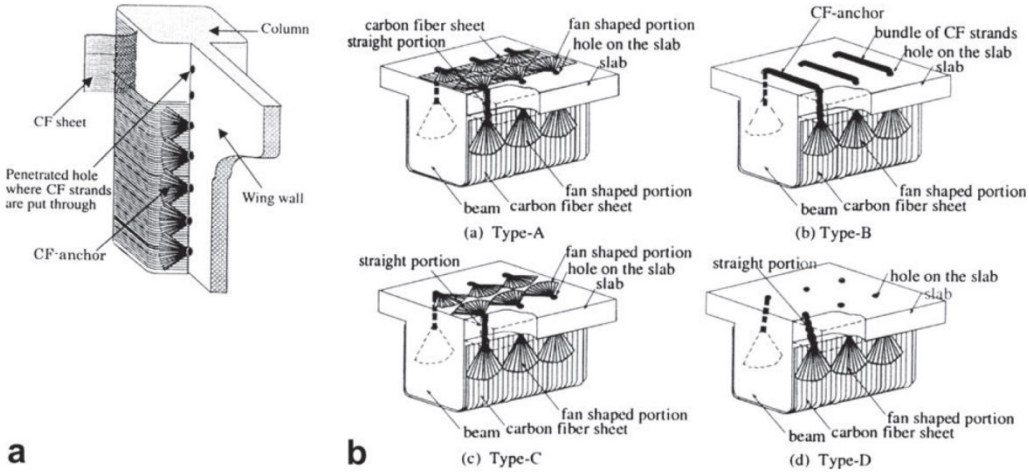

Figure 2.2: Special fan fibres: (a) confinement and (b) Shear strengthening (taken from Koayshi et al. 2001)

Another concept, which was tested by Karantzikis et al. (2005), used spike anchorages to provide effective FRP jacketing at the internal corners of the L-shaped columns. Each anchor consisted of a bundle of uni-directional fibres inserted into holes which were drilled into the concrete. The remaining part of the bundle was spread uniformly outwards, as shown in Figure 2.3. Experimental tests, conducted according to various configurations, showed that the anchorages were effective in terms of deformability and strength increase, depending on the distance of the anchorages.

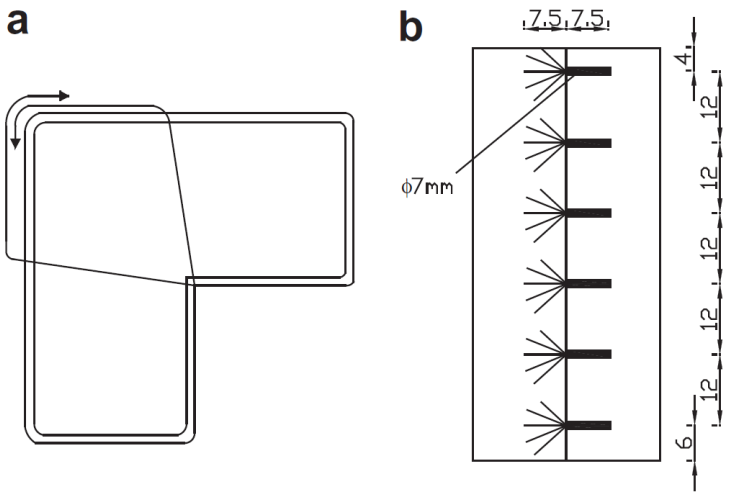

Figure 2.3: Spike anchors (taken from Karantzikis et al.2005)

For beams with flexural strengthening, the use of U-shaped fibre sheets can be a simple and efficient method. In experimental tests on beams performed by Ceroni and Pecce (2005), this type of fixing system increased strength and ductility. Anchorages with U-shaped fibre strips are more efficient at preventing debonding, and they allow tensile fracture of the fibres at the mid-span of the beam if the strips are distributed along the beam instead of concentrated at the ends. In some cases, concentrated end U-shaped strips can suffer local slip, cutting or debonding with a loss of effectiveness, before reaching the tensile strength of the fibre at the mid-span.

Embedding steel U-shaped devices into the concrete provides a simple anchorage system. Blaschko (2001) and Mukhopadhyaya, Swamy and Lynsdale (1998) performed tests on reinforced concrete ties externally bonded with FRP sheets fixed at the end with U-shaped steel. They showed that the anchorage provided not only an increase in the ultimate strength, but also in the ductility of the strengthened member, with higher displacements at ultimate conditions. The subject of ductility is particularly interesting because strengthening the beam with FRP can reduce the beam's ductility, especially when the RC beam has a low number of steel bars; that is the failure is ductile due to the yielding of the steel. CFRP anchorage could significantly increase the flexural ductility of strengthened beams, allowing large post-yielding deformation of the steel before brittle debonding of the FRP.

The concept of improving ductility in externally strengthened elements was investigated by Hall, Schuman and Hamilton III (2002) in masonry elements using a hybrid (steel and FRP) strengthening method which used structural steel at critical locations. The aim was to have a ductile structural steel connection that would improve the connection of strengthened shear walls to the foundation, providing higher energy dissipation for the strengthened system. Results showed that a ductile failure mode could be reached when the connection was designed to yield before the failure of the strengthened component, being the FRP. The most efficient system was the application of U-shaped strips, glued to the longitudinal fibres, which were used as flexural reinforcement at both the wall foot and the base foundation where the T-shaped longitudinal fibres were located. Following this, steel plates were glued onto the U-shaped fibre strips and these were then placed onto the base foundation. The U-shaped anchorages significantly reduced debonding, allowing the fibres to reach

their potential tensile strength and this enhanced the overall ductility of the FRP-strengthened beams using the hybrid strengthening method.

2.4 Flexural Behaviour of RC Beam Strengthened with FRP

Research has been performed on the flexural strengthening of concrete beams using externally bonded composite materials (Chajes et al. 1994). According to the researchers, the bonding of composite materials to the tension face of concrete beams can be divided into two categories: (1) the bonding of composite plates and (2) the bonding of composite fabrics. While FRP composite plates can be used as an effective means of providing additional reinforcement, they do possess some drawbacks, including the need for a flat surface for bonding, the high cost associated with manufacturing large plates, and the difficulty in achieving a sufficient bond between the concrete and the composite plate to prevent debonding from governing the failure mode. Hence, as an alternative to the use of composite plates, Chajes et al. (1994) investigated the use of epoxy bonded composite fabrics made of aramid, glass fibre and graphite fibres. As with the FRP composite plates, the fabrics were non-corrosive and possessed high strength-to-weight ratios. Furthermore, the FRP composite fabrics had other beneficial qualities; for example, they could conform to irregular surface geometries, and because they are usually manufactured in long rolls, they were available in long lengths. Lastly, FRP fabric could also be bonded to beams in such a way as to develop full tensile capacity prior to debonding.

Chajes et al. (1994) tested 12 rectangular beams with three of the beams used as control beams. The remaining nine beams were divided into three sets of three beams; the first set was strengthened with aramid, the second with glass fibre and the third with graphite fibre fabric. Two of the aramid-strengthened beams were bonded with anchorage; the other was bonded with FRP fabric at the tension face. All of the beams were loaded monotonically until failure in a four-point bending configuration. The final failure indicated that the beams strengthened with glass fibre and graphite fibre suffered fabric tensile failure. The beam strengthened with aramid only, failed due to fabric debonding, whereas the two beams strengthened with aramid and anchorages reached the ultimate compression strain of concrete; the beams failed due to the crushing of the concrete before reaching the fabric's tensile capacity. The

average strength of the FRP-strengthened beams was 50 per cent higher than that of the unstrengthened beams. The results of this study indicate that EBR technology can be used to effectively rehabilitate or strengthen concrete beams. Additional anchorage can be easily applied to ensure that any failure will either be concrete compression failure, or tensile rupture of the fabric on the tension side.

Research has also been conducted on the performance of RC beams strengthened with FRP materials (Ceroni 2010). Twenty-one beams were constructed for the research. Five of the beams were tested cyclically, while the rest were tested monotonically. Among those that were tested monotonically, four of the beams were strengthened with U-shaped anchorages. According to Ceroni (2010), the control beams failed due to concrete crushing. Beams that were strengthened with CFRP only (without anchorage) suffered debonding failure at the end of the reinforcement, whereas the beams that were strengthened with anchorages suffered concrete-crushing failure. Ceroni (2010) concluded that the beams strengthened with an FRP–EBR system had strength increments of between 26 per cent and 50 per cent in the case of the lower control beam, and 17 per cent to 33 per cent for the higher control beam. The ductility was reduced due to the brittle failure caused by the end debonding of the FRP reinforcement.

Based on the literature reviewed in this chapter, it is possible to make some predictions about the likely failure modes for the specimens tested in this research. Beams strengthened with both FRP and anchorages are predicted to fail with the crushing of compression concrete. Beams without anchorage systems are predicted to suffer FRP debonding from the plate end, as indicated in Figure 2.1(b).

Chapter 3: Experimental Research

3.1 Introduction

The literature reviewed in Chapter 2 indicates the advantages of using FRP in concrete structures under static loading. Hence in this research, twelve specimens were constructed, each measuring 200 mm wide, 250 mm deep and 3000 mm in length. Ten of the beams were strengthened using one of two types of material: CFRP and GFRP. The remaining two beams were used as control beams to compare the performance of typical RC beams with the performance of FRP-strengthened RC beams. To investigate the effectiveness of anchorages in strengthening beams, eight of the ten FRP-strengthened beams were further reinforced with different types of anchorage at different locations on the beams. Epoxy resin was used as a bonding agent between the concrete surface and the FRP surface. Each of the 12 specimens was labelled with an identifier. Identifiers were H1, H2, H3, H4, H5, H6, H7, J1, J2, J3, J4 and J5 where 'H' and 'J' represents the initial of the researcher who conducted the test for those particular beams. However, due to labelling error, Specimen J4 was tested by the author. Table 3.1 shows the size, length, fitment, amount of reinforcement steel used for each beam and the name of researcher who conducted the test. Although Beam J1, J2, J3 and J5 was labelled with another researcher's initial, however, the author has been instrumental in carrying out the test for these four beams. Hence, the results were included as part of the author's research work.

Table 3.1: Summary of beam specifications

Beam name	Size (mm) (width x depth)	Length (mm)	Fitment	Compressive rebar	Tensile rebar	Tester
H1	200 x 250	3000	23-R10 @ 125 mm	2N12	2N20	Hiew Kee Hon
H2	200 x 250	3000	23-R10 @ 125 mm	2N12	2N20	Hiew Kee Hon
H3	200 x 250	3000	23-R10 @ 125 mm	2N10	2N12	Hiew Kee Hon
H4	200 x 250	3000	23-R10 @ 125 mm	2N10	2N12	Hiew Kee Hon
H5	200 x 250	3000	23-R10 @ 125 mm	2N10	2N12	Hiew Kee Hon
H6	200 x 250	3000	23-R10 @ 125 mm	2N10	2N12	Hiew Kee Hon
H7	200 x 250	3000	23-R10 @ 125 mm	2N10	2N12	Hiew Kee Hon
J1	200 x 250	3000	23-R10 @ 125 mm	2N10	2N12	Jovanco Domazetoski
J2	200 x 250	3000	23-R10 @ 125 mm	2N10	2N12	Jovanco Domazetoski
J3	200 x 250	3000	23-R10 @ 125 mm	2N10	2N12	Jovanco Domazetoski
J4	200 x 250	3000	23-R10 @ 125 mm	2N10	2N12	Hiew Kee Hon
J5	200 x 250	3000	23-R10 @ 125 mm	2N10	2N12	Jovanco Domazetoski

3.2 Design Stage

3.2.1 Beam Design

Twelve beams were constructed for this research. The dimensions of each beam were 3000 mm in length, 200 mm in width and 250 mm in depth. Ten beams were constructed with internal 2N12 tensile reinforcement and two beams were constructed with internal 2N20 tensile reinforcement. The concrete used was commercially supplied and of nominal grade 40MPa. The arrangement of the steel reinforcement is shown in Figure 3.1. Since this research focused on the investigation of the flexural behaviour of control beams in relation to FRP-strengthened beams, all beams were designed to have a significantly high amount of shear capacity compared to flexural capacity.

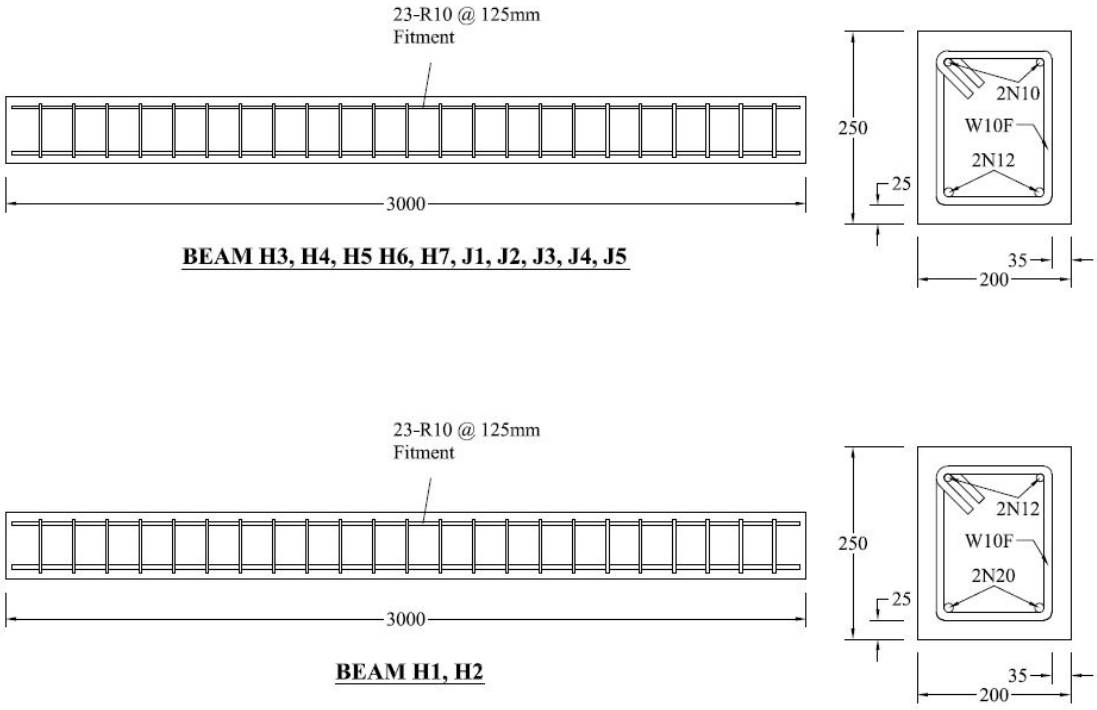

Figure 3.1: Steel bar arrangement

The flexural capacity design was carried out using the strain compatibility method. The FRP-strengthened beams were also designed according to this method. For the FRP-strengthened beam design, it was taken as given that there would be no debonding on the longitudinal plane of the FRP and that the tensile capacity of the FRP components would be fully utilised. The arrangement of the FRP fabric is discussed further in Section 3.2.2. The shear design was designed in accordance with <AS 3600–Clause 8.2.10> (2009; Australia 2009). The design for shear capacity relied on the contribution of tensile reinforcement, the direct shear of the concrete and the contribution of the fitment. Achievement of an adequate amount of shear capacity in the control beams obviated the need to design the shear capacity for the FRP-strengthened beams, as the FRP component in those beams provided extra shear capacity. The summary of the initial design for the beams is tabulated in Table 3.2, and sample calculations for the design of the beams are given in Appendix D and Appendix E.

Table 3.2: Summary of Initial Design

Beam type	Flexural capacity (kN)	Design shear load (kN)	Shear capacity (kN)
Lower control beam (H6)	25.5	38.3	182.8
Upper control beam (H2)	61.1	91.7	194.9
GFRP-strengthened beam (H1, H3, H4, H5, H7, J4)	81.2	121.8	>182.8
CFRP-strengthened beam (J1, J2, J3, J5)	70.0	110.0	>182.8

3.2.2 FRP Fabric Design and Arrangement

In this research, both CFRP and GFRP fabrics were used to strengthen the RC beams. Specimens J1, J2, J3 and J5 were strengthened with three layers of CFRP, while specimens H4, H7 and J4 were strengthened with three layers of GFRP. Specimen H3 and H5 were strengthened with two layers of FRP, with the inner layer being CFRP and the outer layer being GFRP. Specimen H1 was strengthened with a layer of GFRP on the tension face and another layer of GFRP on the compression face. Figure 3.2 shows cross-sections of all FRP-strengthened specimens detailing the layers of FRP. Table 3.3 summarises the materials used in strengthening the RC beams.

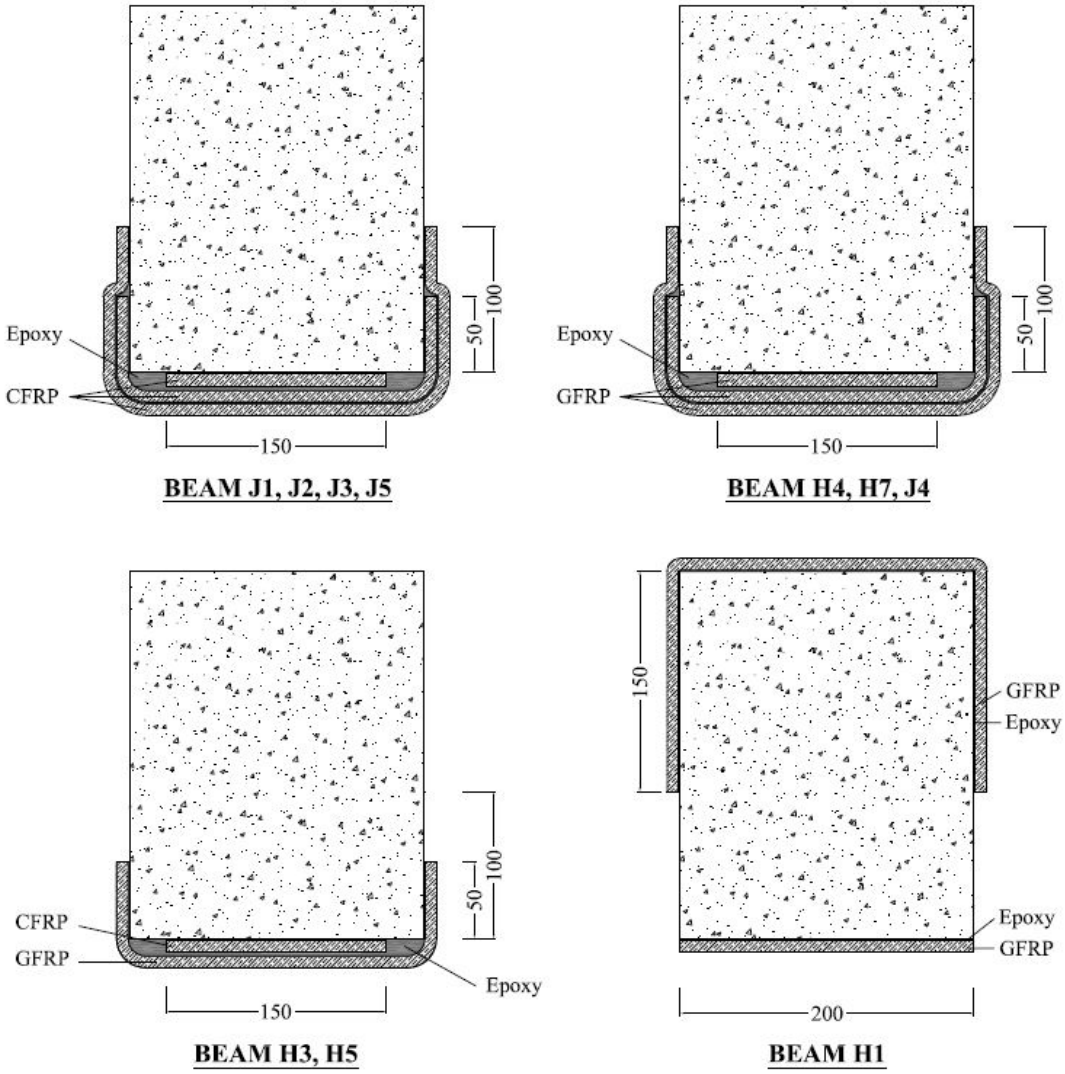

Figure 3.2: Cross-sections of FRP-strengthened specimens

Table 3.3: Summary of strengthening materials used for all Specimens

Specimen	Strengthening material	Description
H1	GFRP	One layer at tension face and one layer at compression face
H2	-	Upper control beam
H3	CFRP & GFRP	CFRP at inner layer and GFRP at outer layer
H4	GFRP	Three layers of GFRP at tension face
H5	CFRP & GFRP	CFRP at inner layer and GFRP at outer layer
H6	-	Lower control beam
H7	GFRP	Three layers of GFRP at tension face
J1	CFRP	Three layers of CFRP at tension face
J2	CFRP	Three layers of CFRP at tension face
J3	CFRP	Three layers of CFRP at tension face
J4	GFRP	Three layers of GFRP at tension face
J5	CFRP	Three layers of CFRP at tension face

3.2.3 Anchorage Design

As discussed in Chapter 2 (Section 2.3), anchorage is used to minimise the debonding failure of FRP in a longitudinal direction. Therefore, for this research, several anchorage designs involving different materials were used to identify both their effectiveness and their debonding performance. The two anchorage designs used were the U-shaped design and the V-shaped design (see Figure 3.3). The U-shaped anchorage design made use of an FRP sheet partially wrapped around the beam vertically at both ends of the RC beam. The V-shaped design made use of an FRP sheet partially wrapped around the beam at an inclined angle. As shown in Figure 3.3, the anchorage of one of the specimens, Beam J4, was wrapped with GFRP, vertically at both ends. Hence, in the section view A-A, the anchorage wrapping of the beam exhibits a U shape. On the other hand, Beam H4 was wrapped with anchorages in an inclined manner. Hence, the elevation view of Beam H4 in Figure 3.3 shows the anchorage exhibiting a V shape. For this reason, the designs of

these two types of anchorages were called U-shaped designs and V-shaped designs respectively.

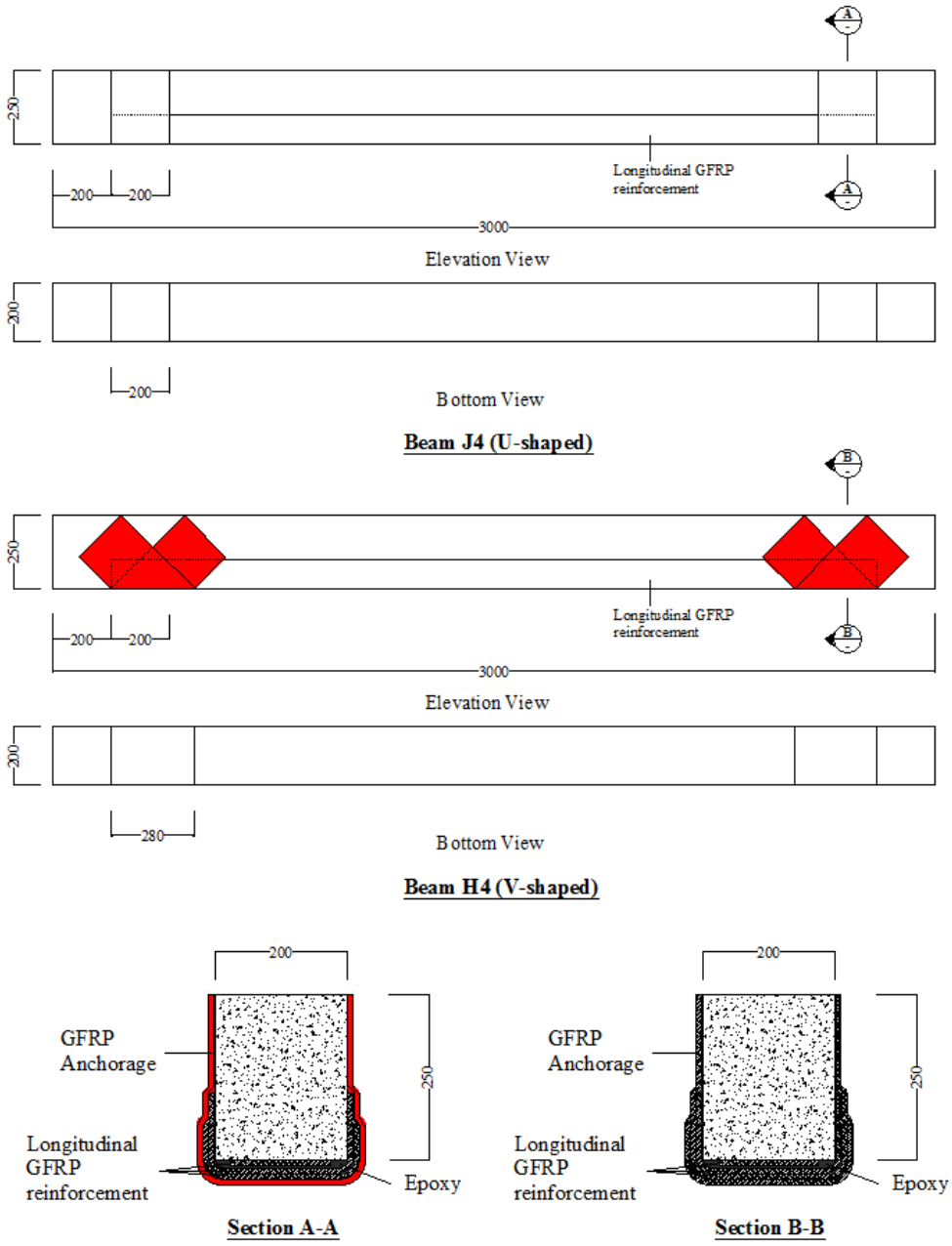

Figure 3.3: U-shaped and V-shaped anchorages

The major difference between these two anchorage designs is the direction of the strap. Since both the CFRP and GFRP used in this project were uni-directional fabrics (see technical data sheet, Appendix A), the fabric was concentrated in one direction only, which meant that the fabric performed well in resisting the tension force in the longitudinal direction, and less well in the transverse direction. Hence, if any internal tension occurred in the longitudinal direction, the U-shaped anchorage would not be able to provide much resistance, as there was no horizontal component

to the design. Therefore, failure occurring in this area would simply tear off the vertical strap. However, with the V-shaped anchorage, the inclined strap provided both horizontal and vertical components which were able to resist any internal action coming from either direction. Figure 3.4 illustrates the internal action of the beam and the FRP behaviour during loading.

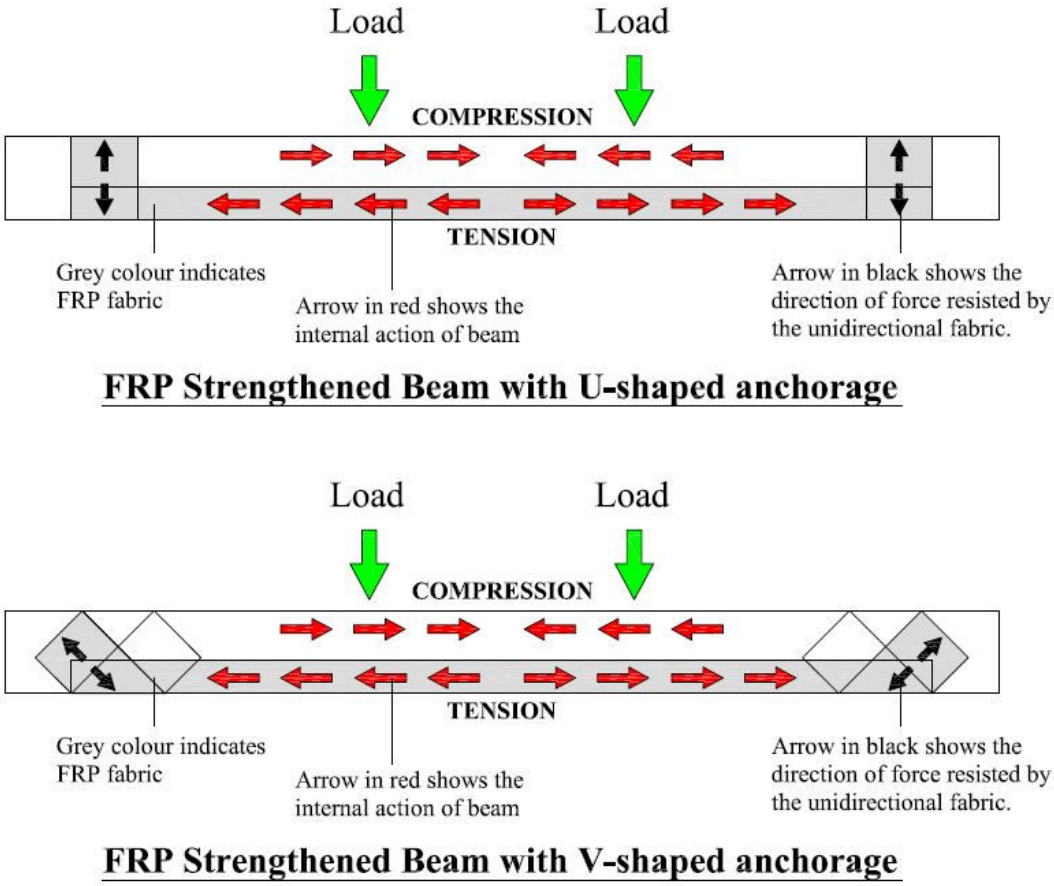

Figure 3.4: Internal action of FRP-strengthened beams with U-Shaped and V-shaped anchorages

As an alternative to FRP material, steel plates were tested for their utility as end anchorages to resist debonding. At the beginning stage of this research, the steel-plate anchorage design proposed was a U-shape anchorage that would simply clamp onto the beam; the anchorage(s) being bolted on with fasteners, or glued on with epoxy resin. However, after careful consideration, it appeared that the U-shaped design was flawed; for example, precise measurements were required in order to bend the steel plate into a perfect U-shape that that would fit onto the beam. Therefore, to reduce such difficulties with the fabrication, two pieces of L-shaped plate mirroring each other, creating a U-shape, were used. With the steel-plate anchorage, there was no necessity to wrap the beam at an inclined direction, as steel

plates placed in any direction perform well at resisting both tension and compression. Figure 3.5 shows the design of steel-plate anchorages used for this research. It should be noted that Figure 3.5 is a not-to-scale illustration (the contact between the beam surface and the steel plate was thinner than indicated; GFRP thickness was 0.4 mm).

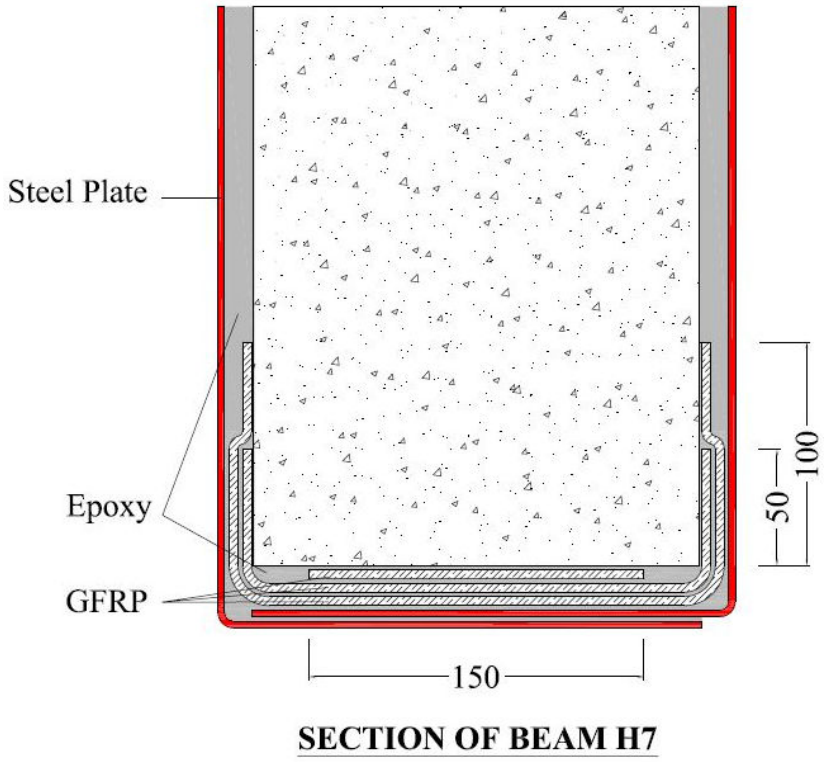

For illustration purpose only. Actual specimen varies

Figure 3.5: Design of steel-plate anchorage

Therefore, in this research, a variety of combinations of anchorage types were applied to determine the results for each design. The designs involved beams fully wrapped with anchorages as well as partially wrapped beams. Beam H1 was wrapped with a layer of GFRP on the tension face and a layer of GFRP on the compression face at mid-span. No anchorages were applied onto this specimen. Beam H2 was tested as an upper control beam. Beam H3 was strengthened with a layer of CFRP on the first layer and a second layer of GFRP on the outer layer; V-shaped anchorages were applied onto this specimen. Beam H4 was strengthened with three layers of GFRP and V-shaped anchorages applied. Beam H5 had the same configuration as Beam H3 but with no anchorage applied at the ends of the beam. Beam H6 was not strengthened with any FRP material and was tested as a lower control beam. Beam H7 was strengthened with three layers of GFRP and steel-plate

anchorages applied. Beam J1 was strengthened with three layers of CFRP, and V-shaped anchorages were applied onto the entire length of the beam. Beam J2 had the same configuration as Beam H4, but used CFRP material instead of GFRP. Three layers of CFRP were used to strengthen the beam, followed by the application of V-shaped anchorages. Beams J3 and J4 were strengthened with three layers of CFRP and GFRP respectively and U-shaped anchorages were applied to both. Lastly, Beam J5 was strengthened with three layers of CFRP, and V-shaped anchorages were applied onto the entire length of the beam, as was the case with Beam J1. However, the anchorage width of Beam J5 was less than that of Beam J1. A summary of the designs of the anchorages is tabulated in Table 3.4. Figure 3.6 illustrates the anchorage arrangement of all FRP-strengthened beams.

Table 3.4: Summary of designs of specimens

Specimen	Anchorage	Anchorage material	Description
H1	Nil	Nil	No anchorage wrapping at either end of the longitudinal GFRP layer
H2	Nil	Nil	Upper control beam
H3	V-shaped	GFRP	V-shaped GFRP anchorage wrapping at both ends of the longitudinal hybrid FRP layer
H4	V-shaped	GFRP	V-shaped GFRP anchorage wrapping at both ends of the longitudinal GFRP layer
H5	Nil	Nil	No anchorage wrapping at either end of the longitudinal hybrid FRP layer
H6	Nil	Nil	Lower control beam
H7	U-shaped	Steel plate	U-shaped steel-plate anchorage wrapping at both ends of the longitudinal GFRP layer
J1	V-shaped	CFRP	V-shaped CFRP anchorage wrapping the entire length of the longitudinal CFRP layer
J2	V-shaped	CFRP	V-shaped CFRP anchorage wrapping at both ends of the longitudinal CFRP layer
J3	U-shaped	CFRP	U-shaped CFRP anchorage wrapping at both ends of the longitudinal CFRP layer
J4	U-shaped	GFRP	U-shaped GFRP anchorage wrapping at both ends of the longitudinal GFRP layer
J5	V-shaped	CFRP	V-shaped CFRP anchorage wrapping the entire length of the longitudinal CFRP layer

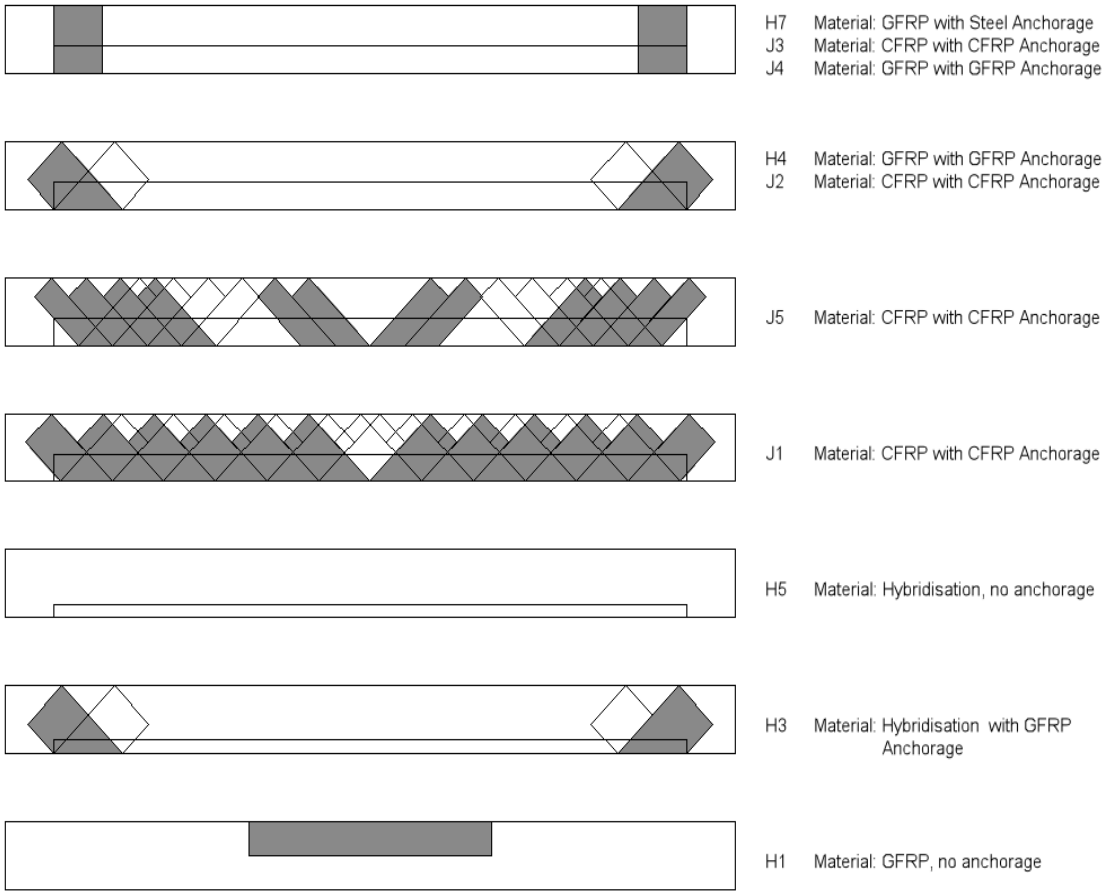

Figure 3.6: Anchorage arrangements of FRP-strengthened specimens

3.3 Construction Stage

3.3.1 Formwork Construction

Prior to the start of the project, a formwork bed was erected with moulds of galvanised parallel flange channel (PFC). Twelve six-metre lengths of PFCs were clamped and welded onto the formwork bed to form the moulds for the specimens.

3.3.2 Steel Reinforcement Construction

The tensile reinforcements used were reinforced N10, N12 and N20 steel bars, supplied by an accredited ACES Australia supplier. Prior to tying the tensile bars with the fitment, each steel bar was cut to an appropriate length to suit the design parameters of the project. Fitments were then tied to each reinforcement bar using wires. It the final process Bar chairs were then tied up to cover 25 mm of the concrete. Figure 3.7 shows the location of all specimens on the formwork bed with

Figure 3.8 showing the steel reinforcement held in place on the concrete mould ready to be cast.

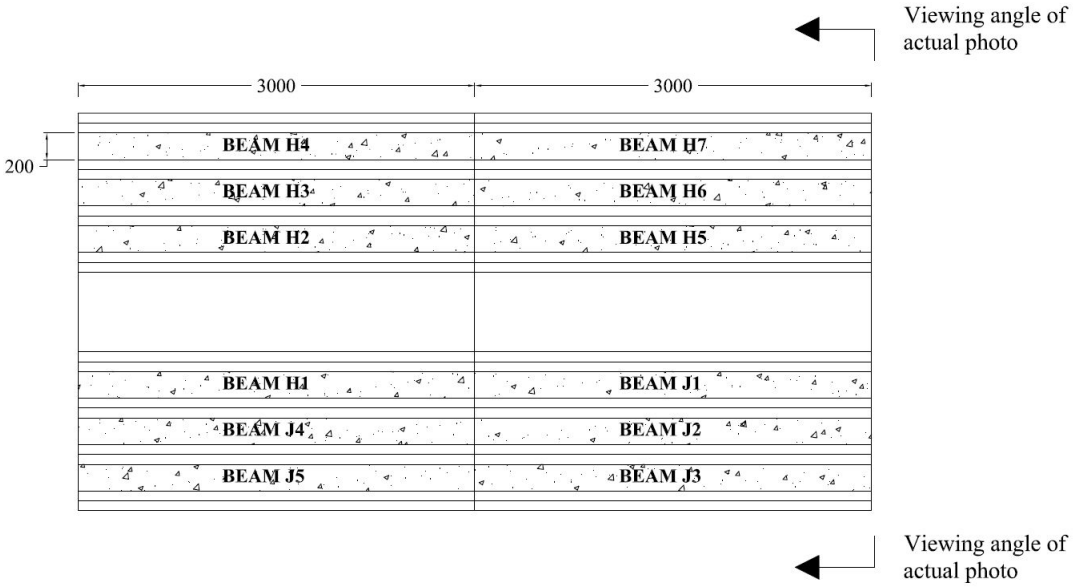

Figure 3.7: Location of specimens on the formwork bed

Figure 3.8: Steel reinforcement in the concrete mould

3.3.3 Beam Construction

Prior to pouring the concrete, each mould surface was applied with formwork release oil in order to ease the process of de-moulding and lift-up. All steel reinforcements were then put into place and readied for pouring. The concrete was of the ready-mix type of nominal grade 40 MPa. Prior to pouring, standard procedures such as the slump test were carried out to ensure that there was no excessive water content in the

concrete. Concrete cylinders of 100 mm in diameter and 200 mm in height were cleaned and greased in advance in order to be filled for cylinder sampling. In the meantime, the moulds were poured and filled with wet concrete. A vibrator was used during the pouring process to remove any air bubbles. A two-foot anchor was inserted into the surface of each beam for lifting. After three days, the de-moulding process was carried out, the formwork was dismantled and the beams lifted out using face lifting. Swiftlift clutches were connected to the anchor-head by inserting the anchor-head into the slot of the lifting clutch. The lifting clutch was then connected to a metal chain. The beam, which was connected to the lifting clutch, was raised using a forklift. All of the beams were then placed into an open-air environment and moist-cured for 28 days.

3.4 Pre-FRP Installation Stage

Prior to the testing stage, preparations involving all necessary work were carried out. These included the surface treatment of each specimen to ensure that the FRP fabric and concrete would bond strongly. In addition, several pre-installation procedures were required during the installation of the FRP fabric.

3.4.1 Scabbling

Scabbling is the process of reducing concrete or stone. In this research, each beam surface was mechanically scabbled using a needle gun connected to an air compressor, which left the surface of the concrete beam roughened, with aggregates exposed. It is advisable that scabbling be carried out at an early stage, before the concrete reaches its maximum compressive strength, as this makes it easier to remove the soft concrete matrices. Only the beams requiring strengthening work needed to be scabbled, and this process was vital to efforts to enhance the bonding strength between the beam surface and the FRP fabric. After scabbling, the beam surface was cleaned with either an air gun or water to remove dust. Methylated spirit was used to remove any remaining dust particles. Figure 3.9 shows the difference between a smooth concrete surface (Beam H2, left) and a scabbled concrete surface (Beam H1, right).

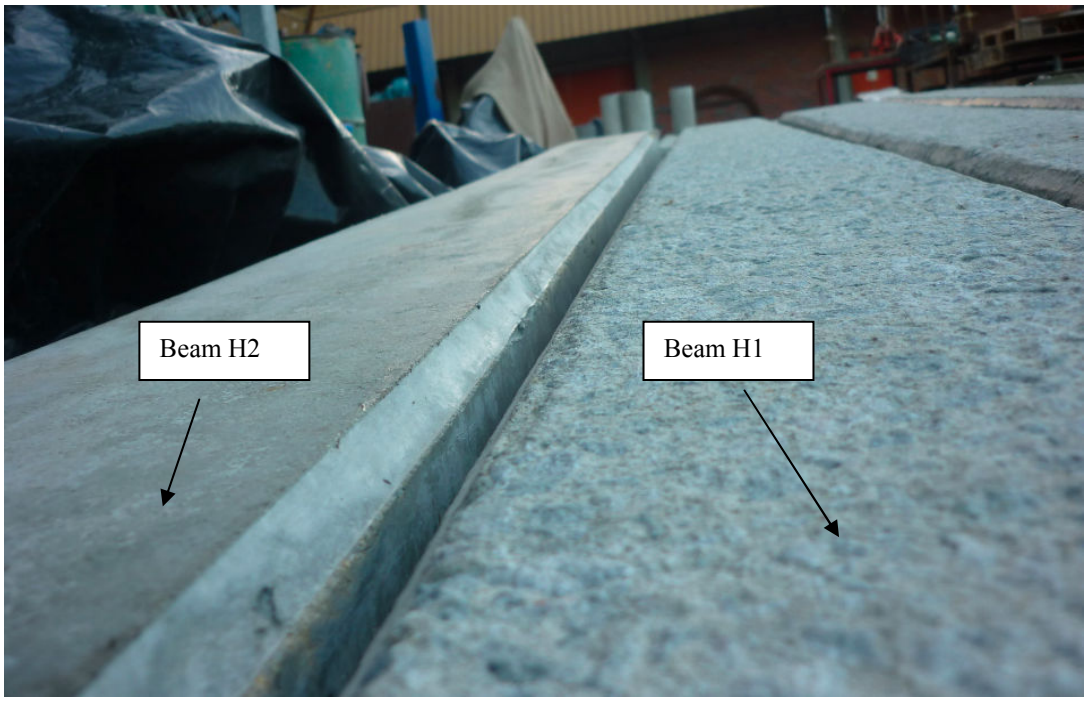

Figure 3.9: Difference between a smooth surface and a rough (scabbled) surface

3.4.2 Installation of FRP Fabric

3.4.2.1 Pre-installation

Several pre-installation procedures were carried out before the FRP fabric was applied to the concrete specimens. These procedures included cutting the fabric into various dimensions to suit the design parameters, mixing epoxy resin and mixing primer. FRP fabric comes in rolls; the fabric was measured to the correct dimensions and then cut with a rotary cutter. Appropriate safety precautions were taken in line with Occupational Health and Safety requirements as outlined in the Material Safety Data Sheet (see Appendix B).

The bonding products used in this research were primer and epoxy, which were sourced from a supplier. Both products came in Part A and Part B packaging, and they required mixing prior to the installation process.

3.4.2.2 Installation

The first stage involved final cleaning to ensure dust particles were removed. Then, the well-mixed primer (Part A and Part B mixed together) was brushed onto the concrete surface using a paintbrush. The wet primer was then evenly distributed onto

the sides of each specimen where the FRP fabric was to be installed. To ensure that the second layer (epoxy resin) was applied effectively before attaching the FRP fabric, the primer layer needed to become 'tacky'. Approximately one hour was needed for the primer to become tacky, as the chemical reaction between the Part A and Part B portions was slow.

As with the primer, the epoxy resin was well mixed prior to being brushed on top of the first layer of concrete. When the epoxy had been well distributed, a layer of fabric was instantly applied over the top. A roller was used to roll across the fabric to ensure the fabric interstices were completely filled with wet epoxy. The rolling also removed any possibility of air bubbles being trapped between the concrete surface and the FRP fabric. The removal of air bubbles was crucial to ensure that the quality of the strengthening work was maintained. Air bubbles trapped inside eventually form air pockets, which prevent bonding from occurring between the fabric and the resin. Depending on the design parameters, different amounts of each of the above layers were applied onto each specimen.

3.4.2.3 Post-Installation

After the application of the FRP fabric, curing time was required to allow the epoxy to bond fully with the concrete surface and the FRP fabric layer. Based on the supplied technical data sheet, suggested curing time is seven days at a temperature of 28 °C. Because winter night temperatures can drop to as low as 6 °C, a total curing time of three weeks was allowed for the specimen to strengthen completely before flexural testing commenced.

3.5 Setup Stage

After the installation, the setup procedure was carried out while waiting for the strengthened beams to cure fully. Any equipment needed during the testing stage was set up and prepared.

3.5.1 Equipment and Apparatus

3.5.1.1 Jack and Support

The specimens were tested in a heavy testing area where supports were prepared and built prior to the testing. Supports were held in place and tie-down rods with nuts were used to fix the supports to the floor, ensuring that the supports would not move during the test. Two 20-tonne jacks were used as a four-point bending test to carry out the flexural bending test. With swivel hinges bolted onto the testing frame, the jacks were lifted and positioned by engaging the hinge pin. Nuts were then screwed onto the pin to secure the pin position. In order to obtain digital readings and data from the jacks, load cells were connected to each jack. The load cells used for this project were code-named PS-10 and Kyowa.

3.5.1.2 LVDT

When measuring the deflection of the specimens during the flexural bending test, it was necessary to employ equipment to obtain accurate results. Hence, LVDTs were used in this research. An LVDT, which is a type of electrical transformer used to measure linear displacement, can provide an accurate measurement of three significant figures in millimetres. The LVDT consisted of copper coils wrapped around a metallic core rod. The voltage signal in an LVDT is proportionally related to displacement. Once the LVDT was connected to a data acquisition system, called Nicolet, the LVDT displacement results were measured electronically. The only disadvantage in using an LVDT was that it could only monitor a one-dimensional displacement. Figure 3.10 shows the layout of the LVDT.

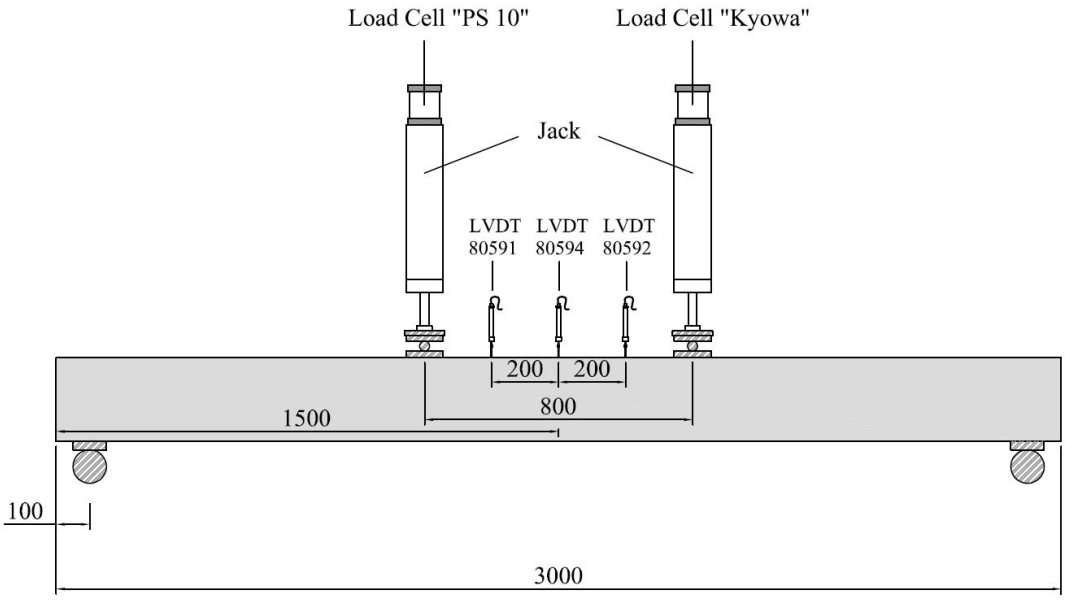

Figure 3.10: Layout of LVDT

3.5.2 Close-range photogrammetry

In this research, it was important to record the failure mode of each specimen for analysis. Prior to the testing, it had been predicted that most failures would result from the debonding of the FRP. Due to the nature of failure during the flexural bending test, it was necessary to use another type of technology to record displacement, as an LVDT can produce errors from time to time. Hence, close-range photogrammetry was introduced to capture all of the supplementary data. Photogrammetry is defined as the practice of determining the geometric properties of objects from photographic images. Cameras were used to capture the light which was reflected from reflective targets. To ensure that the reflected light was properly captured, camera flashes were used. This ensured that the reflective targets would reflect the light back to the camera lens. To increase the accuracy of results, it was necessary to place the cameras in predetermined positions so that during the analysis of the photographs, the triangulation of the targets could be ascertained properly. The photos were analysed using Australis software.

Generally, the more cameras used, the more accurate the results. Therefore, for this research, six single-lens reflex cameras were used to capture images of the specimens during the testing stage. An advantage of photogrammetry is that it can provide three-dimensional displacement, whereas LVDT can provide only one-

dimensional displacement. However, a major disadvantage of photogrammetry is that any malfunction of the cameras will compromise the accuracy of results. For this reason, the photogrammetry required lengthier preparation than would have been the case if the LVDT alone had been used. Figure 3.11 shows the placement of reflective dots for the photogrammetry.

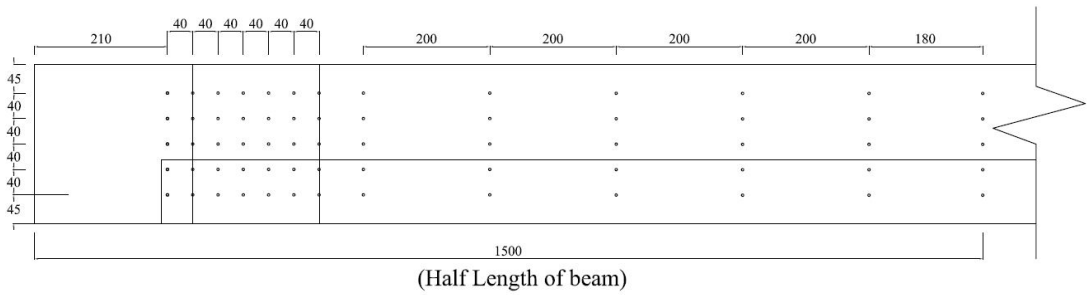

Dot Arrangement of Beam J4

Figure 3.11: Placement of reflective dots

3.5.2.1 Camera Calibration

Before setting up the equipment for photogrammetry, all cameras were calibrated to a specific focal length and shutter speed to suit the testing environment. Due to the repetitive testing required for each specimen, duct tape was applied to the camera lens to avoid the possibility of accidentally altering the focal length of the cameras. Several images were then taken from a specific distance at a calibration board prepared in advance. Images were then imported into the same software used for the data analysis. Further calibration was carried out using the software.

Once the calibration was completed, the cameras were ready to be positioned onto the camera frames. Due to the testing environment, the frames were constructed from galvanised iron pipes which were braced to minimise movement.

3.5.2.2 Reference Boards

In order for the Australis software to analyse the displacement of target points based on reference points, two reference boards were built using plywood, each with 12 reflective target points. These boards were than bolted onto a static frame, which had

to be handled with extreme caution; the slightest knock would have changed the coordinates of the target points, which would have affected the results. The coordinates of the target points on the reference boards were determined using a total station. Coordinates of all the points were then imported into the Australis software to create a coordinates file. This file was required in order to determine the position of the reflective targets during data analysis.

3.5.2.3 Reflective Target Points

The reflective target dots were cut from retro-reflective tape. Each dot measured four millimetres in diameter. Each target was positioned by hand onto the surface of the specimens in the location where the displacement information was required. These locations included the end anchorages at the mid-span, and at both ends of the FRP in a longitudinal direction. These locations were chosen as displacement information from these locations was impossible to collect via the LVDT. It was important to wear gloves while positioning the dots as human skin contains oils that might block the retro-reflective dots, which would have affected the results.

Images were to be taken during the testing at different load magnitudes until failure occurred. Since there would be movement during the bending test, these images would contain the coordinates of target points relative to the static reference boards. To analyse the images, the software would track the three-dimensional movement of the dots. Any movement of the FRP fabric, such as slippage, would be detected.

3.6 Testing Stage

The final part of the experimental program in this research was the testing stage, which involved various tests, such as the compression test, the indirect tensile test and testing the elastic modulus of the concrete cylinders. In addition to the main flexural test, a steel tensile test and FRP fabric tensile test were carried out.

3.6.1 Compression Test of Concrete Cylinders

The compression test was carried out to determine the compressive strength of the concrete. Compressive strength test results were used primarily to determine if the concrete mixture that was delivered and used, met the required specific strength of the design parameters. The compression test carried out in this project was set up in accordance with AS 1012.9–1999. The machine used to test the cylinders was a 300 tonne compression machine called MCC8. Prior to testing, the dimensions and weight of the cylinders were taken. The standard dimensions of concrete cylinders were 100 mm in diameter and 200 mm in height.

Three cylinders were tested at each stipulated day to obtain the average compressive strength of the concrete. Cylinders were tested on the third, seventh, fourteenth, twenty-first and twenty-eighth day after the concrete was poured. Compression tests were also carried out after each flexural bending test to obtain the exact compressive strength of the concrete during that period. The results are presented in Chapter 4, Section 4.1.

3.6.2 Indirect Tensile Test of Concrete Cylinders

An indirect tensile test was performed by applying the load diametrically across the circular cross-section of the concrete cylinder. The applied loading created a tensile deformation, causing the cylindrical specimen to split vertically in the same direction as the load. As with the compression test, the machine that was used to carry out the indirect tensile test was the MCC8, which was set up according to AS 1012.8–1999. Dimensions and weight were measured prior to testing. Dimensions used for this type of testing of the cylinders were to the Standard, being 150 mm in diameter and 300 mm in height. Three cylinders were used for the testing to obtain an average value. The results are presented in Chapter 4, Section 4.2.

3.6.3 Steel Tensile Test

A steel tensile test was carried out to determine the stress and strain relationship of the steel bars. Tests were carried out on the N10, N12 and N20 reinforcement bars as

well as on the W10F fitment. Tests were conducted before the steel reinforcement/cages were constructed and after the flexural test. The tensile test of the reinforcement bars was carried out before the construction of the steel cages, to check if the materials accorded with the specifications and to check the design parameters. Offcut bars that had been cut from the main rebar were tested. Some tests were carried out using the Instron tensile testing machine at Curtin University; others were sent out to an accredited external national association of testing authorities (NATA) laboratory for a full stress and stress relationship test. Appendix C shows the results supplied by the external NATA-accredited laboratory. The results of the steel tensile test are shown in Chapter 4, Section 4.4.

3.6.4 FRP Fabric Tensile Test

Tensile tests were also conducted on the FRP fabric that was used to strengthen the specimens. Ten samples were tested: five CFRP samples and five GFRP samples. Each sample was 600 mm in length and 50 mm in width. Two steel plates of 100 mm in length and 50 mm in width were clamped onto each end using epoxy resin and then allowed to cure for three days inside an oven at a temperature of 40 °C. However, the fabric itself was not covered in epoxy as only the tensile capacity of the pure fabric was needed. All the samples were prepared in the heavy testing laboratory.

3.6.5 Beam Flexural Test

The beam flexural test was the final stage of testing. 12 beams were tested in the project in an iterative procedure. Once the preparation stage was completed, the RC beam was lifted into the heavy testing area and onto the support via a forklift. The roller supports were wedged and the bearing plates were then placed on top of the support. Plaster was applied onto the face of the bearing plate before the beam was put in place. The beam was then positioned squarely, using a variety of equipment such as plum bobs and spirit levels. Two more plates were plastered and placed below the two jacks, creating a four-point bending test configuration. Prior to the start of testing, three photographs were taken for photographic and data referencing. Full flexural testing commenced by applying the loading jacks at a relatively low

load magnitude for several cycles, to allow for the uncracked stiffness of the beam to be inspected. See Chapter 5 (Section 5.3) for specific load versus time, amount of load cycles and explanations of both. Higher loads were then applied to the beam where cracks were expected to appear. A marker pen was used to draw the crack pattern on the beam. It was expected that further vertical displacement of the loading jacks would deform the concrete beam, and eventually failures such as crushing of concrete at the compression zone, tensile rupture of FRP or debonding of FRP would occur at high load magnitude.

3.7 Summary

In summary, twelve beams were constructed where ten of the beams were strengthened with CFRP and GFRP and the remaining two beams were tested as control beams. All the strengthened beams were pre-treated with scabbling before the installation of FRP. During the installation stage, it was crucial to make sure that the FRP and concrete surface is effectively bonded. These were achieved through allowing sufficient time for the primer to undergo chemical reaction and the removal of air bubbles trapped between concrete surface and FRP fabric. Post-installation was also important by ensuring the strengthened beams were fully cured to achieve complete strengthening before commencing with flexural test. The flexural test results are presented in Chapter 5.

Chapter 4: Material Testing Results

This chapter discusses the results of the tests conducted on the materials used in this research, including tests of concrete compression, indirect tensile strength, FRP fabric tensile strength and the properties of reinforcement bars. The results of these tests were used to determine the characteristics of the materials for the data analysis of the strengthened RC beams.

4.1 Concrete Cylinders Compression Test

The concrete used for this research was ordered from and delivered to Curtin University Concrete Laboratory by a commercial ready-mix supplier. The concrete specifications were of a nominal compressive strength of 40 MPa, a maximum aggregate size of 20 mm and a slump of 80 mm high. More than 60 large and small cylinders were cast and cured along with the 12 specimens. All the specimens and the RC beams were sprayed with water for a period of 28 days and covered with plastic to keep them hydrated.

As discussed in Chapter 3 (Section 3.6.1), the concrete cylinder compression test was carried out in accordance with AS 1012.9–1999. During the early stage, cylinders were tested at the designated marks of 3, 7, 14, 21 and 27 days. After carrying out each flexural bending test on the concrete beams, cylinders were then retested to determine their strength at that time. Therefore tests were carried out at marks of 60, 62, 102, 178 and 188 days. Three cylinders were tested at each ‘lot’ of days (i.e., at the 60 day mark, at the 102 day mark etc.), and mean strength was taken. Table 4.1 shows the summarised test results. The strength of the concrete gradually increased as shown in Table 4.1. There was a slight decrease at the 21 day mark, possibly due to a sampling error. However, the compressive strength continued to increase and eventually achieved the nominal strength by the twenty-eighth day. Figure 4.1 shows the increase in concrete strength over time.

Table 4.1: Summary of concrete compressive strength

Date of testing	Sample	Age (days)	Individual stress, f'cm (MPa)	Mean stress, f'cm (MPa)	Beams tested
8 March 2010	1	3	26.8	27.9 ± 1.3	
	2		27.6		
	3		29.3		
12 March 2010	1	7	35.0	33.8 ± 1.7	
	2		32.6		
19 March 2010	1	14	40.2	40.5 ± 0.9	
	2		41.5		
	3		39.8		
26 March 2010	1	21	39.3	38.9 ± 1.3	
	2		37.4		
	3		40.0		
1 April 2010	1	27	44.6	41.7 ± 2.7	
	2		39.2		
	3		41.3		
4 May 2010	1	60	47.2	44.3 ± 4.1	J2, J3
	2		46.0		
	3		39.6		
6 May 2010	1	62	49.3	46.9 ± 2.4	H2, H6, J1, J5
	2		44.6		
	3		46.9		
16 June 2010	1	102	47.7	46.9 ± 0.9	H4, H7, J4
	2		46.0		
	3		46.9		
31 Aug 2010	1	179	43.5	47.5 ± 3.5	H1, H3, H5
	2		50.0		
	3		49.1		

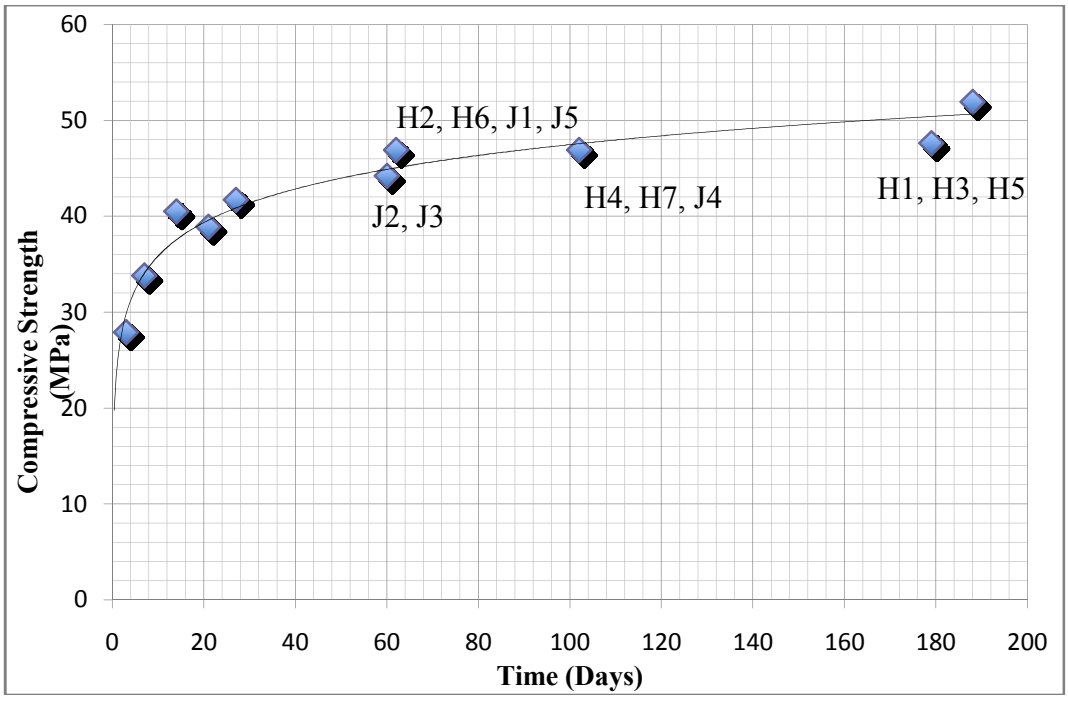

Figure 4.1: Concrete compressive strength v. time

4.2 Indirect Tensile Test/Brazilian Test

The dimensions of the concrete cylinders that were used to carry out the indirect tensile test were 150 mm in diameter and 300 mm in height. All cylinders were cast and cured by the same method used for the small cylinders and the RC beams.

The indirect tensile test was carried out in accordance with AS 1012.10–2000. Three cylinders were tested, and the mean stress computed. Tests were carried out after the flexural bending test on the RC beams. Table 4.2 shows the summary of the tensile strength of cylinders at different ages. All figures, such as load and dimensions, were taken as averages. The formulae used to compute the average tensile strength were:

$$\text{Splitting tensile strength} = \frac{2P}{\pi LD} \qquad \text{(Equation 1)}$$

where P = Load (N), L = Height of cylinder (mm), D = Diameter of cylinder (mm)

Table 4.2: Summary of concrete cylinders tensile strength

Date of test	Sample	Beams tested	Age (days)	Diameter (mm)	Average height (mm)	Load, P (kN)	Tensile strength (MPa)	Mean tensile strength (MPa)
4 May 2010	1	H2, H6, J1, J2, J3, J5	60	149.6	298	228.8	3.3	3.3 ± 0.1
	2			149.8	297	234.2	3.4	
	3			148.6	298	226.4	3.3	
18 June 2010	1	H4, H7, J4	104	147.9	298	227.7	3.3	3.7 ± 0.4
	2			147.6	298	279.2	4.0	
	3			147.4	300	256.4	3.7	
1 Sept 2010	1	H1, H3, H5	181	148.2	300	273.3	3.9	4.1 ± 0.2
	2			148.5	303	297.4	4.2	
	3			147.2	303	288.4	4.1	

4.3 FRP Fabric Tensile Test

As discussed in Chapter 3, fabric specimens were glued with steel plates to prevent the jaws tearing the fabric apart. Although results from the tensile test were consistent, they differed significantly from the indications in the technical data sheet (see Appendix A). This may have been due to improper storage of the FRP and/or the expiry of its shelf life. Another factor that may have affected the results is the failure mode. Ideally, when the FRP fabric fails, it should fracture apart with a uniform separation perpendicular to its length. However, the failure mode in the test conducted was on an inclined separation. Unlike steel, the failure mode of the FRP was a brittle failure rather than a ductile failure. The aforesaid factors might explain why the tensile capacity of the FRP differed from the specifications. See Figure 4.2 for photos of the GFRP tensile test setup and the failure of the GFRP. Tables 4.3 and 4.4 summarise the tensile strengths of the FRP fabric with all samples being 300 mm in length and 50 mm in width. All the fabric were cut to the aforementioned size using rotary cutter while the thickness of fabric were measured using vernier caliper.

Table 4.3: Average tensile strength of carbon fabric

Sample	Material	Measured thickness (mm)	Area (mm^2)	Load rate (kN/min)	Load (kN)	Stress (MPa or N/mm^2)
1	Carbon	0.14	7	5	15.6	2229
2	Carbon	0.14	7	3	14.1	2014
3	Carbon	0.14	7	3	14.9	2129
4	Carbon	0.14	7	2	16.1	2300
5	Carbon	0.18	9	2	14.4	1600
					Mean tensile strength	2054 ± 276

Table 4.4: Average tensile strength of glass fabric

Sample	Material	Measured thickness (mm)	Area (mm^2)	Load rate (kN/min)	Load (kN)	Stress (MPa or N/mm^2)
1	Glass	0.46	23	5	19.0	826
2	Glass	0.40	20	3	18.7	935
3	Glass	0.40	20	3	20.2	1010
4	Glass	0.44	22	2	21.6	982
5	Glass	0.44	22	2	20.3	923
					Mean tensile strength	935 ± 70

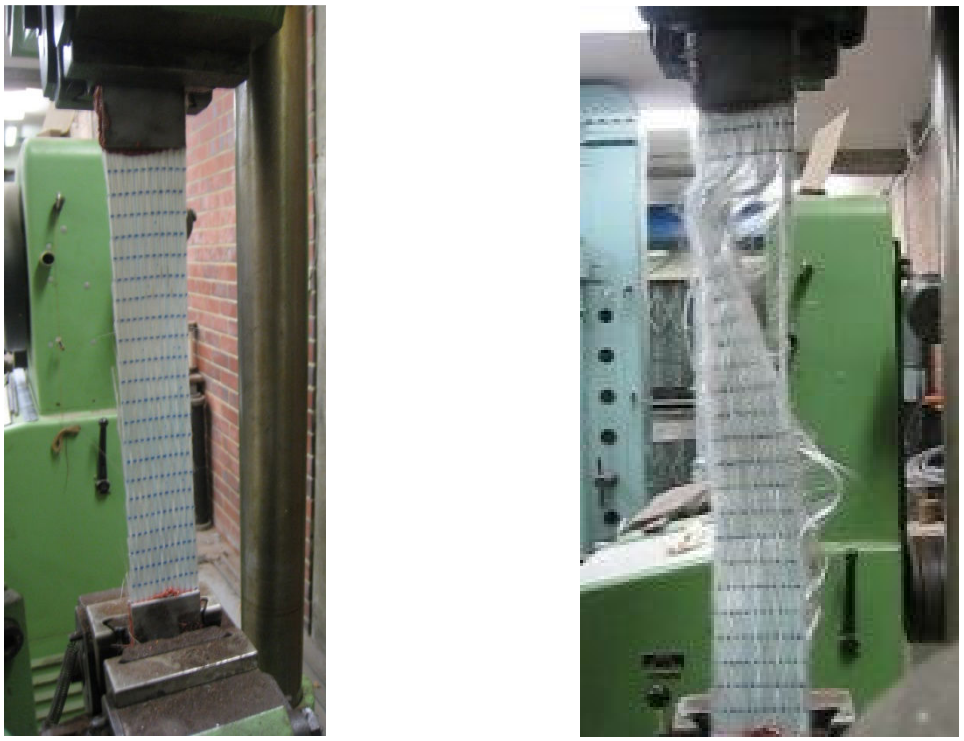

Figure 4.2: Setup of GFRP tensile test and failure of GFRP

4.4 Properties of Reinforcement Bars

The reinforcement bars were tested prior to beam fabrication. Sample bars were tested at the heavy testing laboratory using the Instron machine. Certain offcuts of the reinforcement bars for the beams were tested by Melbourne Testing Services (MTS) to determine the tensile properties of the reinforcement bars. The reinforcement bars tested by MTS using the TE machine were in accordance with AS 1391–2007. Appendix C shows the sample stress versus strain profile of the bars N10, N12 and N20. The specimen details and tensile properties of the bars are tabulated in Table 4.5. Figure 4.3 shows sections of the beams exposing the locations of the steel bars.

Table 4.5: Summary of properties of reinforcement bars

Beam	N10 bars	Tensile strength (MPa)	Yield strength (MPa)	N12 bars	Tensile strength (MPa)	Yield strength (MPa)	N20 bars	Tensile strength (MPa)	Yield strength (MPa)
H6	#7	670	567	#11	699	535	-	-	-
	#8	674	566	#12	700	537	-	-	-
H2	-	-	-	#3	689	534	3	666	579
	-	-	-	#4	691	535	4	666	577
J4	#11	677	567	#15	698	535	-	-	-
	#12	680	569	#16	688	538	-	-	-
H4	#3	670	551	#7	677	540	-	-	-
	#4	666	548	#8	690	530	-	-	-
H7	#9	673	555	#13	683	534	-	-	-
	#10	671	566	#14	686	536	-	-	-
H5	#5	668	568	#9	691	542	-	-	-
	#6	673	559	#10	693	531	-	-	-
H3	#1	674	560	#5	683	533	-	-	-
	#2	677	567	#6	688	544	-	-	-
H1	-	-	-	#1	687	545	1	658	568
	-	-	-	#2	690	530	2	657	562
J3	N/A	665	550	N/A	701	550	-	-	-
	N/A	665	550	N/A	701	550	-	-	-
J2	N/A	665	550	N/A	701	550	-	-	-
	N/A	665	550	N/A	701	550	-	-	-
J5	N/A	665	550	N/A	701	550	-	-	-
	N/A	665	550	N/A	701	550	-	-	-
J1	N/A	665	550	N/A	701	550	-	-	-
	N/A	665	550	N/A	701	550	-	-	-

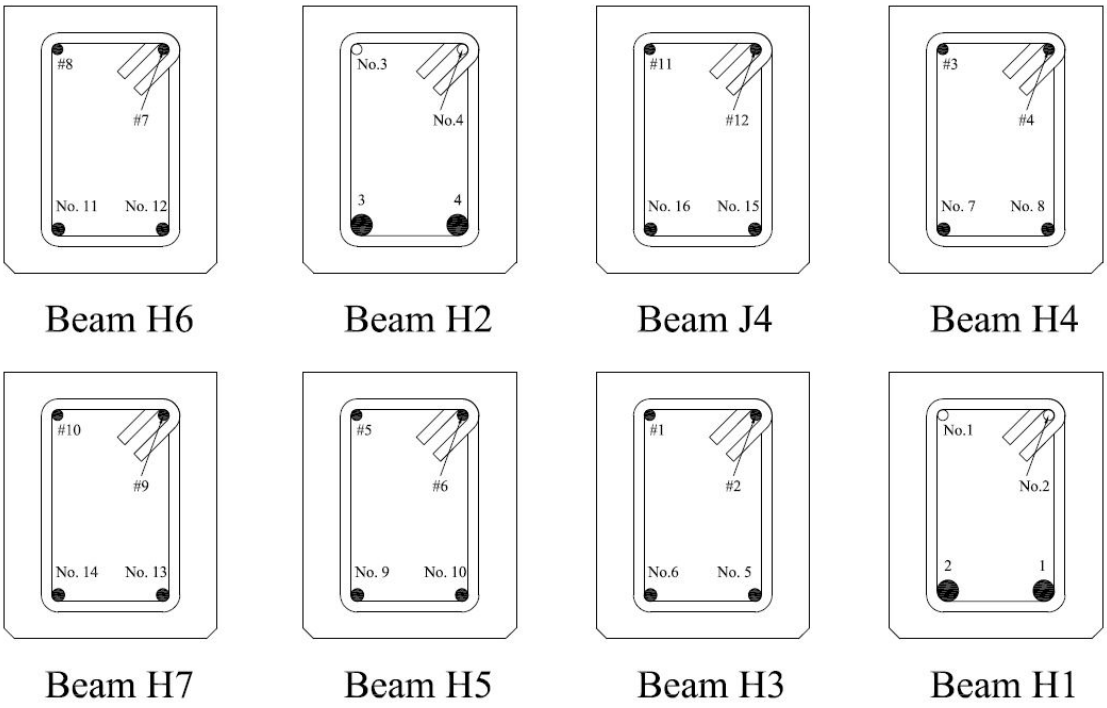

Figure 4.3: Sections of beams showing the locations of the steel bars

Chapter 5: Beam Flexural Testing Results

5.1 Presentation of Results

In this chapter, the experimental results are presented for the 12 beams described in Chapter 3. Discussion of individual results is provided in Section 5.3. This presentation of results commences with the lower control beam H6 and the upper control beam H2, followed by all of the GFRP-strengthened and CFRP-strengthened beams. The order of presentation of the results is shown in Table 5.1.

Table 5.1: Order of presentation of results

Test no.	Beam	Beam description	Tester
1	H6	Lower control beam	Hiew Kee Hon
2	H2	Upper control beam	Hiew Kee Hon
3	J4	GFRP-strengthened beam with U-shaped anchorages	Hiew Kee Hon
4	H4	GFRP-strengthened beam with V-shaped anchorages	Hiew Kee Hon
5	H7	GFRP-strengthened with U-shaped mechanical anchorages	Hiew Kee Hon
6	H5	Hybrid FRP-strengthened beam with no anchorages	Hiew Kee Hon
7	H3	Hybrid FRP-strengthened beam with V-shaped anchorages	Hiew Kee Hon
8	H1	GFRP-strengthened beam with no anchorage; another layer of GFRP strengthening on compression zone	Hiew Kee Hon
9	J3	CFRP-strengthened with U-shaped anchorages	Jovanco Domazetoski
10	J2	CFRP-strengthened with V-shaped anchorages	Jovanco Domazetoski
11	J5	CFRP-strengthened with V-shaped anchorages on entire length	Jovanco Domazetoski
12	J1	CFRP-strengthened with V-shaped anchorages on entire length	Jovanco Domazetoski

5.2 Loading Method

Each specimen was loaded from datum to failure throughout the entire testing stage. At the initial stage, specimens were loaded to a particularly low magnitude, ranging from two to eight kN to ensure that the specimen did not crack. This was particularly the case for the unstrengthened control beams, which were likely to start exhibiting cracks at low magnitude. The magnitude and number of cycles varied for each specimen. The relationship between load and time was plotted for each specimen. This relationship is shown at the end of the discussion for each specimen. Each figure shows the entire loading process from datum until failure and indicates the number of cycles repeated for each loading magnitude.

5.3 Beam Test Results

The beam flexural test results indicate the gain in flexural strength of the post-strengthened concrete beams with externally bonded FRP. The flexural tests are summarised in Table 5.2. The table compares the theoretical and experimental ultimate load with the sample calculation for the theoretical ultimate load included in Appendix F. The theoretical calculations are based on constructed beam sections.

Table 5.2: Beam flexural test results

Beam	Theoretical ultimate load (kN)	Experimental ultimate load (kN)	Ratio of Theoretical/Experimental Ultimate Load
H6	27.0	31	0.87
H2	67.3	67	1.0
J4	82.3	84	0.98
H4	82.2	82	1.0
H7	83.4	78	1.07
H5	58.6	64	0.92
H3	59.7	64	0.93
H1	78.4	80	0.98
J3	70.0	67	1.04
J2	70.0	74	0.95
J5	71.0	79	0.90
J1	70.0	78	0.90

5.3.1 Specimen H6

Specimen H6 was tested as a lower control beam. As H6 was a typical RC beam, the expected failure mode for Specimen H6 was the yielding of tensile steel followed by the failing of the beam in a ductile manner. Specimen H6 was initially loaded to 6 kN for two cycles and then loaded up to 8 kN. It was then loaded up to 16 kN for three cycles and then eventually up to yielding load, which was 25 kN. The loading jack was then released back to 8 kN for another cycle to check whether yielding load has achieved, and it was then reloaded until failure. All loading cycles for Specimen H6 are illustrated in Figure 5.1.

The first sign of cracking appeared at a load magnitude of 6 kN near the mid-span of the beam. As mentioned in Chapter 2 (Section 2.2), these cracks, known as flexural cracks, emanated upwards. The hairline cracks at this stage were so fine that a crack-detection microscope was needed to measure the crack width (see Figure 5.3). The crack width at that time was about 0.5 mm. With progressive loading, the cracks grew wider to measure about 1.0 to 2.0 mm. After reaching the yielding load of 25 kN, the internal tensile rebar started to exhibit plastic deformation. This is shown in the load-deflection graph in Figure 5.2 where the gradient of slope after 25 kN is less steep than the gradient at earlier loadings. Subsequently, the beam began to exhibit concrete compression failure at the mid-span of the compression zone (Figure 5.4). Further loading caused the tensile reinforcement to fracture and eventually fail. This is shown in Figures 5.5 and 5.6.

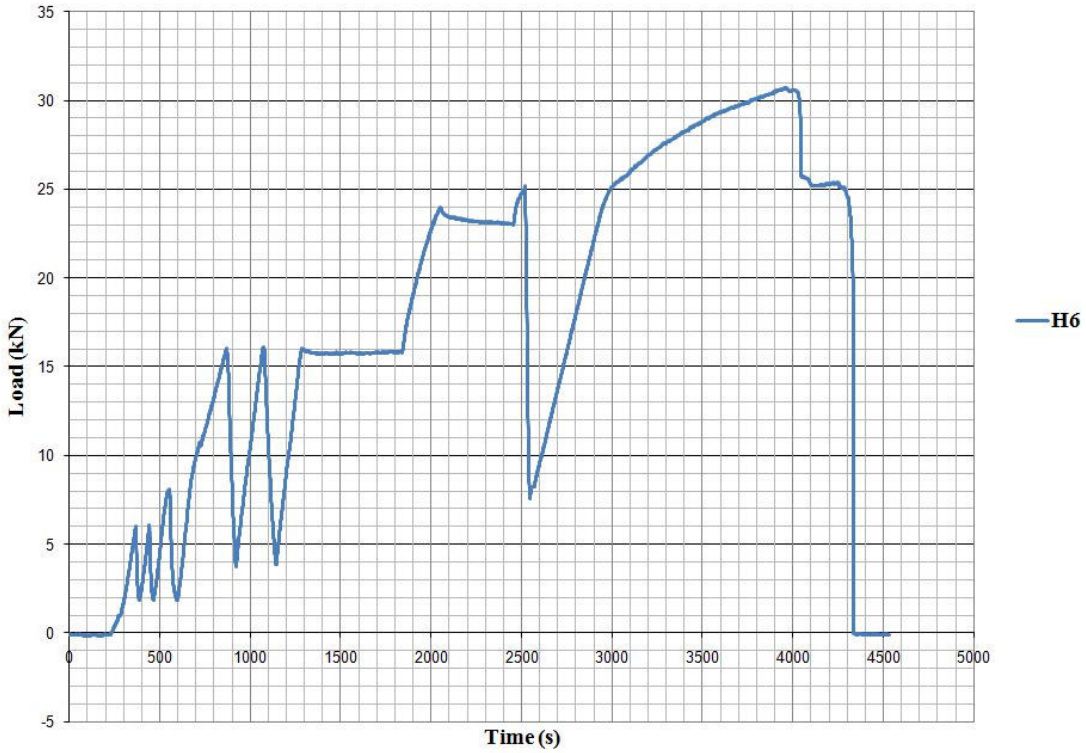

Figure 5.1: Loading cycles for Specimen H6

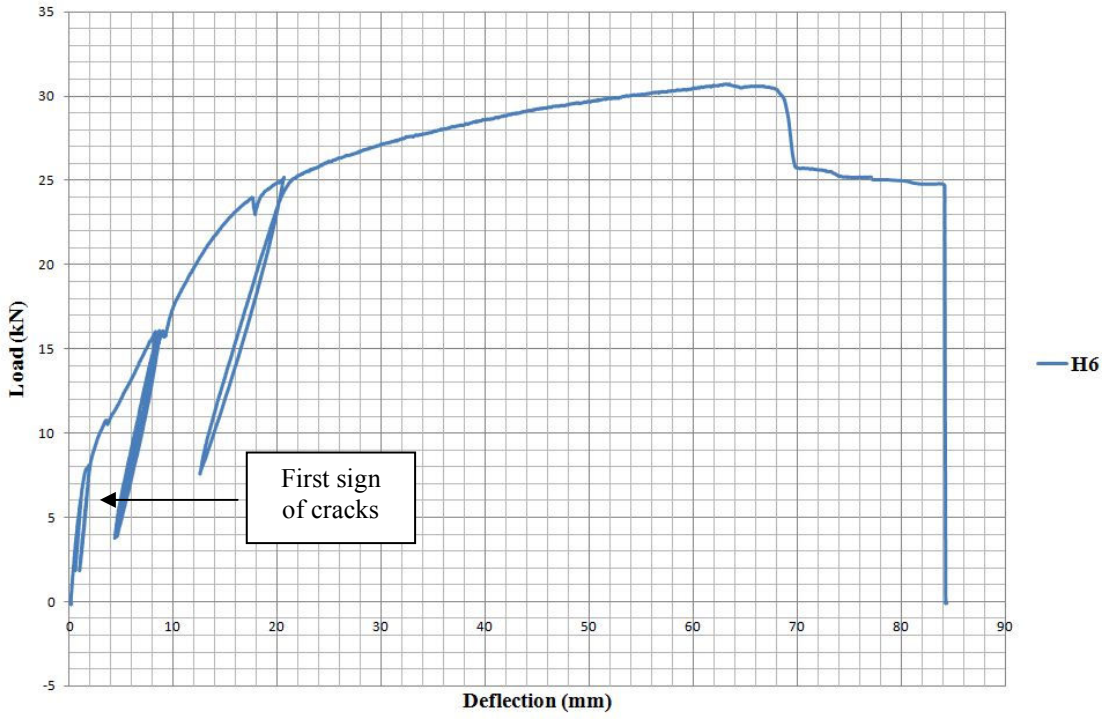

Figure 5.2: Load v. deflection graph for Specimen H6

Figure 5.3: Cracks in Specimen H6 sighted using crack-detection microscope

Figure 5.4: Concrete compression, Specimen H6

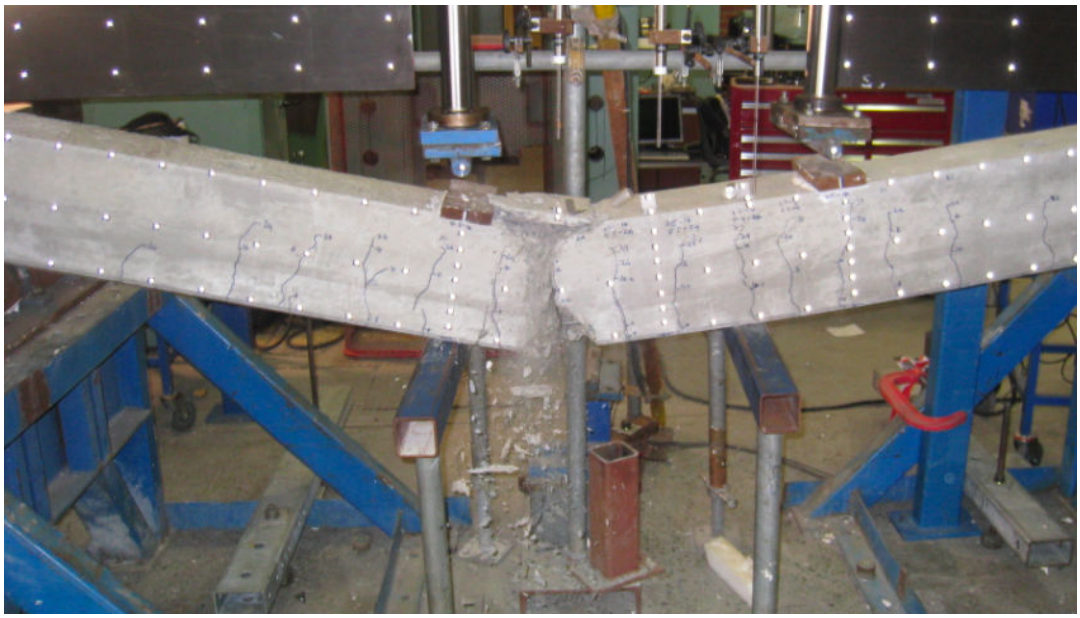

Figure 5.5: Total failure of Specimen H6

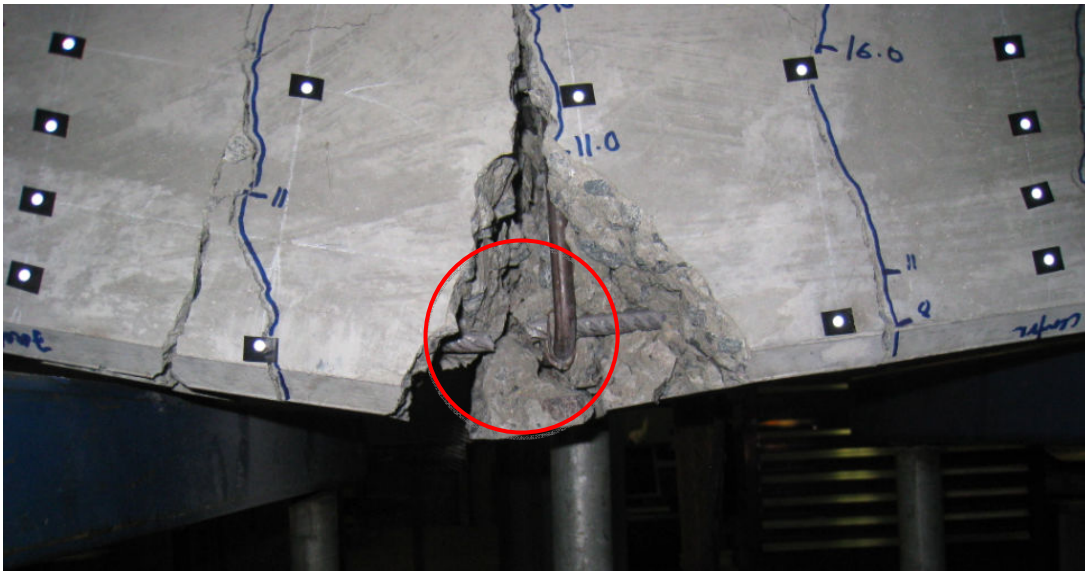

Figure 5.6: Tensile reinforcement fracture, Specimen H6

5.3.2 Specimen H2

Specimen H2, which was not strengthened with FRP, was tested as an upper control beam. Since it was an unstrengthened control beam, Specimen H2 was initially loaded to 6 kN for three cycles as shown in Figure 5.7. The first sign of cracking occurred at a load magnitude of 8 kN; the cracks were about 0.3 mm, which widened further with the increase in load magnitude. The beam ultimately failed at 66 kN. The first noticeable failure of Specimen H2 was the crushing of the concrete at the compression zone. The entire beam then started to buckle laterally, which was

unexpected. For this reason, after the completion of the flexural, test the beam was sawn in half to check the steel bar location. As shown in Figure 5.9, the two N20 tensile reinforcements and the two N10 compressive reinforcements were located at different depths, causing the beam to produce an unequal neutral axis. This is shown by the shaded area in Figure 5.9. The shaded area contained more concrete and therefore a greater compressive force with which to resist greater tensile force. This caused the load magnitude to be distributed towards the shaded area, which caused the entire beam to buckle laterally during the flexural test. Figure 5.10 shows only one buckled compressive reinforcement bar visible, as the other compressive reinforcement is further down. Figure 5.8 shows the load versus deflection graph for Specimen H2 during the flexural bending test. The beam deflected up to 22 mm upon reaching the peak load. The beam then continued to sustain the load while deflecting up to 30 mm. Meanwhile, concrete crushing and buckling of the compressive reinforcement bar occurred. With the further vertical displacement that came from the loading jacks, the beam continued to deflect and eventually failed.

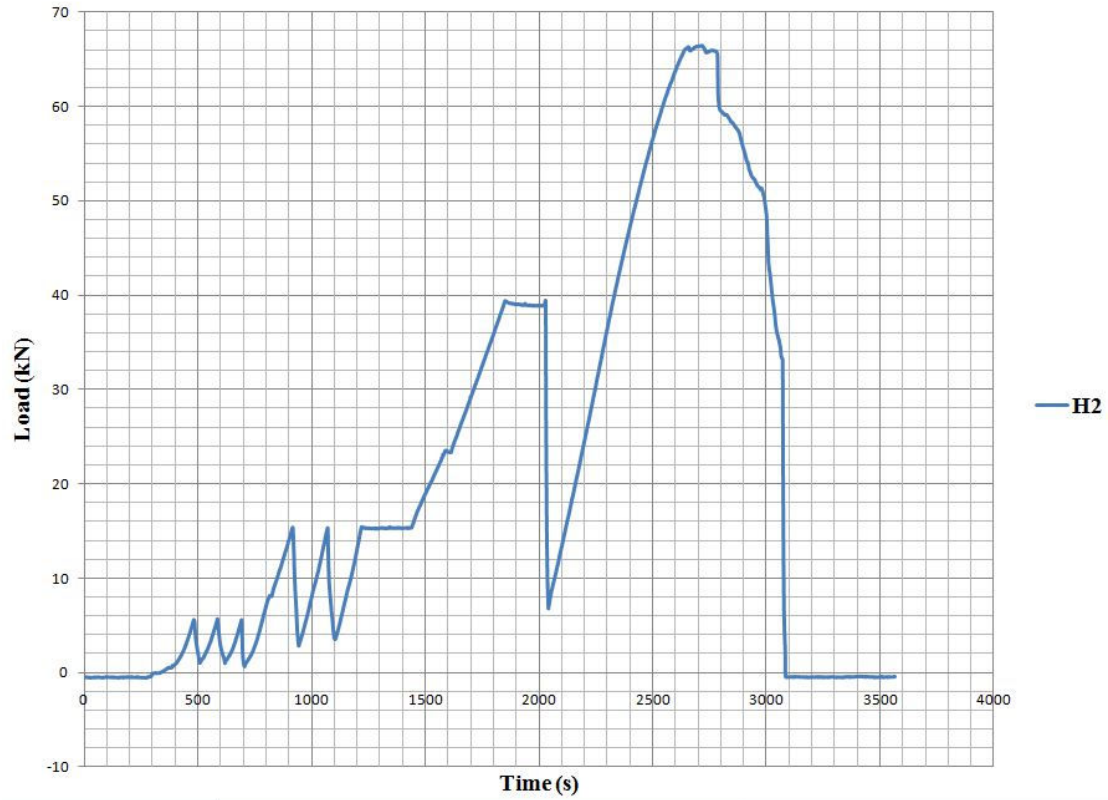

Figure 5.7: Loading cycles for Specimen H2

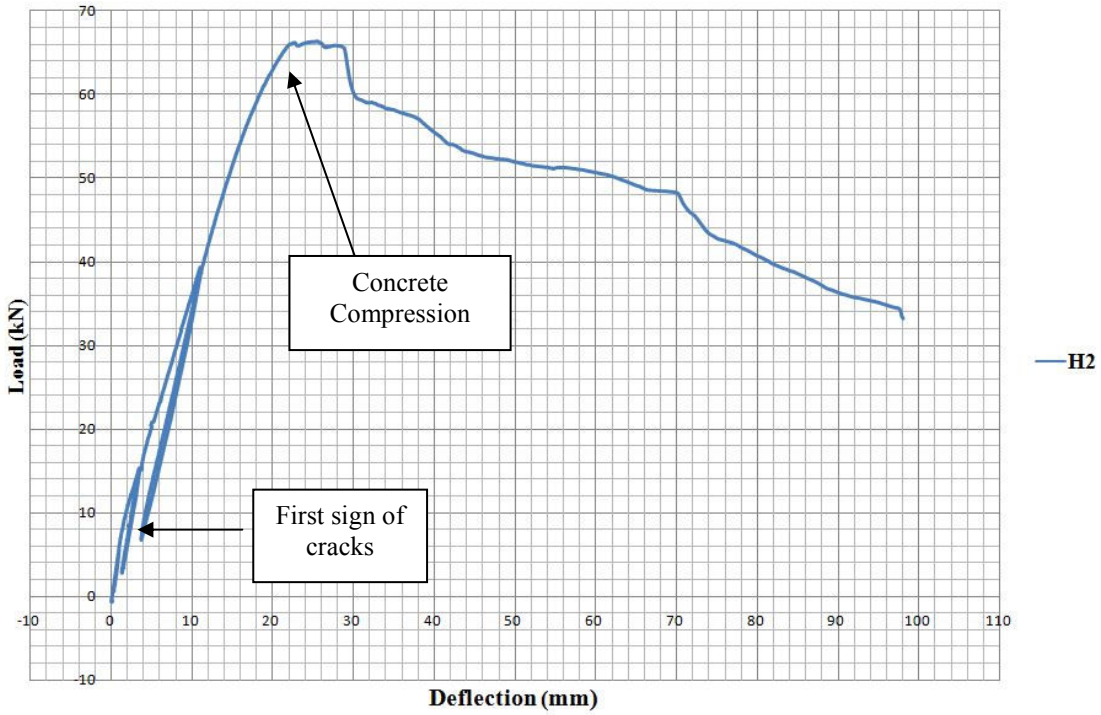

Figure 5.8: Load v. deflection graph for Specimen H2

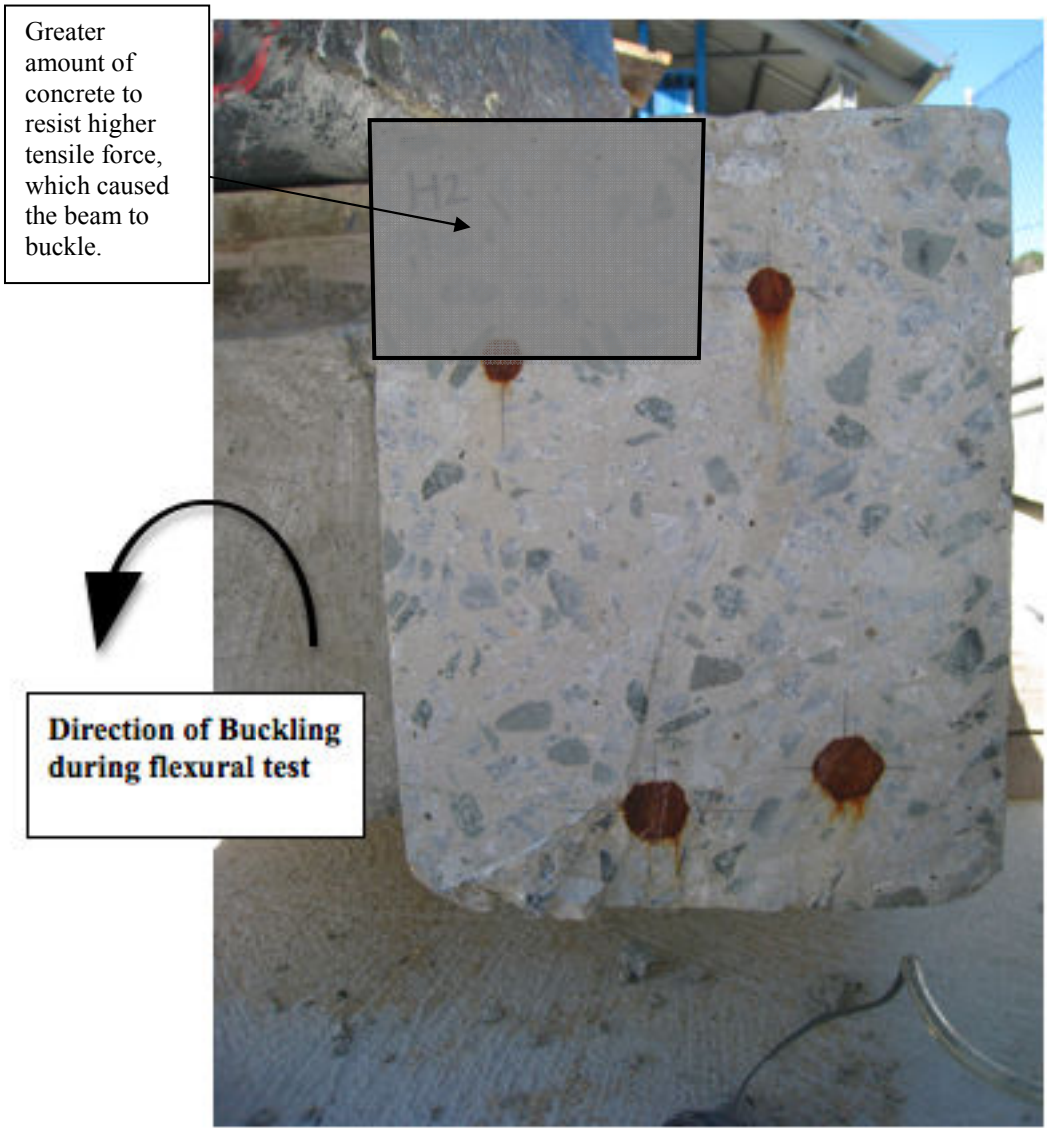

Figure 5.9: Uneven steel positioning in Specimen H2

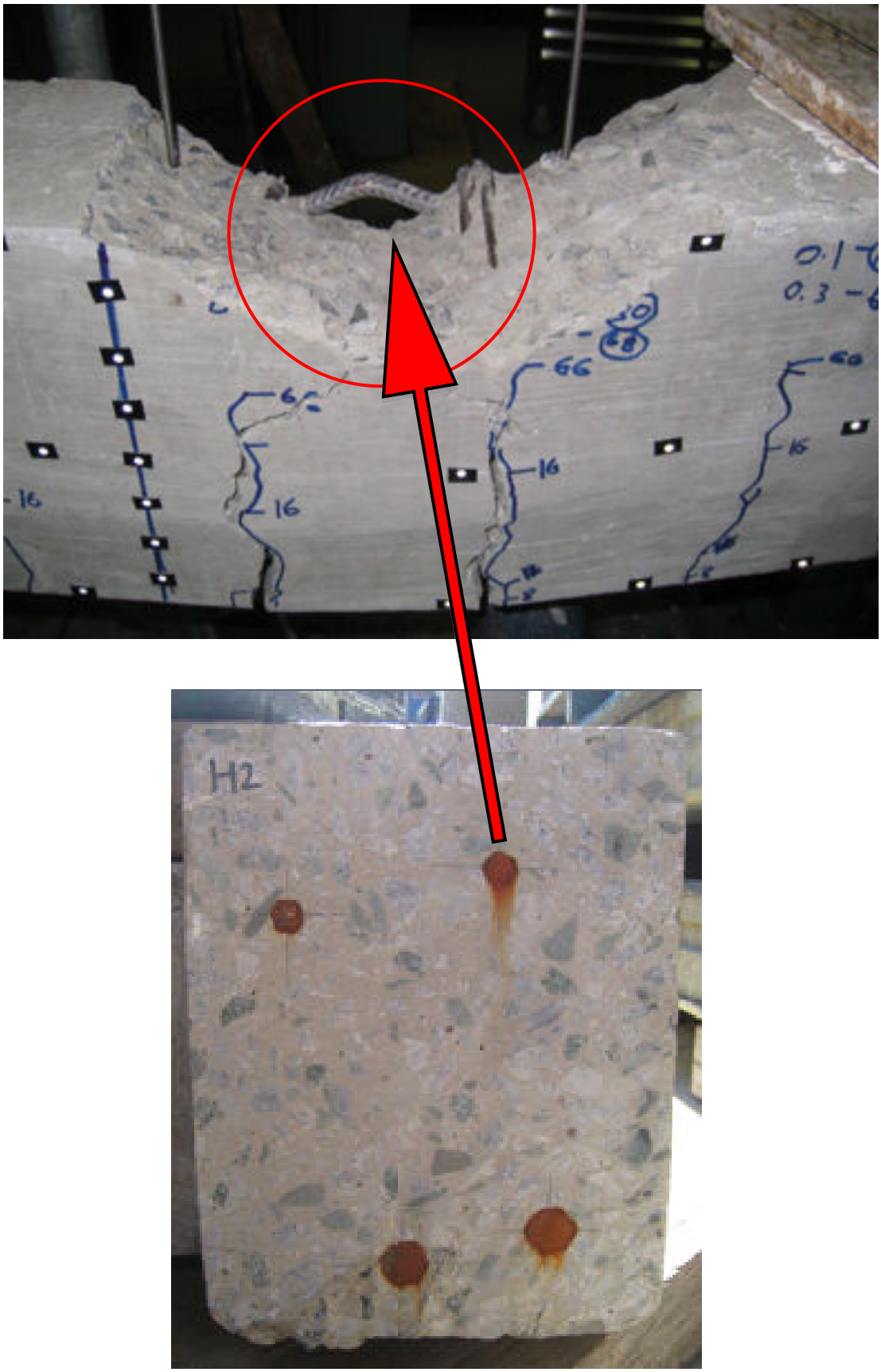

Figure 5.10: Buckling of compressive reinforcement, Specimen H2

5.3.3 Specimen J4

Specimen J4 was strengthened with three layers of GFRP with a typical U-shaped anchorage at each end (the end anchorages). As usual, the beam was loaded for several cycles at the initial testing stage. The first sign of cracks occurred at the 33 kN load, with more cracks showing at 40 kN and above. Shear cracks also appeared near the end support of the beam at a load magnitude of 40 kN, as shown in Figure 5.13. Specimen J4 continued to sustain loading up to 82 kN, when the primary failure occurred in the compression zone of the beam at mid-span where the concrete appeared to undergo concrete crushing; this is shown in Figure 5.14. Meanwhile, no sign of tensile rupture or debonding of the GFRP was detected. With further vertical displacement from the loading jack, the tensile capacity of the GFRP was fully utilised. A 'tickling' sound was heard, and the GFRP at the tension face fractured due to tensile rupture. The end anchorage exhibited shear failure (Figure 5.15) and eventually debonded (Figure 5.16). Figure 5.12 shows the load-deflection graph for Specimen J4, demonstrating that the specimen had a brittle failure as the load decreased rapidly after the concrete-crushing failure. Figure 5.11 illustrates the loading cycles for Specimen J4.

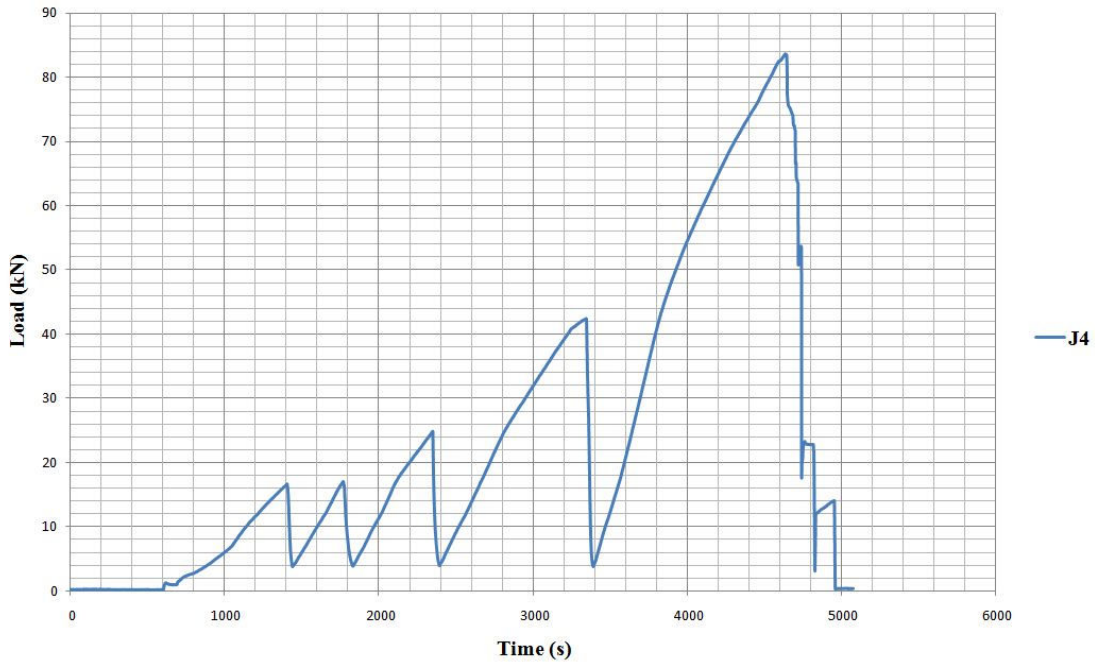

Figure 5.11: Loading cycles for Specimen J4

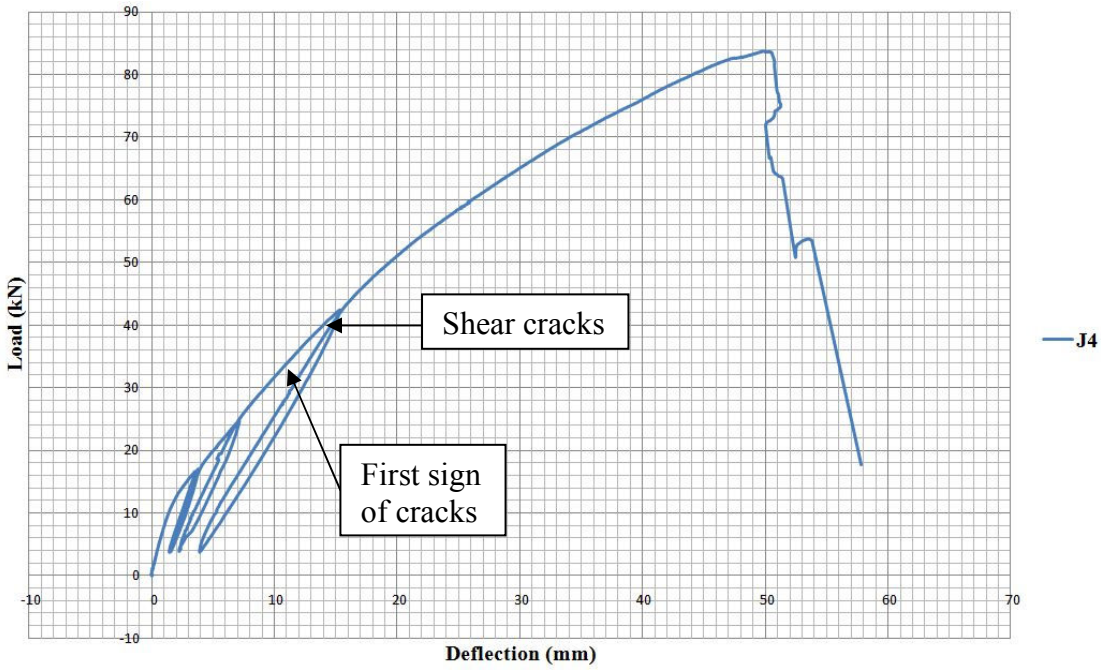

Figure 5.12: Load v. deflection graph for Specimen J4

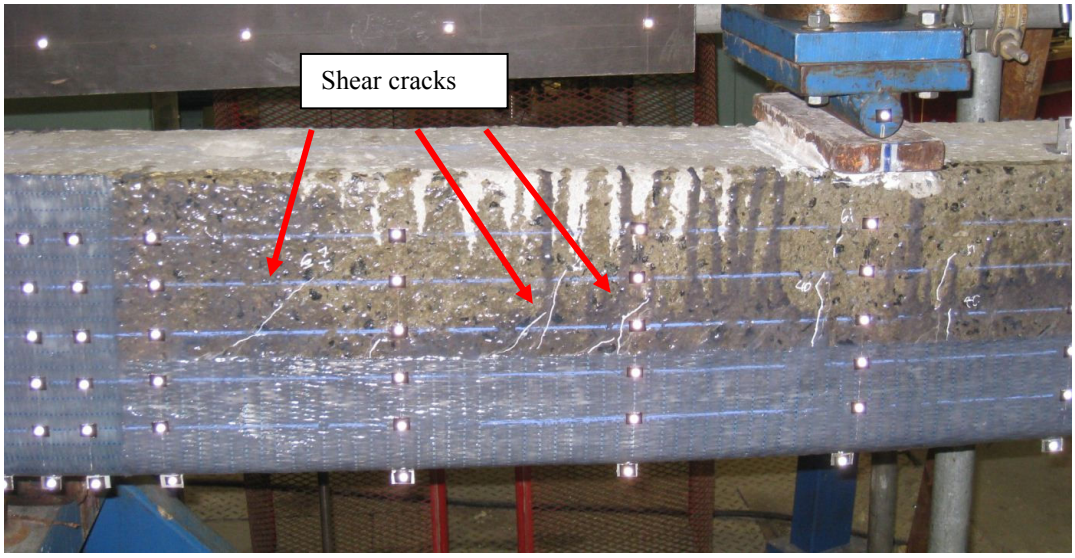

Figure 5.13: Shear cracks, Specimen J4

Figure 5.14: Concrete crushing at compression zone followed by debonding of GFRP, Specimen J4

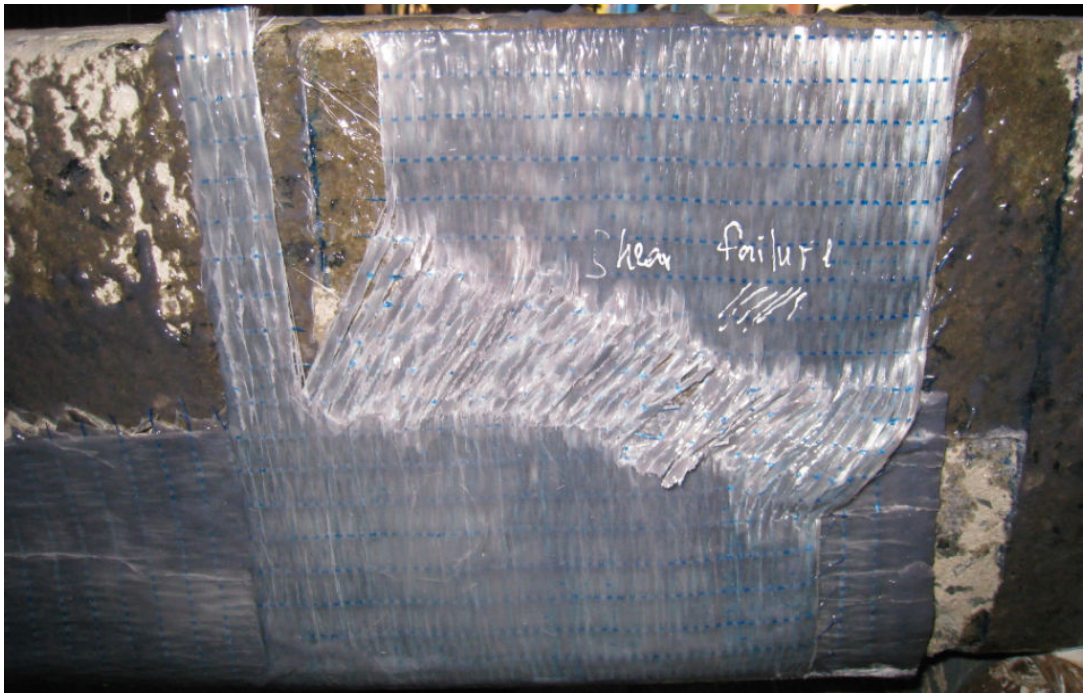

Figure 5.15: Shear failure at end anchorage, Specimen J4

Figure 5.16: Debonding of end anchorage, Specimen J4

5.3.4 Specimen H4

Specimen H4 was strengthened with three layers of GFRP on the tension face and V-shaped anchorages at each end. The beam was loaded for several cycles: 16 kN for two cycles, 24 kN for one cycle and 40 kN for one cycle, and it was then loaded until failure. The loading cycles for Specimen H4 are shown in Figure 5.17. As shown in Figure 5.18, the beam deflected constantly with increased load magnitude. The first signs of cracking occurred at the mid-span area at a load of 24 kN. With further loading, more cracks appeared. Shear cracks appeared near the end support of the beam at 54 kN; all tended to crack towards the position of the loading jack and extended to about three-quarters of the depth of the beam. This is shown in Figure 5.19. Upon reaching the peak load of 82 kN, the concrete at the mid-span of the compression zone started to fail due to concrete crushing. Figure 5.20 shows the compressive reinforcement exposed due to concrete crushing. However, the GFRPs were so well bonded that neither the GFRP at the end anchorages nor the GFRP at the tension face debonded. With further vertical displacement from the jacks, the beam continued to sustain the load with the help of the bonding of the GFRP. Meanwhile, the GFRP was experiencing its ultimate tensile stress as a 'tickling' sound was heard everywhere with the load decreasing. When the load dropped back

to 71 kN at a deflection of 68 mm, both ends of the GFRP at the tension face started to debond. However, the end anchorages prevented this from happening. Figure 5.21 shows the shear failure of the end anchorage where it was being stretched by the GFRP at the tension face but the anchorage was still intact. Total failure happened at a load of 50 kN when the GFRP fractured at mid-span due to tensile rupturing with a sudden brittle failure. After the flexural test, the fabric was cut away using an angle grinder to inspect the interior damage to the beam. Figure 5.22 shows the interior damage to the beam after the test; nearly all of the concrete at the tension face was damaged. Figure 5.23 shows how well the epoxy bonded the GFRP to the concrete surface; some concrete can still be seen where it adhered to the surface of the GFRP.

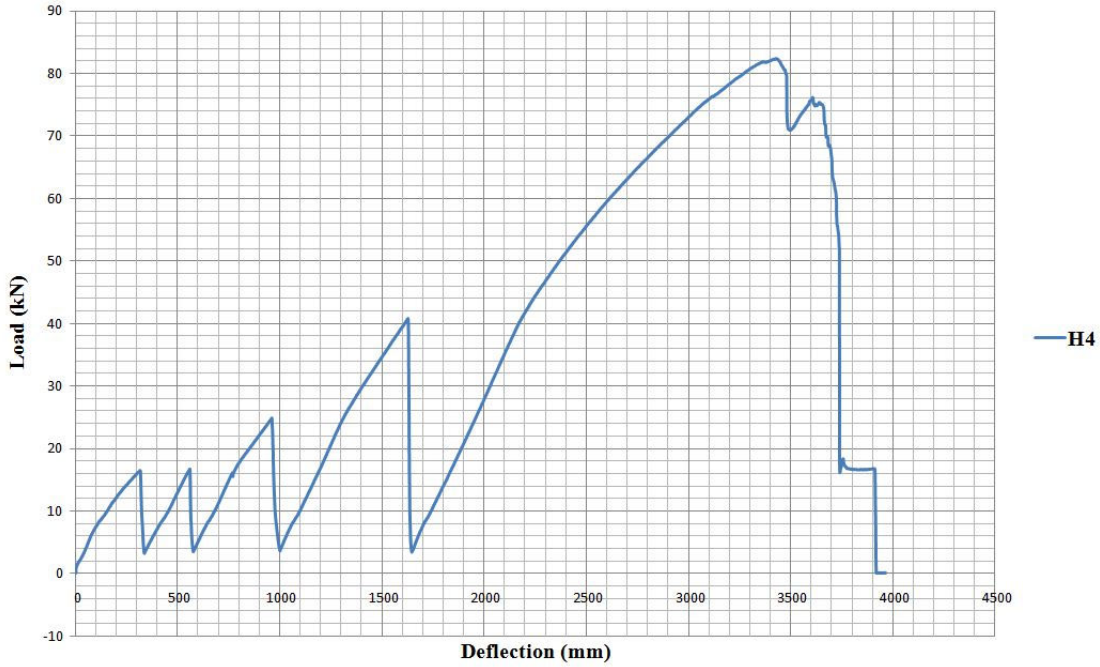

Figure 5.17: Loading cycles for Specimen H4

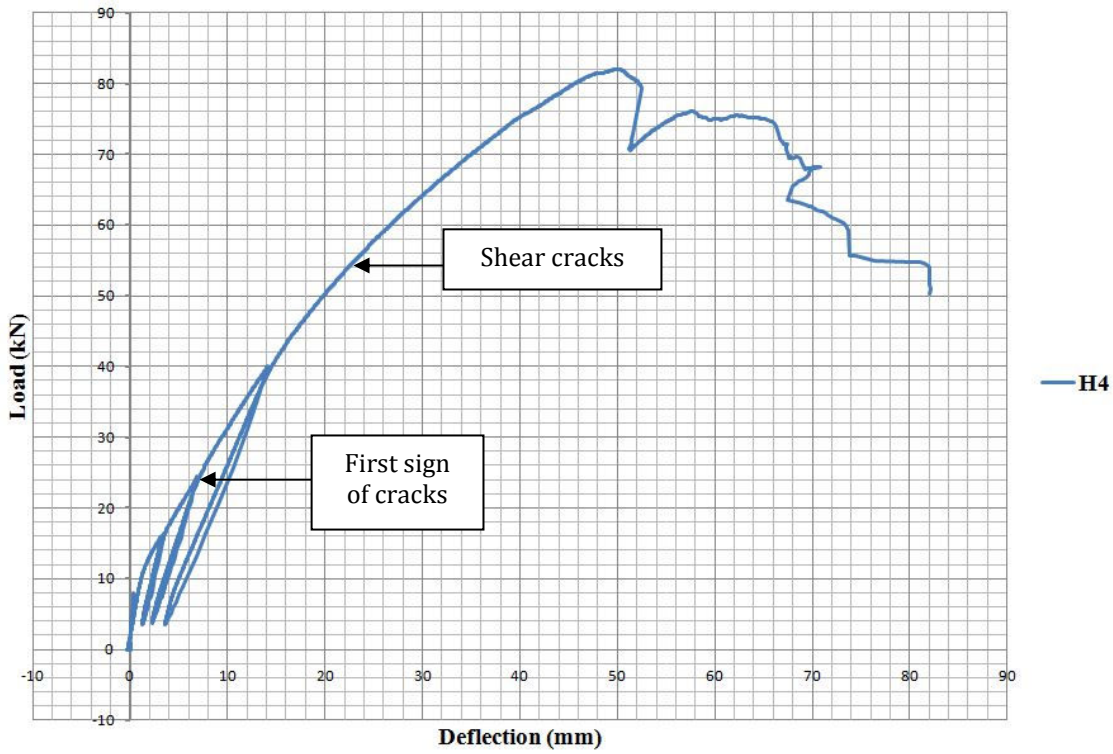

Figure 5.18: Load v. deflection graph for Specimen H4

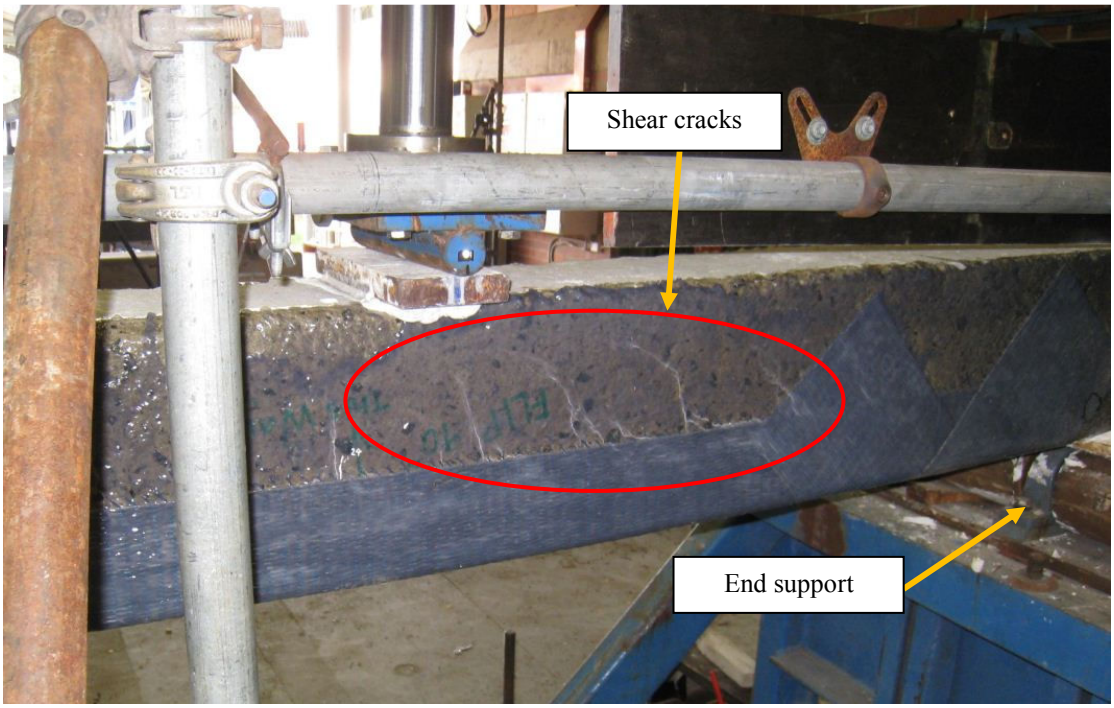

Figure 5.19: Shear cracks near the end support of Specimen H4

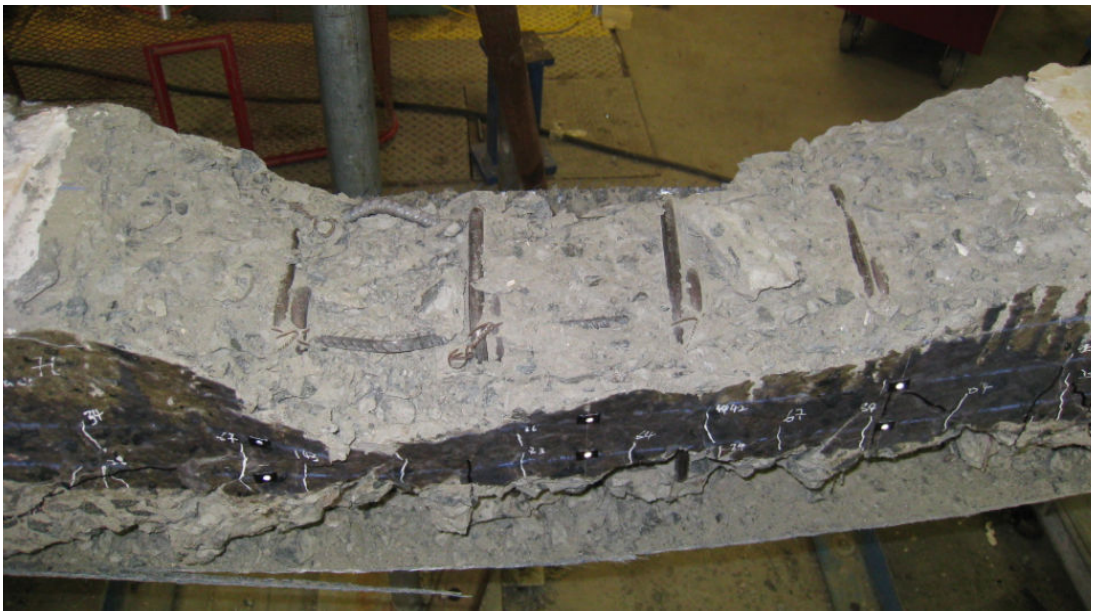

Figure 5.20: Compressive reinforcement exposed due to concrete crushing and spalling, Specimen H4

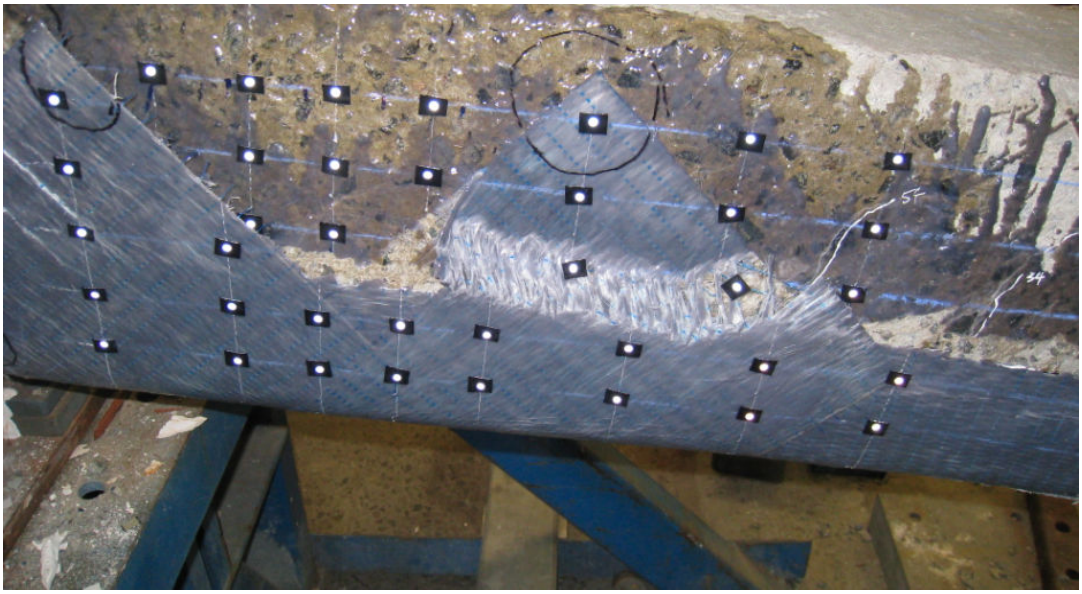

Figure 5.21: Shear failure of end anchorage, Specimen H4

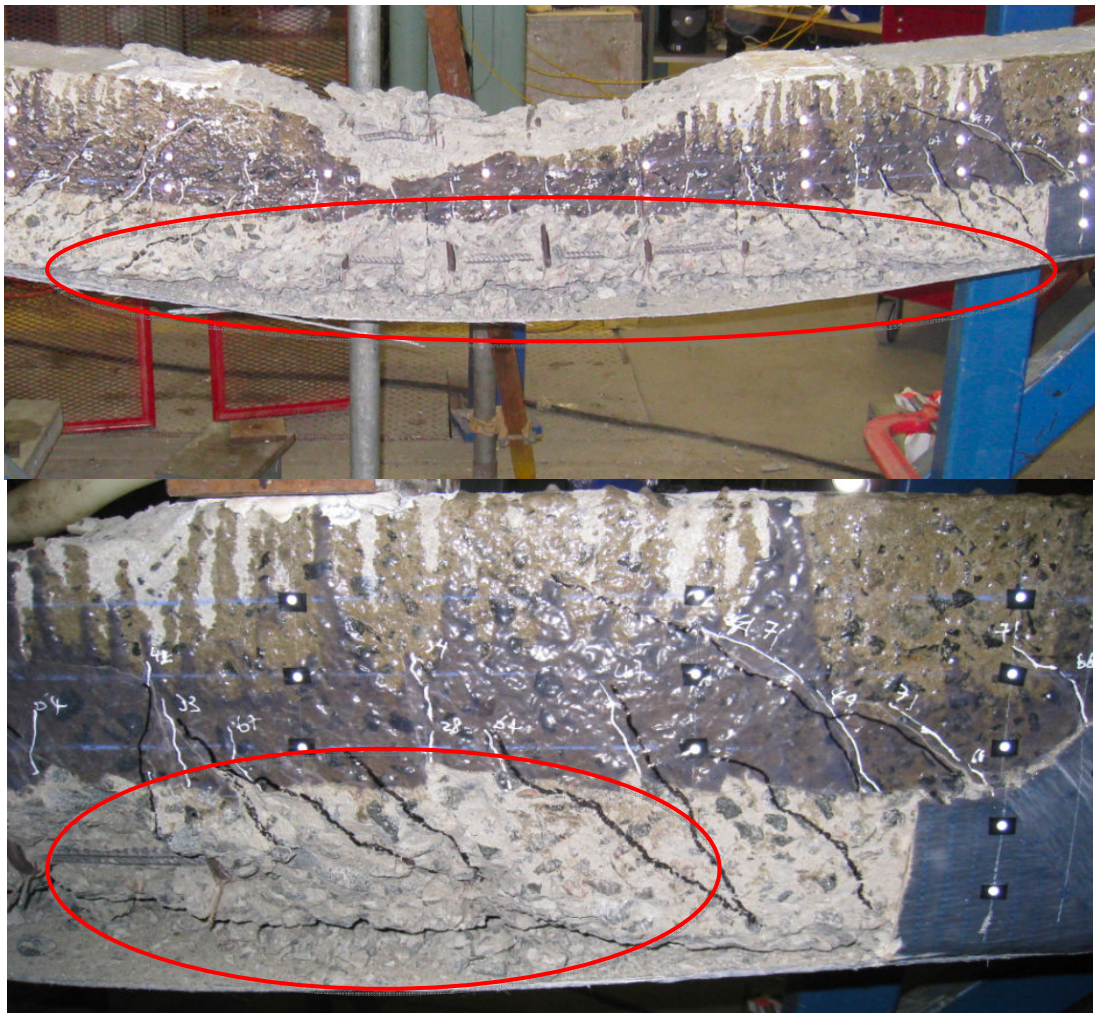

Figure 5.22: Interior damage to Specimen H4

Figure 5.23: Concrete still adhered to the GFRP surface, Specimen H4

5.3.5 Specimen H7

Specimen H7 was strengthened with GFRP and was the only specimen where a mechanical strengthening method was used to install the end anchorages onto the beam. Since the beam was wrapped with GFRP to a height of 100 mm from the soffit, cracks were not visible at low load magnitude. Cracks became visible at 24 kN as they propagated above the GFRP zone. Shear cracks started to appear at 34 kN. The crack pattern is shown in Figure 5.26 and Figure 5.27. The first sign of failure started with concrete compression at 78 kN, which was also the ultimate load. The load started to drop rapidly with major failure from the crushing of the concrete. Meanwhile, the GFRP held onto the beam with no signs of debonding. With further vertical displacement from the loading jack, the GFRP started to undergo ultimate tensile stress at 46 mm deflection. The first major failure of the GFRP was the tensile rupture of the GFRP from the side, as shown in Figure 5.28. With further displacement, the beam eventually failed with debonding of the steel plate anchorage (Figure 5.29). Inspection after the flexural test showed that the compressive reinforcement had buckled, as shown in Figure 5.30. In conclusion, the beam failed with concrete crushing failure followed by debonding of the GFRP. The load versus deflection graph for Specimen H7 is shown in Figure 5.25. Figure 5.24 shows the loading cycles for Specimen H7.

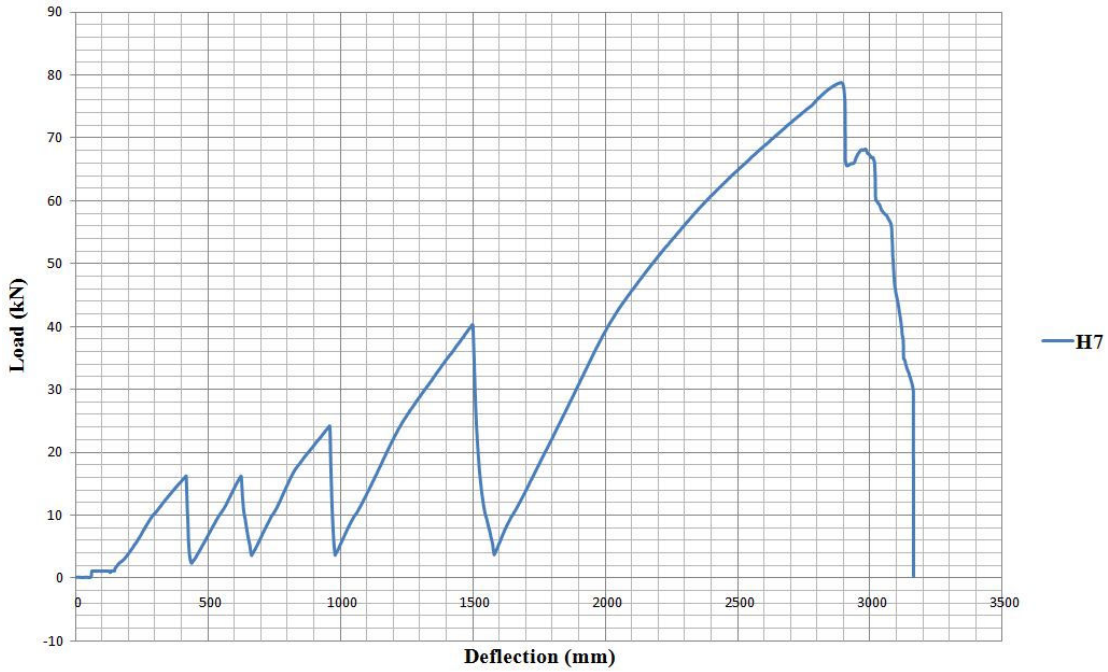

Figure 5.24: Loading cycles for Specimen H7

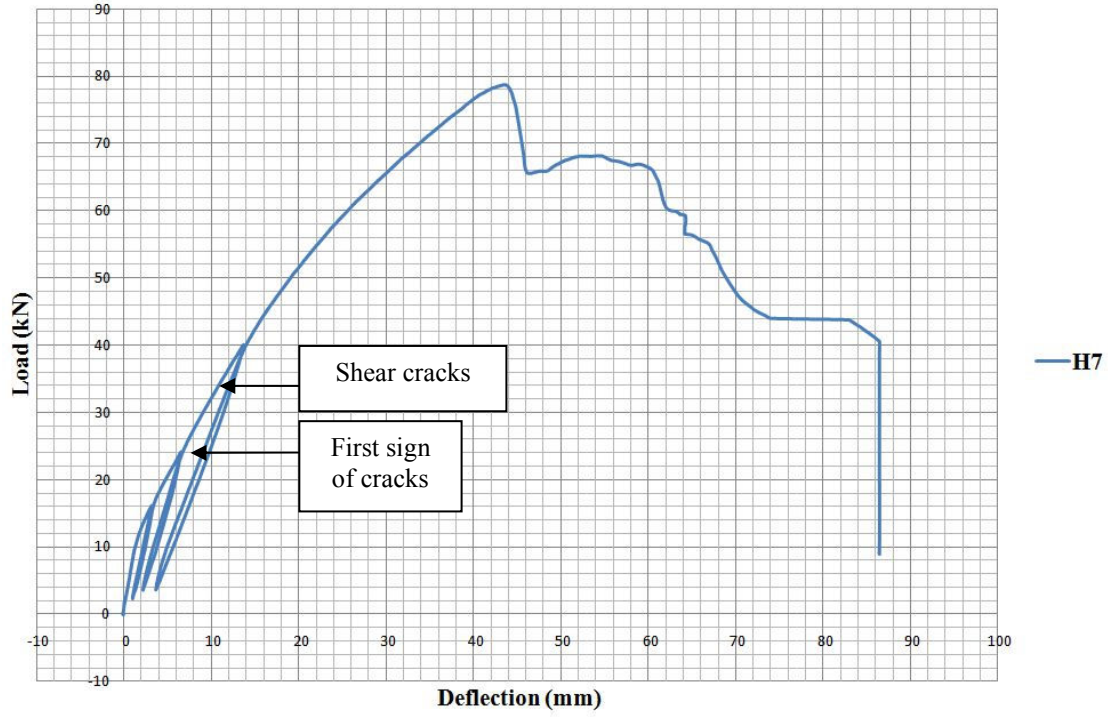

Figure 5.25: Load v. deflection graph for Specimen H7

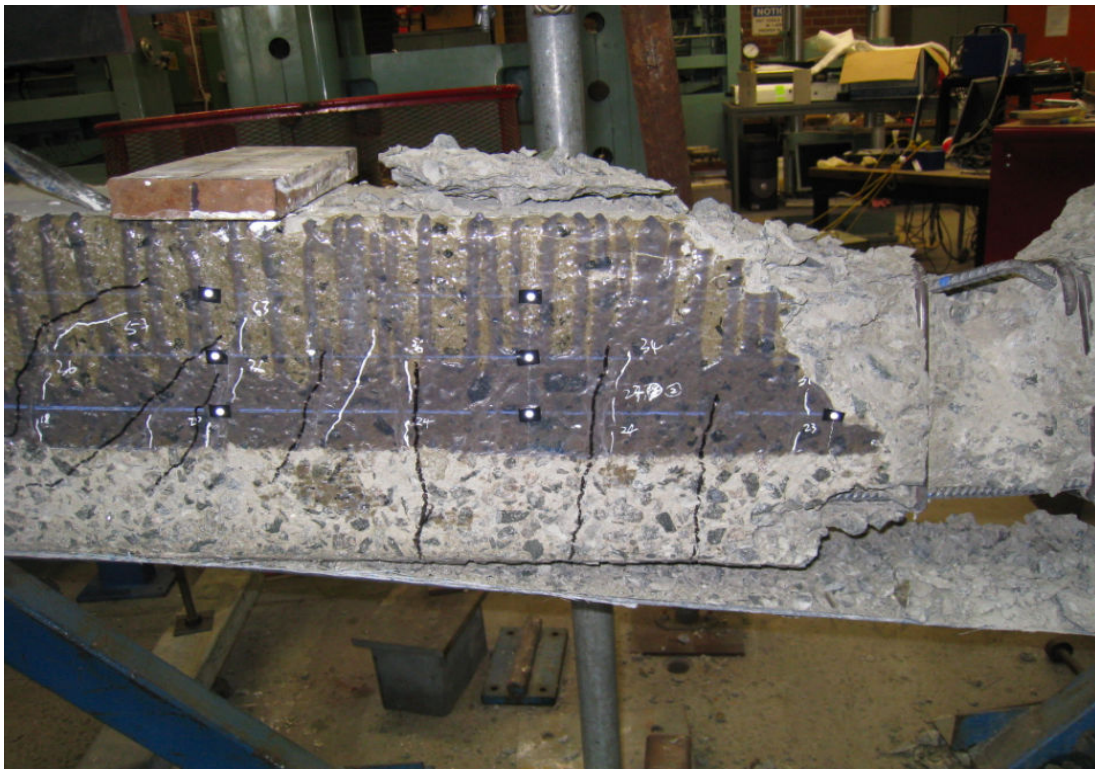

Figure 5.26: Flexure crack pattern of Specimen H7

Figure 5.27: Shear crack pattern of Specimen H7

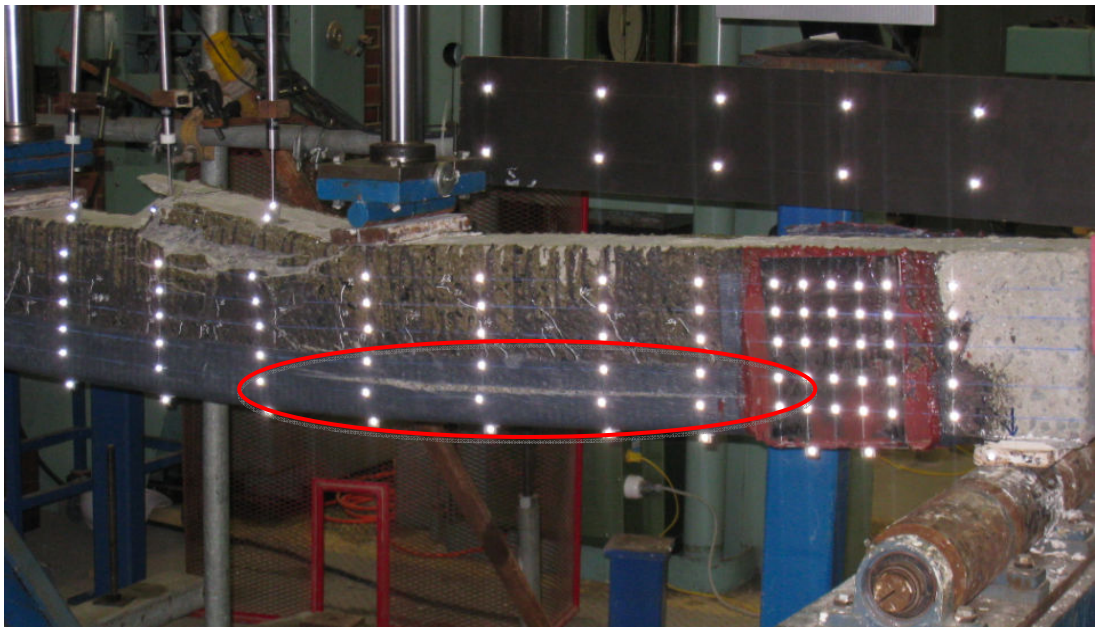

Figure 5.28: Debonding of side FRP, Specimen H7

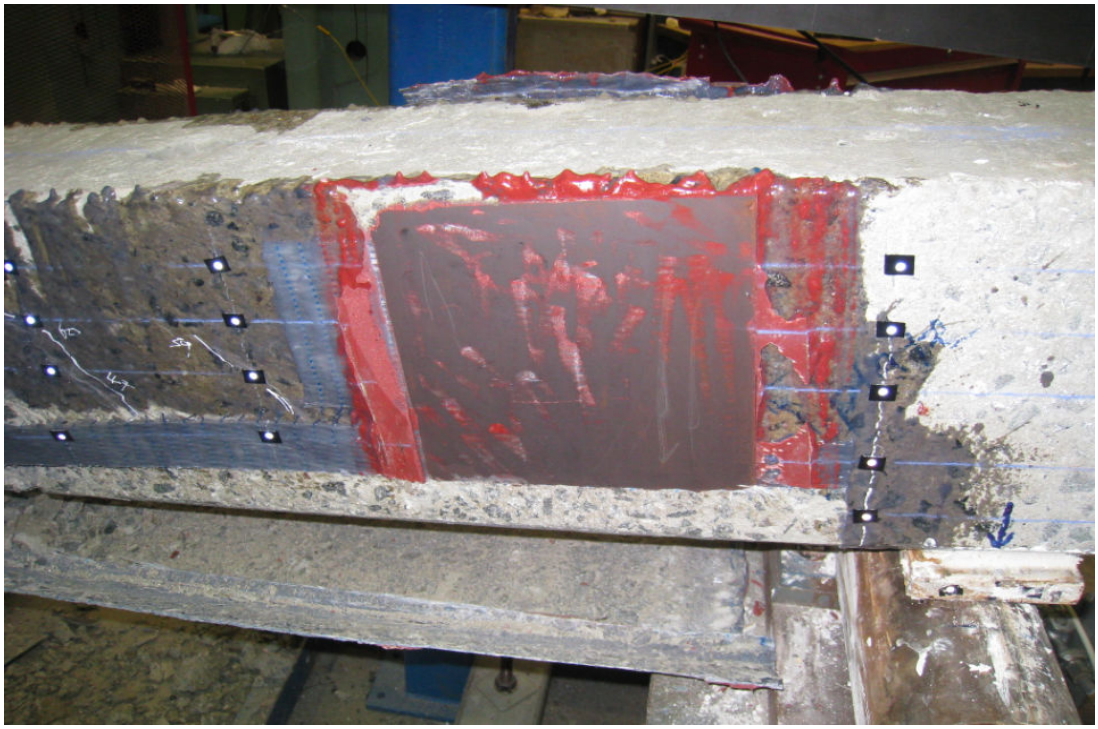

Figure 5.29: Steel plate anchorage debonded, Specimen H7

Figure 5.30: Total failure of compression zone and buckling of compressive reinforcement, Specimen H7

5.3.6 Specimen H5

Specimen H5 was strengthened with FRP using the hybridisation method. It was strengthened with a layer of CFRP at the inner layer, while a layer of GFRP served as the outer layer. Specimen H5 was not strengthened with end anchorages. Since this specimen was only strengthened with two layers of FRP, it was expected that at the beginning of the flexural test it would be weaker than those specimens strengthened with three layers of FRP. During the flexural bending test, the first signs of cracking appeared at a load magnitude of 20 kN, as shown in Figure 5.33. As expected, further loading caused more cracks to appear, with shear cracks also appearing at 36 kN near the ends of the beam (Figure 5.34). The beam had an ultimate load bearing strength of 64 kN with a deflection of 46 mm at that point, as shown in the load versus deflection graph in Figure 5.32. The first sign of failure was the fracture of the FRP layers at the mid-span of the tension face. A critical failure occurred at the point when almost all of the FRP reinforcement at mid-span fractured due to tensile rupture of the GFRP (Figure 5.35). Further vertical displacement of the loading jacks caused the concrete to crush at the compression zone, as shown in

Figure 5.36. The final failure occurred when the side strap at one end of the beam completely debonded. This is shown in Figure 5.37. The loading cycles for Specimen H5 are shown in Figure 5.31.

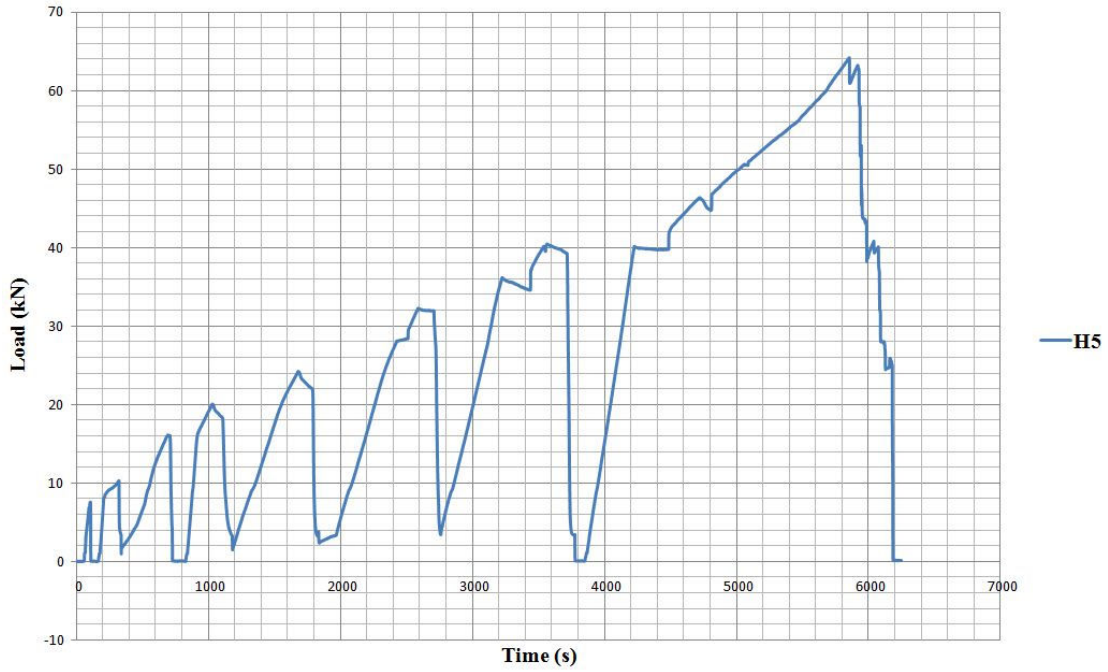

Figure 5.31: Loading cycles for Specimen H5

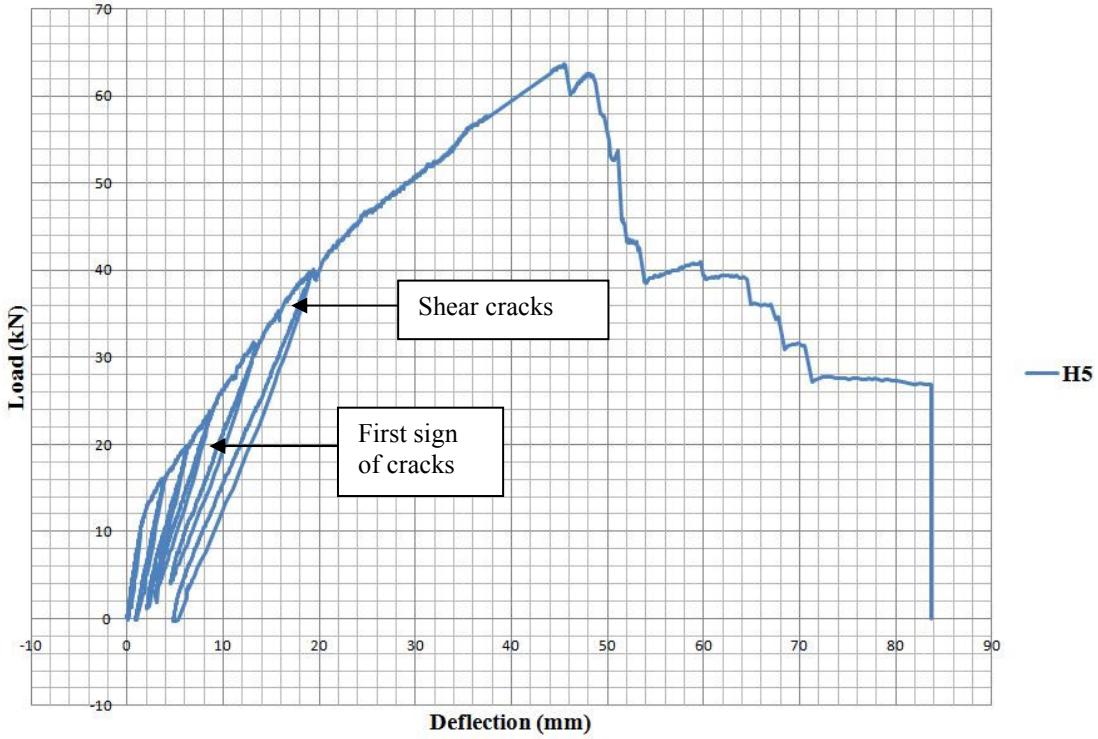

Figure 5.32: Load v. deflection graph for Specimen H5

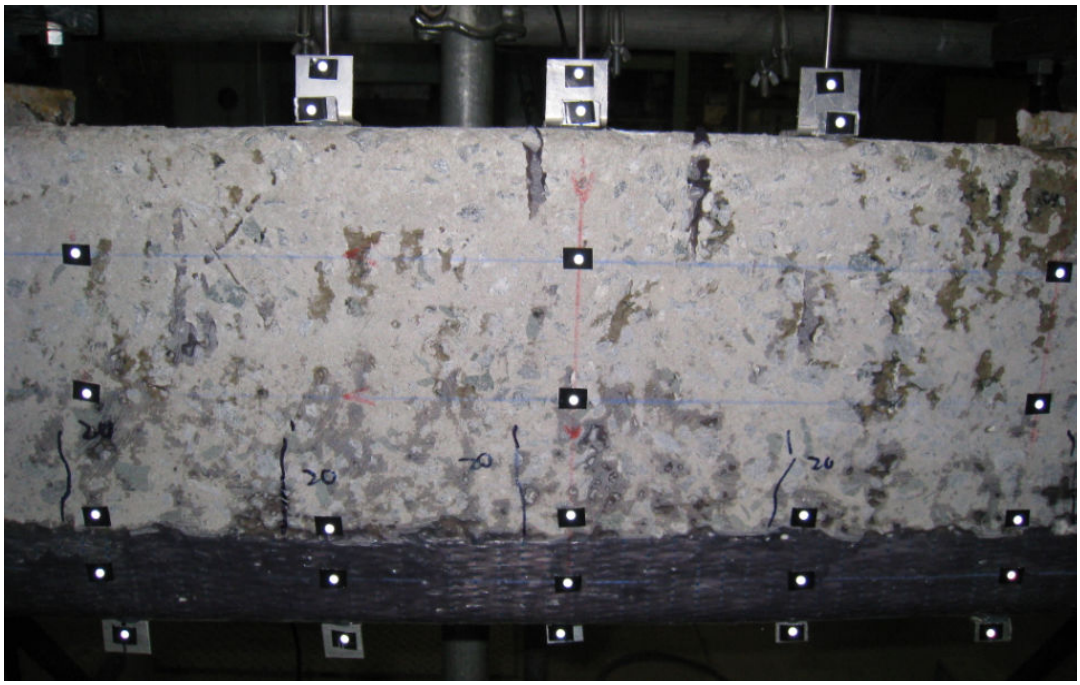

Figure 5.33: Cracks appeared at 20 kN, Specimen H5

Figure 5.34: Shear cracks appeared at high load magnitude, Specimen H5

Figure 5.35: FRP fractured at mid-span, Specimen H5

Figure 5.36: concrete crushed at compression zone, Specimen H5

Figure 5.37: Side FRP completely debonded, Specimen H5

5.3.7 Specimen H3

Specimen H3 was strengthened with FRP using the hybridisation method; the same configuration as used with Specimen H5. However, both ends of Specimen H3 were strengthened with V-shaped end anchorages of GFRP material. At the beginning of the flexural test, the beam was loaded for three cycles at low load magnitudes: 10 kN, 12 kN and 16 kN, as shown in Figure 5.38. Cracks were first observed at a load magnitude of 20 kN (Figure 5.40). It is possible that the cracks appeared before 20 kN but were not visible due the side of the beam being covered with GFRP. Cracks were only visible once they had extended beyond the height of the GFRP. The beam sustained flexural loading until 64 kN when the longitudinal FRP started to fail as a 'tickling' sound was heard. The V-shaped anchorages remained bonded to both ends of the beam even at a high load magnitude of 64 kN, which then forced the FRP to fail at the mid-span of the beam. This is shown in Figure 5.41. The failure started with the tensile rupture of the FRP at mid-span, with fracturing first at the side, and then at the tension face of the beam. Meanwhile, there was concrete crushing at the compression zone (Figure 5.42). The sustained load dropped drastically to 40 kN

where it remained for about three minutes before dropping to 27 kN at 100 mm deflection, as shown in Figure 5.38. This was where the beam became independent from the strength of the FRP. It continued to sustain a constant load with increased deflection. Final failure occurred at 130 mm deflection, at which point the beam fractured in half, as shown in Figure 5.43. After final failure, an inspection was made and, as shown in Figure 5.44, the end anchorages were still well bonded to the concrete surface of the beam. This shows the effectiveness of V-shaped anchorages. The load versus deflection graph for Specimen H3 is shown in Figure 5.39.

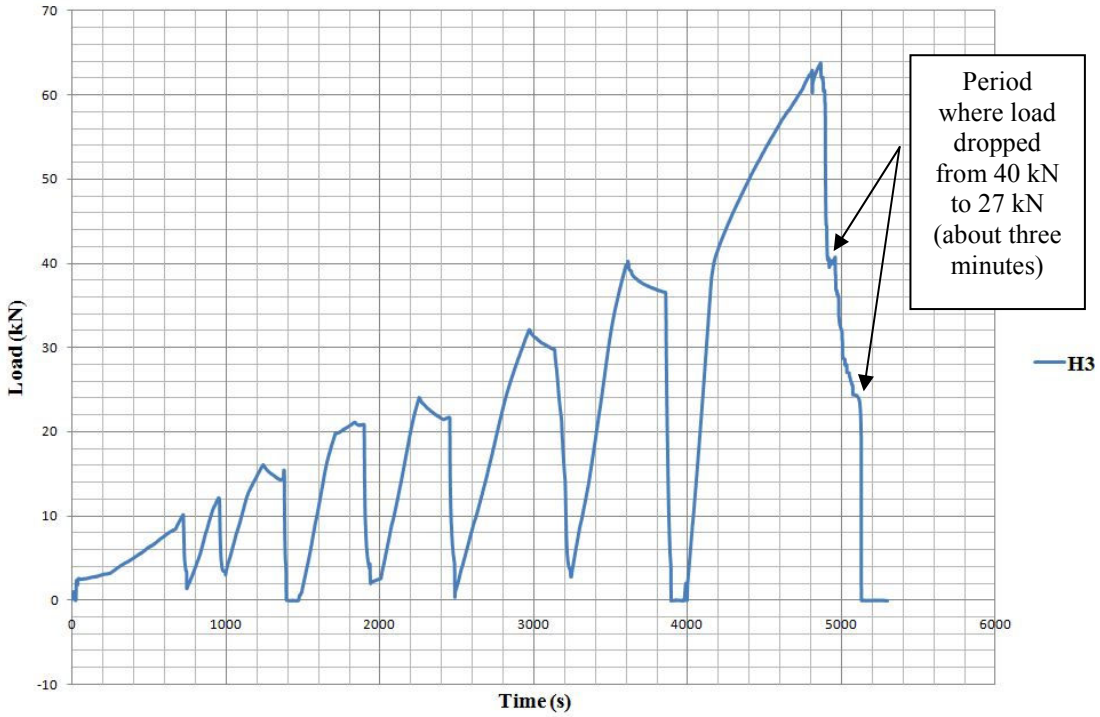

Figure 5.38: loading cycles for Specimen H3

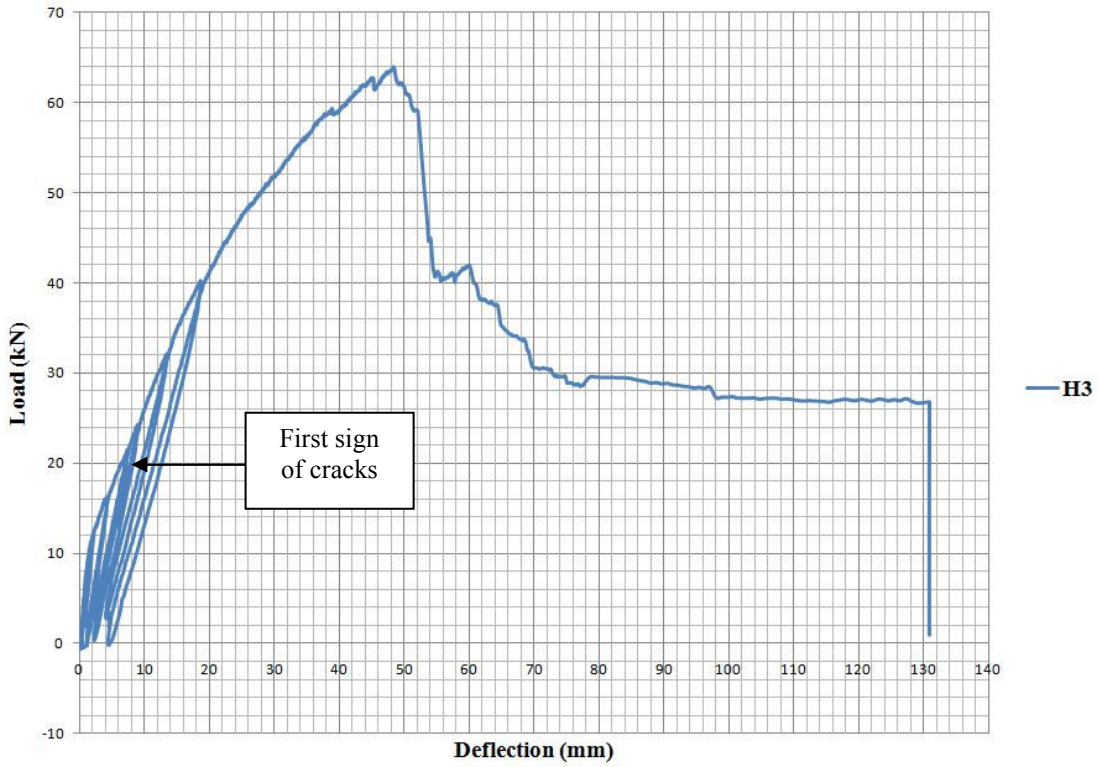

Figure 5.39: Load v. deflection graph for Specimen H3

Figure 5.40: Observation of cracks at 20 kN, Specimen H3

Figure 5.41: Debonding of FRP at side and tension face of Specimen H3

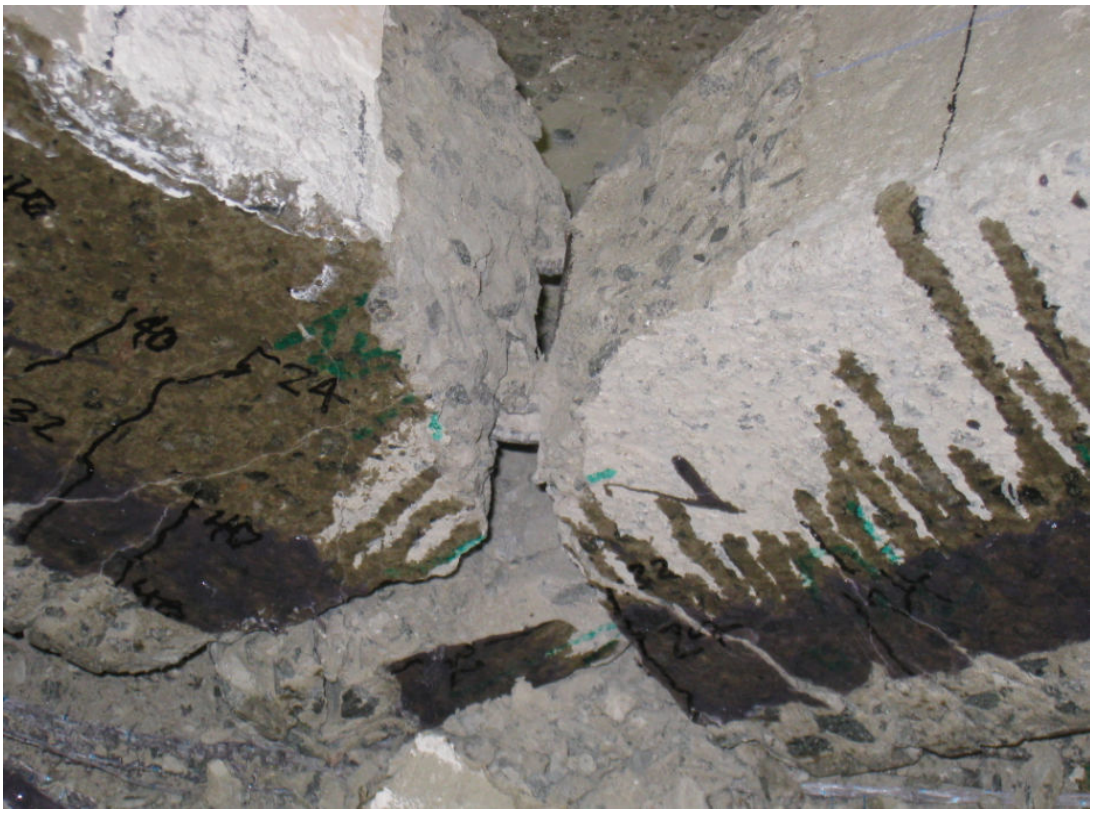

Figure 5.42: Concrete crushing at compression zone, Specimen H3

Figure 5.43: Specimen H3 fractured in half at final failure

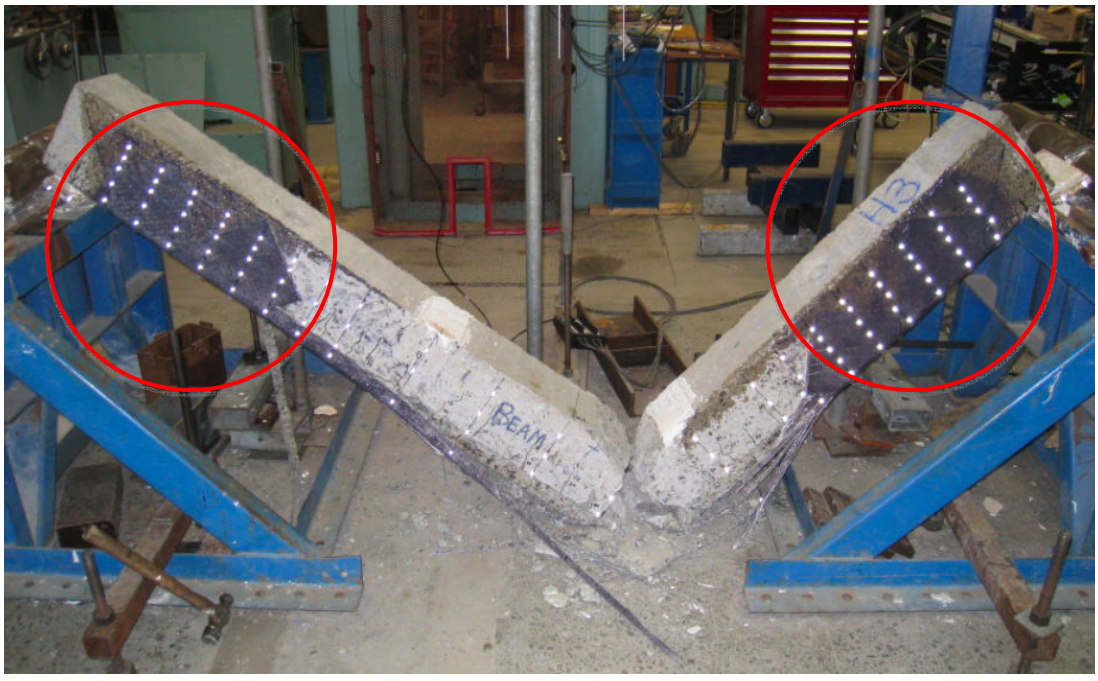

Figure 5.44: End anchorages remain well bonded with the concrete after failure, Specimen H3

5.3.8 Specimen H1

Specimen H1 had the same internal rebar configuration as the upper control beam, Specimen H2. However, Specimen H1 was strengthened with a layer of GFRP of 2600 mm in length at the tension face, and another layer of GFRP of 1000 mm in length at the compression face at mid-span. GFRP was used at the compression zone to prevent the crushing of the concrete. No end anchorages were applied to this specimen. Figure 5.47 shows the setup of Specimen H1. Initial cracks started to appear at magnitude 16 kN (Figure 5.48). The specimen started to exhibit a typical cracking pattern at the position of fitment. With the increase in load magnitude, cracks started to expand to a width of about 0.5 mm. Cracks then widened further with high load magnitudes of 40 kN and above; the zones between the initial cracks began to exhibit cracks, as shown in Figure 5.49. This phenomenon only occurred with FRP-strengthened specimens. 'Tickling' sounds occurred at 70 kN, which indicated that the fibre had started to rupture. The specimen continued to be loaded until a peak load of 80 kN was reached. During this period, the compression zone of the beam was experiencing compressive failure, which was the crushing of the concrete. The compressive failure was resisted temporarily because the compression zone had been strengthened with a layer of GFRP. However, with further vertical displacement from the loading jack, compression failure eventually occurred at a peak load of 80 kN when the compressive reinforcement bar buckled. These two occurrences are shown in Figures 5.50 and Figure 5.51 respectively. After the peak load of 80 kN, another failure occurred when the GFRP at the tension face gradually debonded due to the absence of end anchorages. Once the debonding had occurred, the load magnitude sustained by the beam began to decrease until it dropped to 68 kN. A brittle failure then occurred when the GFRP on the tension side completely debonded, as shown in Figure 5.52. Figure 5.46 shows the load versus deflection graph for Specimen H1 during the flexural bending test. Figure 5.45 shows the full loading process with loading cycles for Specimen H1.

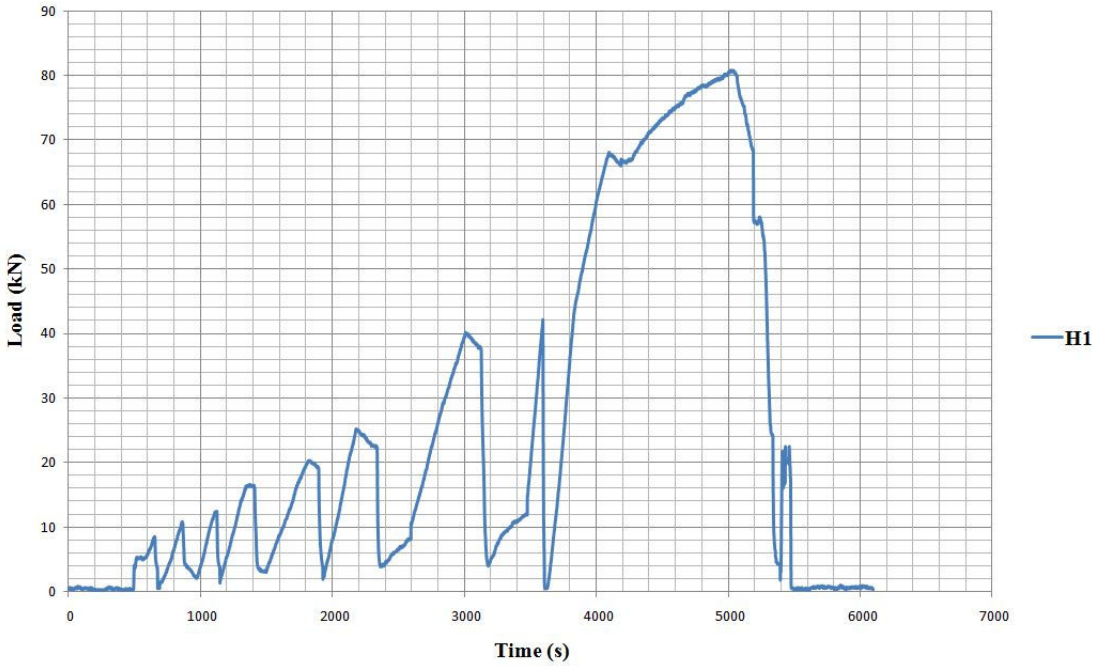

Figure 5.45: Loading cycles for Specimen H1

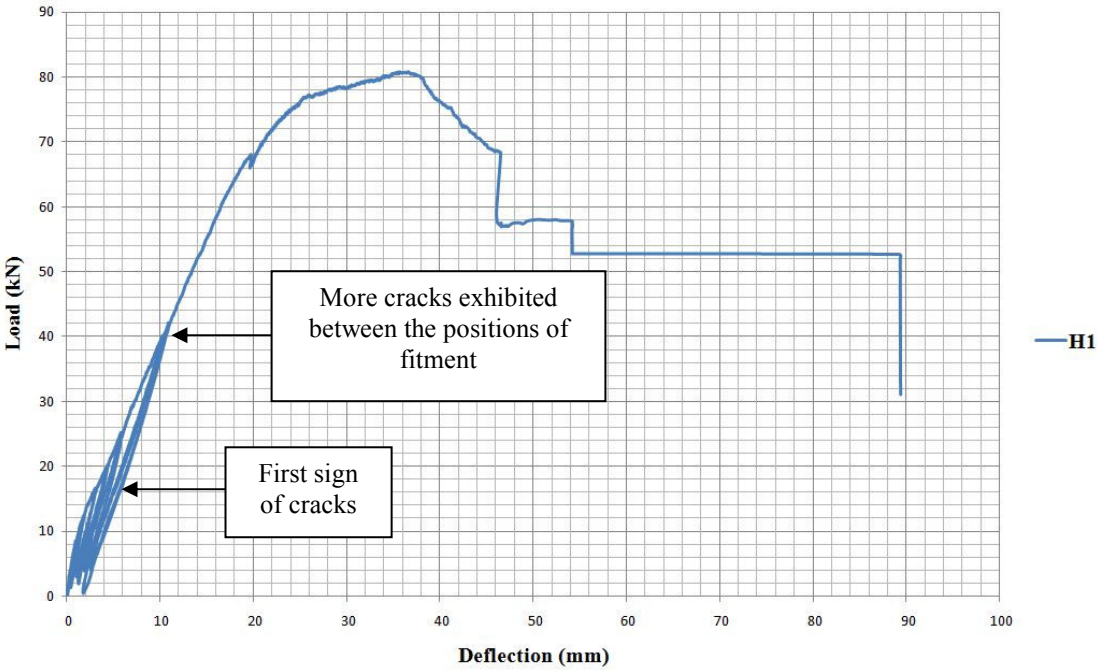

Figure 5.46: Load v. deflection graph for Specimen H1

Figure 5.47: Set-up of Specimen H1

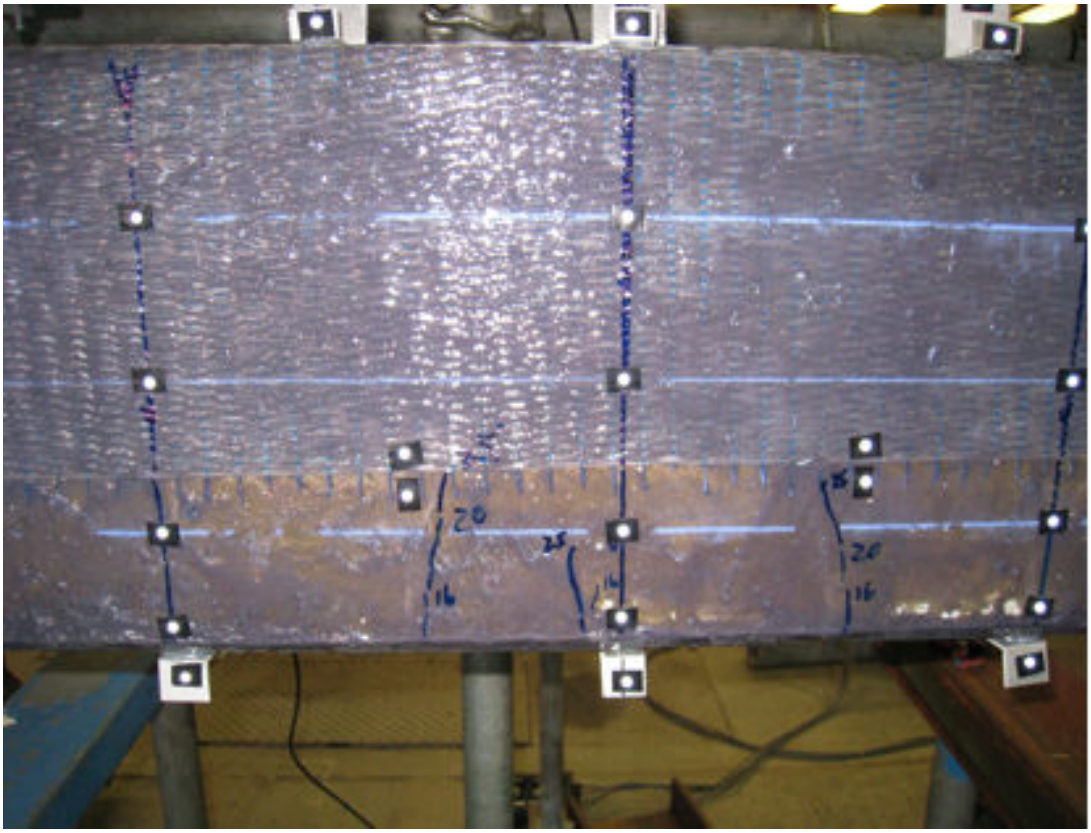

Figure 5.48: Cracks start to show at 16 kN, Specimen H1

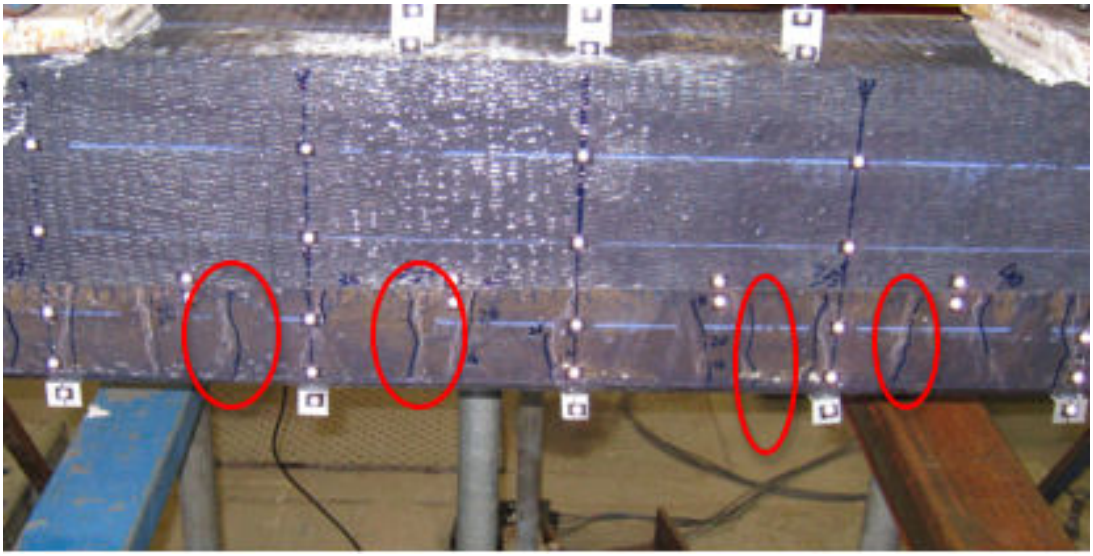

Figure 5.49: More cracks shown between the positions of fitment at 40 kN and above, Specimen H1

Figure 5.50: Crushing of the concrete at the compression zone, Specimen H1

Figure 5.51: Compressive reinforcement bar buckled, Specimen H1

Figure 5.52: Debonding of the GFRP, Specimen H1

5.3.9 Specimen J3

Specimen J3 was a CFRP-strengthened concrete beam with U-shaped end anchorages at both ends. Specimen J3 was the earliest type of specimen to be tested by Jovanco Domazetoski. According to Domazetoski's statement, the U-shaped end anchorage was considered least effective as it did not double-wrap the beam nor provide an inclined CFRP fabric sheet to resist opposing forces, as did the V-shaped anchorage. The typical setup for a flexural test as used for Specimen J3 is shown in Figure 5.55. The first noticeable failure in this flexural test was the anchorage failure at a load magnitude of 66 kN. This happened when the CFRP U-shaped anchorages were pulled by the CFRP at the tension side of the beam. As discussed, U-shaped anchorages do not provide resistance transversely. Therefore, with the debonding of the CFRP at the tension face, combined with the restraining force of the CFRP, the end anchorages were torn apart at 66 kN, as shown in Figure 5.56. Concrete compression also occurred with further vertical displacement from the loading jacks (Figure 5.57). Figure 5.54 shows the load versus deflection graph for Specimen J3, indicating a brittle failure as the load decreased rapidly from peak load to 34 kN. A

full loading process illustrating the loading cycles for Specimen J3 is shown in Figure 5.53.

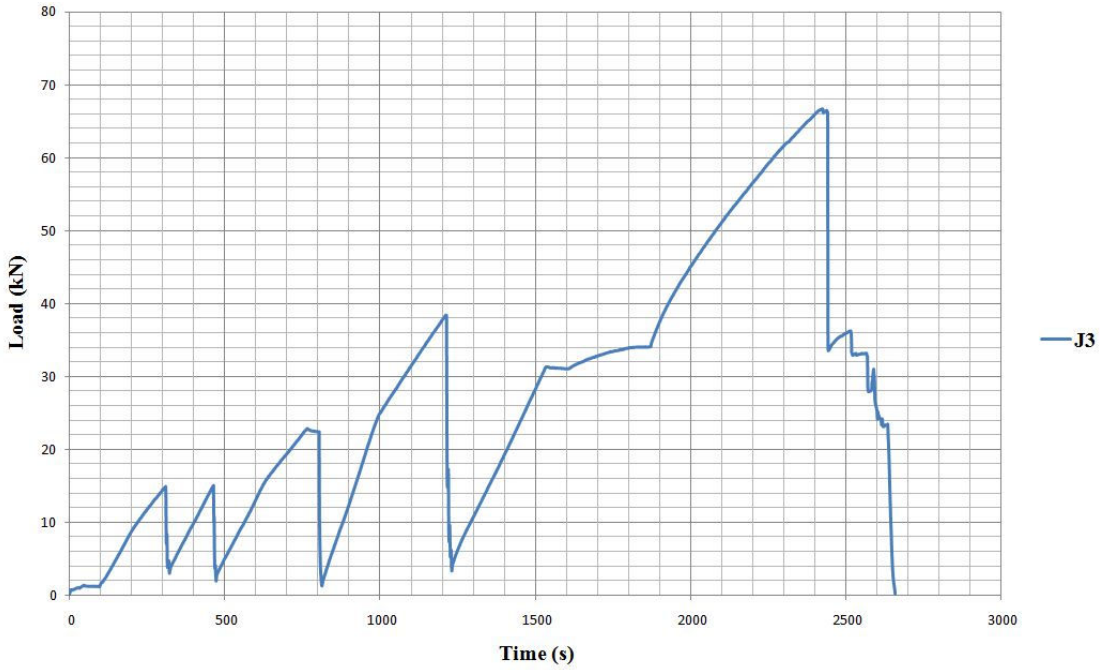

Figure 5.53: Loading cycles for Specimen J3

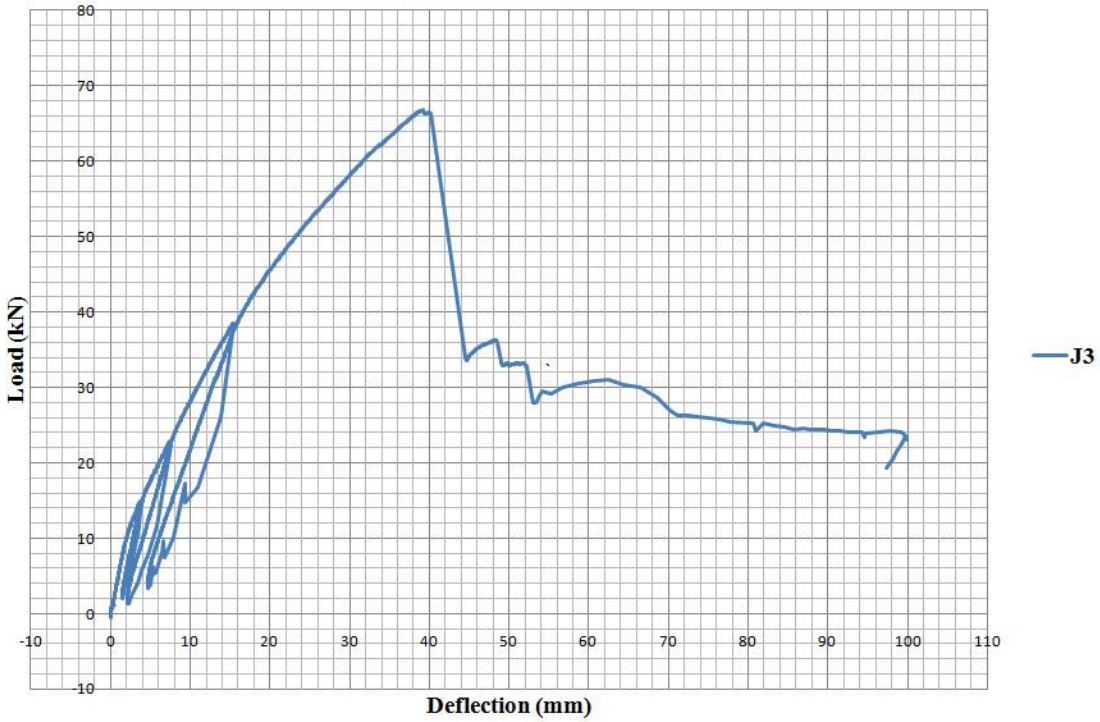

Figure 5.54: Load v. deflection graph for Specimen J3

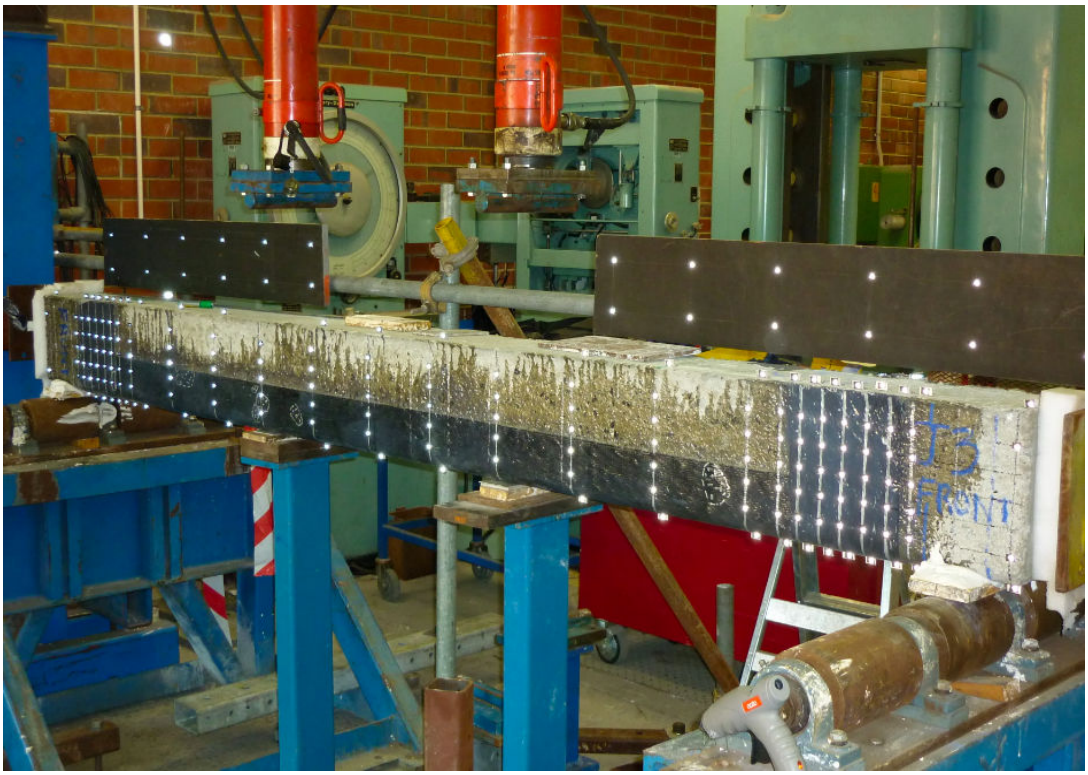

Figure 5.55: Typical Setup for Specimen J3

Figure 5.56: Debonding of longitudinal CFRP tore apart the end anchorage, Specimen J3

Figure 5.57: Concrete compression of Specimen J3

5.3.10 Specimen J2

Specimen J2 was strengthened with three layers of longitudinal CFRP as well as V-shaped end anchorages on both ends of the beam. The major failure of Specimen J2, which happened at a load magnitude of 74 kN, was the tensile rupture of the CFRP at the longitudinal face, which indicates that the tensile capacity of the CFRP layers was fully utilised. The CFRP layer at the tension face underwent tensile rupture, as did the CFRP at the side face of the beam (see Figure 5.60), followed by the crushing of the concrete at the compression zone at mid-span (see Figure 5.61). Neither side of the end anchorages exhibited tensile rupture or debonding throughout the entire testing stage. However, Specimen J2 had an extremely brittle failure, as shown in the load versus deflection graph in Figure 5.59, with the load magnitude decreasing rapidly from 72 kN to 30kN due to the tensile rupture of the CFRP. The beam continued to sustain vertical displacement from 50 mm to 100 mm, experiencing concrete crushing at this stage. A full loading process illustrating the loading cycles for Specimen J2 is shown in Figure 5.58.

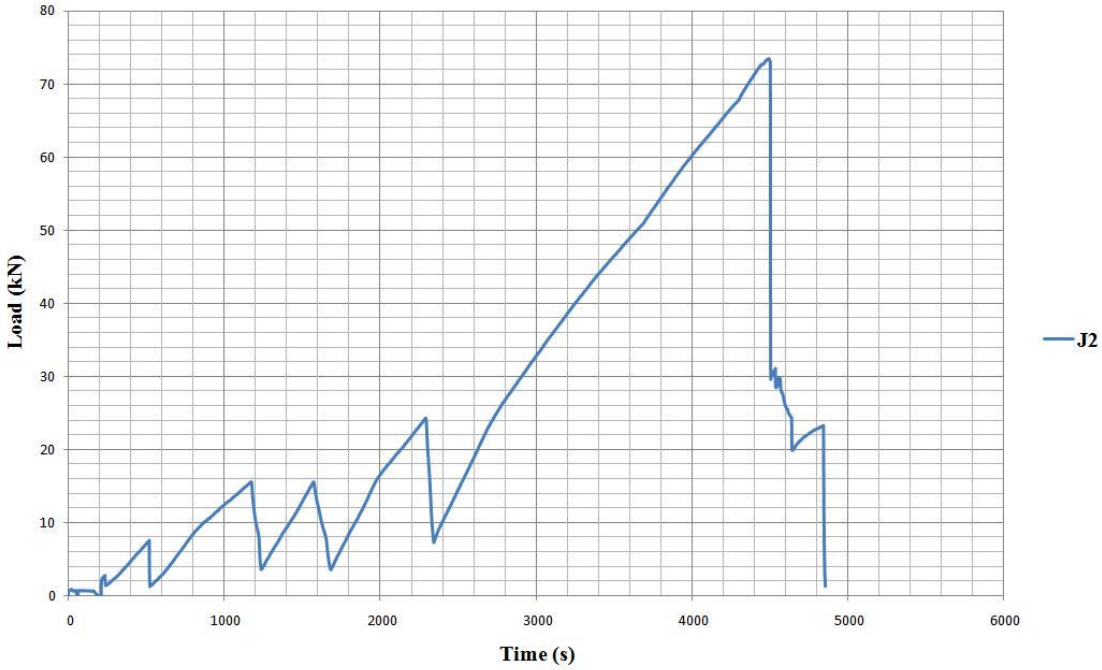

Figure 5.58: Loading cycles for Specimen J2

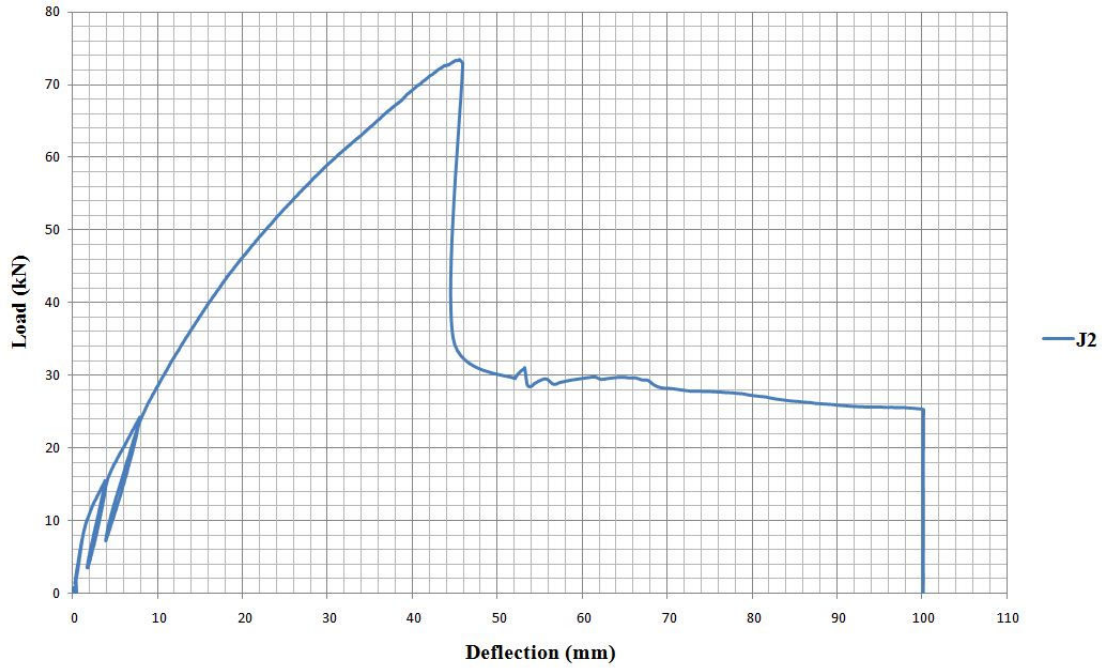

Figure 5.59: Load v. deflection graph for Specimen J2

Figure 5.60: Tensile rupture of longitudinal CFRP, Specimen J2

Figure 5.61: Crushing of concrete at compression zone, Specimen J2

5.3.11 Specimen J5

Specimen J5 was a CFRP-strengthened concrete beam with a similar configuration to Specimen J1. It was strengthened with V-shaped anchorages wrapped across the entire beam. Specimen J5 utilised 24 pieces of 810 mm by 100 mm CFRP sheet anchorages. According to Domazetoski, each end of the beam utilised eight CFRP sheet anchorages, which were double-wrapped. The middle section of the beam was also strengthened with eight double-wrapped CFRP sheet anchorages. With six times the anchorage of Specimen J2, Specimen J5 was significantly better anchored. Therefore, it was assumed that the failure mode of Specimen J5 would not be debonding of the CFRP. At the end of the flexural test, this assumption was proven correct, as the beam eventually failed due to the tensile rupture of the CFRP sheets at the tension face. Since the longitudinal CFRP arrangement of Specimen J5 was the same as that of Specimen J2, it was assumed that Specimen J5 could sustain at least the same flexural load as had Specimen J2. Eventually, Specimen J5 failed at a high load of 79 kN, which was 8 kN more than the load at which Specimen J2 failed. See Figure 5.63 for the load versus deflection graph for Specimen J5. The additional load came from the extra tensile force provided by the anchorage at the middle section of the beam. The first noticeable failure was concrete compression at the mid-span of the beam (see Figure 5.64). Shortly after the crushing of the concrete, the tensile capacity of the longitudinal CFRP was fully utilised when it exhibited tensile rupture (see Figure 5.65). The full loading cycles for Specimen J5 are shown in Figure 5.62.

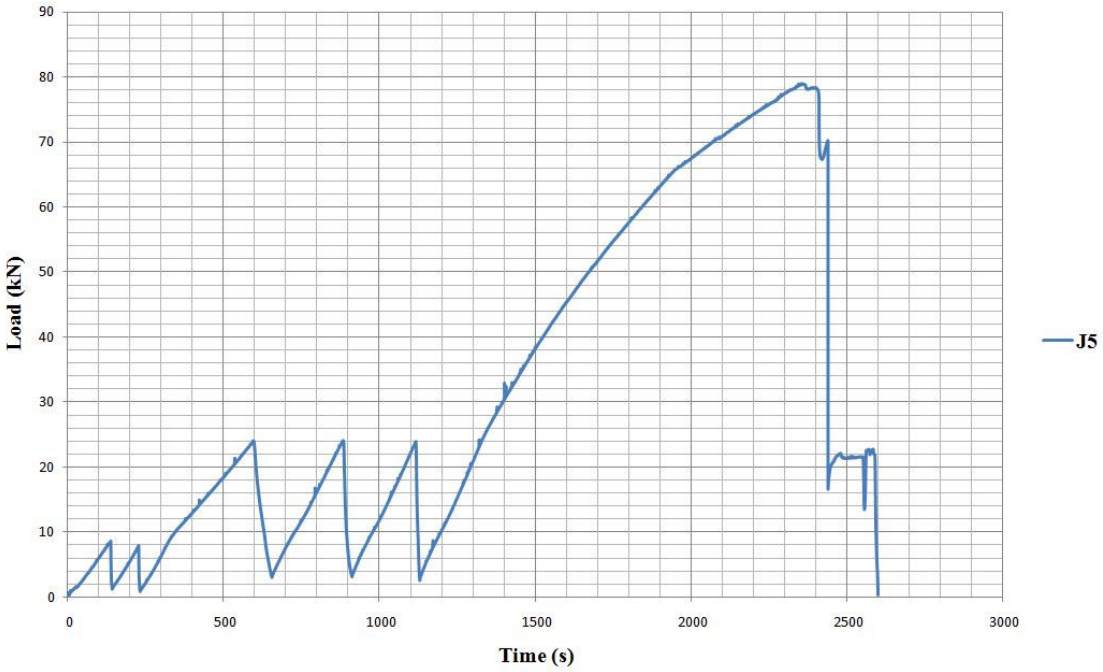

Figure 5.62: Loading cycles for Specimen J5

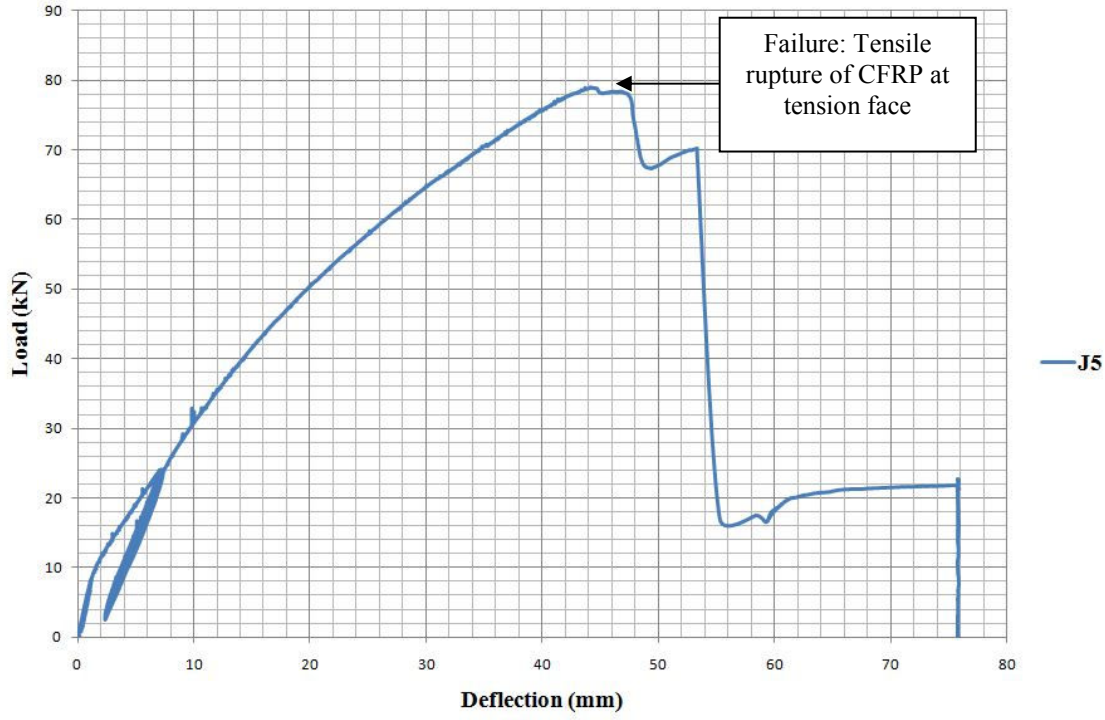

Figure 5.63: Load v. Deflection graph for Specimen J5

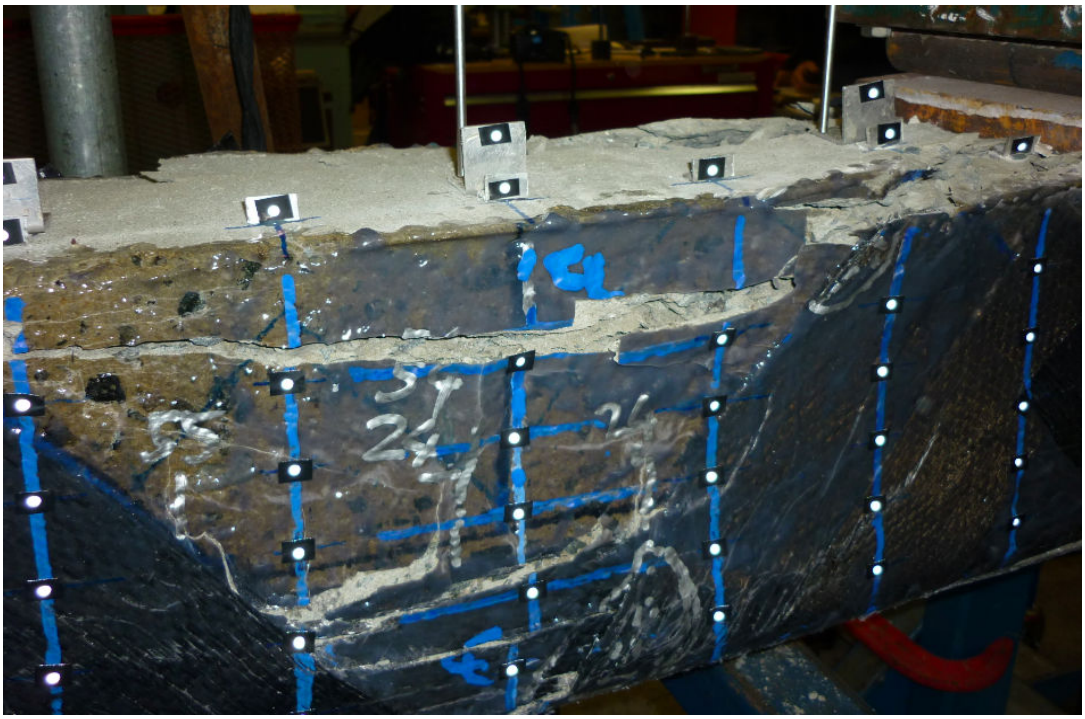

Figure 5.64: Concrete compression, Specimen J5

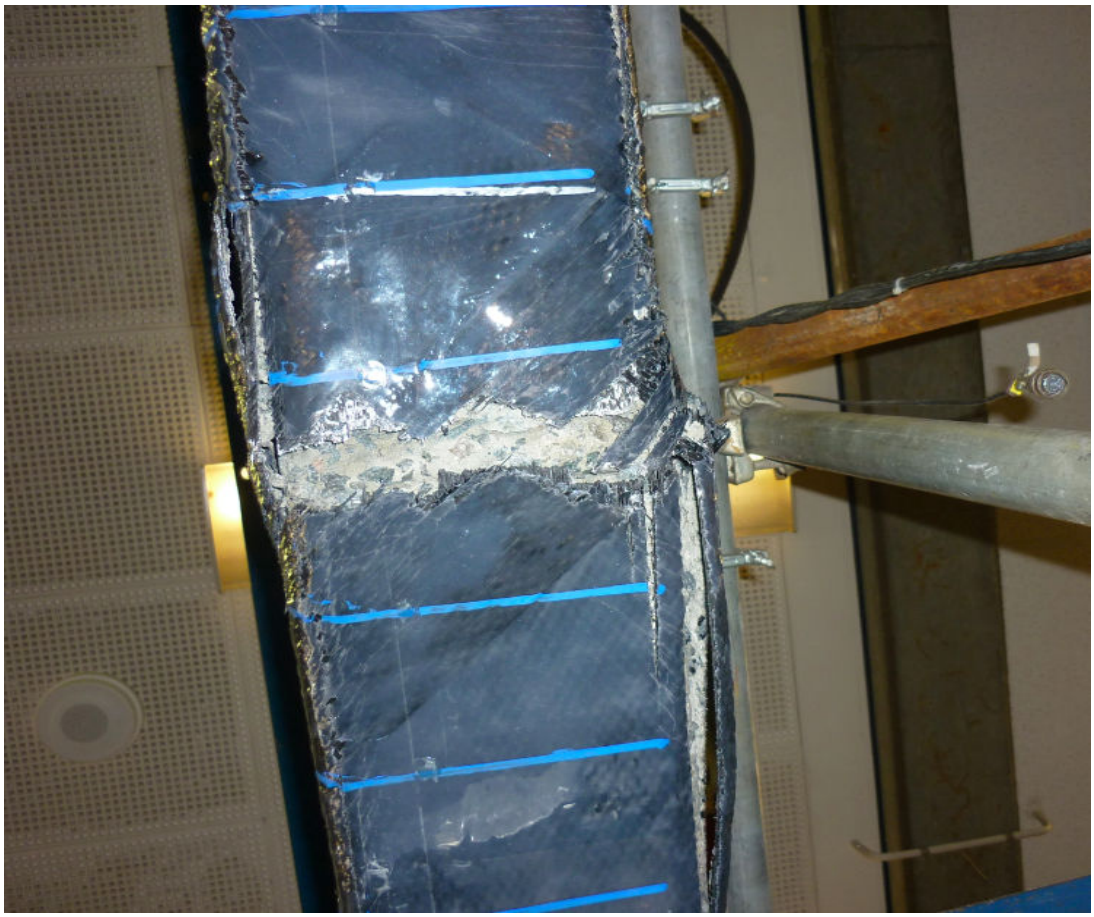

Figure 5.65: Tensile rupture on the tension face, Specimen J5

5.3.12 Specimen J1

Specimen J1 was strengthened with three layers of CFRP on the tension face of the beam. The entire length of the specimen was strengthened with 20 sheets of 150 mm by 760 mm V-shaped anchorages. The V-shaped anchorages were wider than for Specimen J5. According to Domazetoski, it was initially planned that Specimen J1 would be strengthened with 26 sheets of CFRP anchorage. However, due to hardening of the epoxy during the installation of the CFRP fabric, the middle section of the beam was not covered with CFRP anchorage. It seems for this reason, Specimen J1 failed at a failure load of 77 kN. The first noticeable failure was the tensile rupture of CFRP at the tension face (see Figure 5.68), followed by the crushing of the concrete at the compression zone at mid-span. This is shown in Figure 5.69. Due to the lack of CFRP sheeting at the middle section of the beam, Specimen J1 had less significant tensile force in the middle section, causing the CFRP to have a tensile rupture and eventually fail. Figure 5.67 shows the load versus deflection graph for Specimen J1. It can be seen that after the specimen reached the peak load, the beam exhibited an extremely brittle failure as the load capacity dropped rapidly from 68 kN to 20 kN. This suggests the requirement for further investigation to improve the ductility of the beam. Figure 5.66 shows the loading cycles for J1.

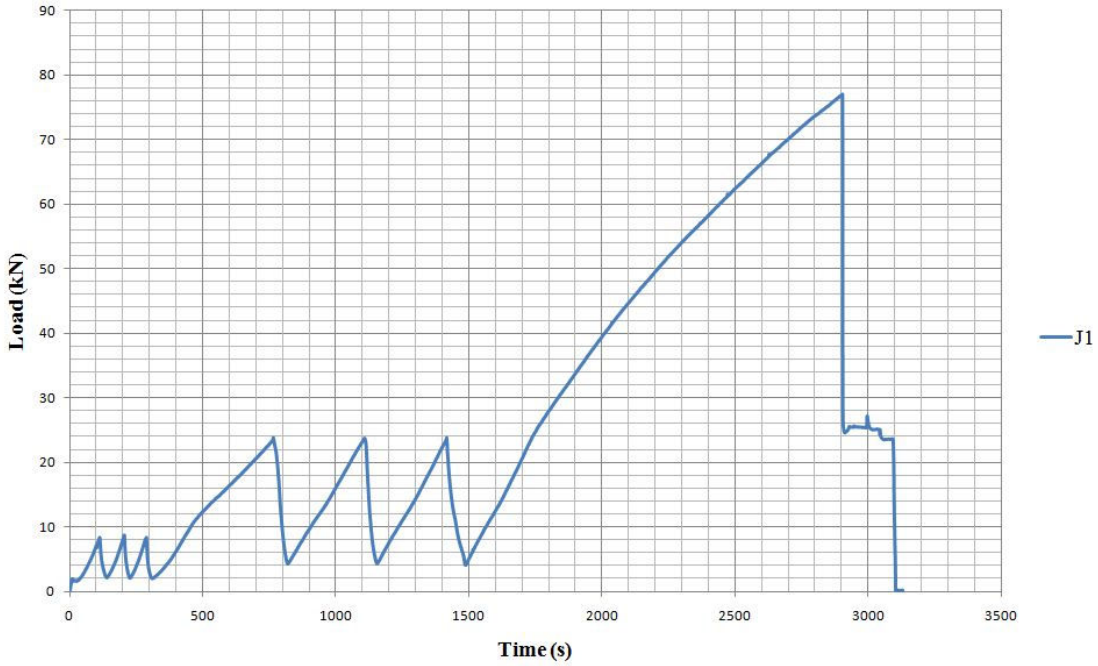

Figure 5.66 Loading cycles for Specimen J1

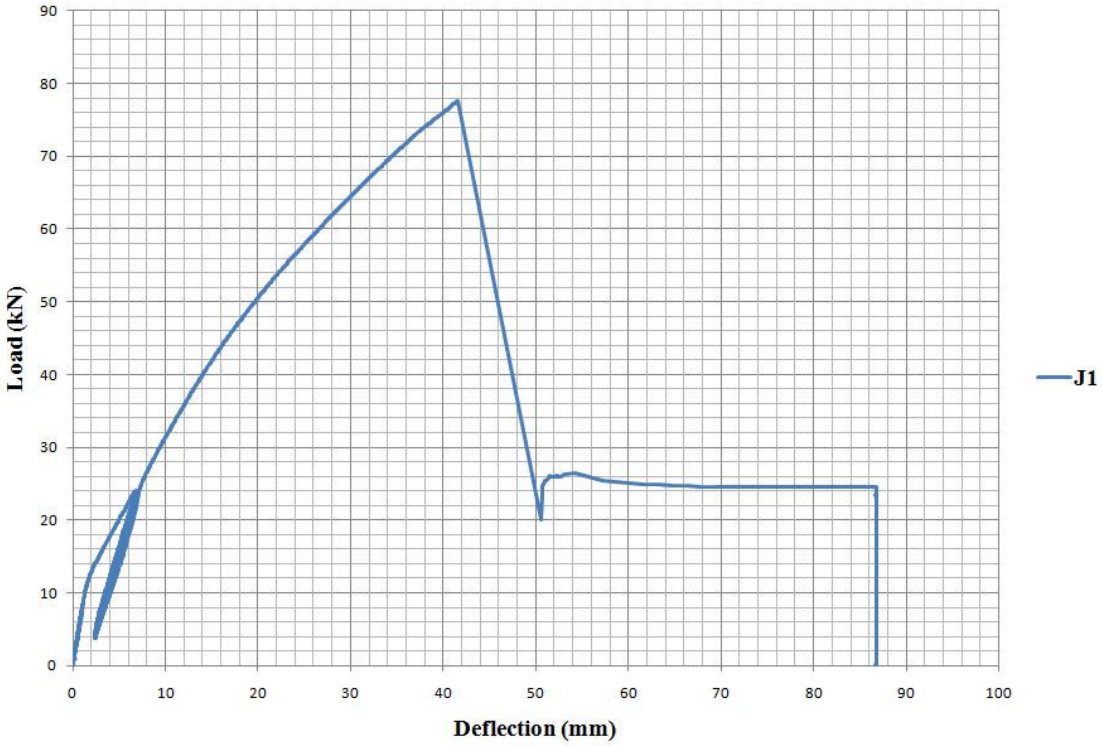

Figure 5.67: Load v. Deflection graph for Specimen J1

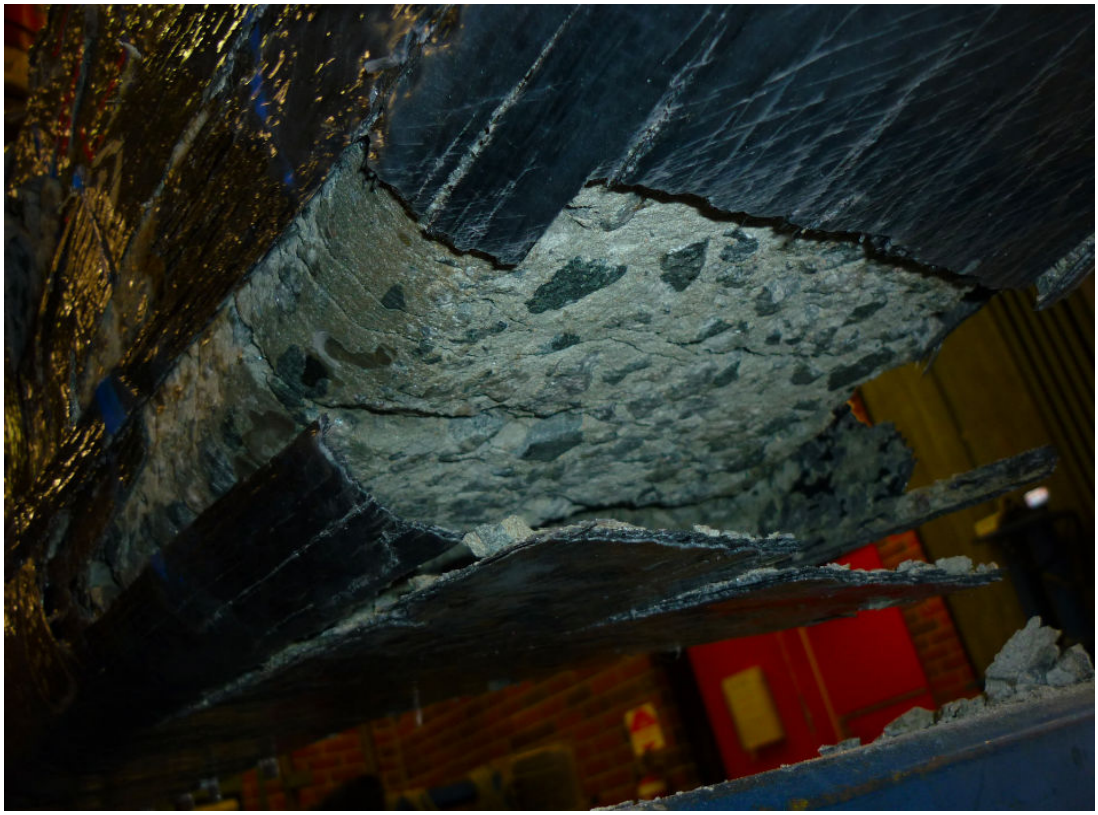

Figure 5.68: Tensile rupture at tension face, Specimen J1

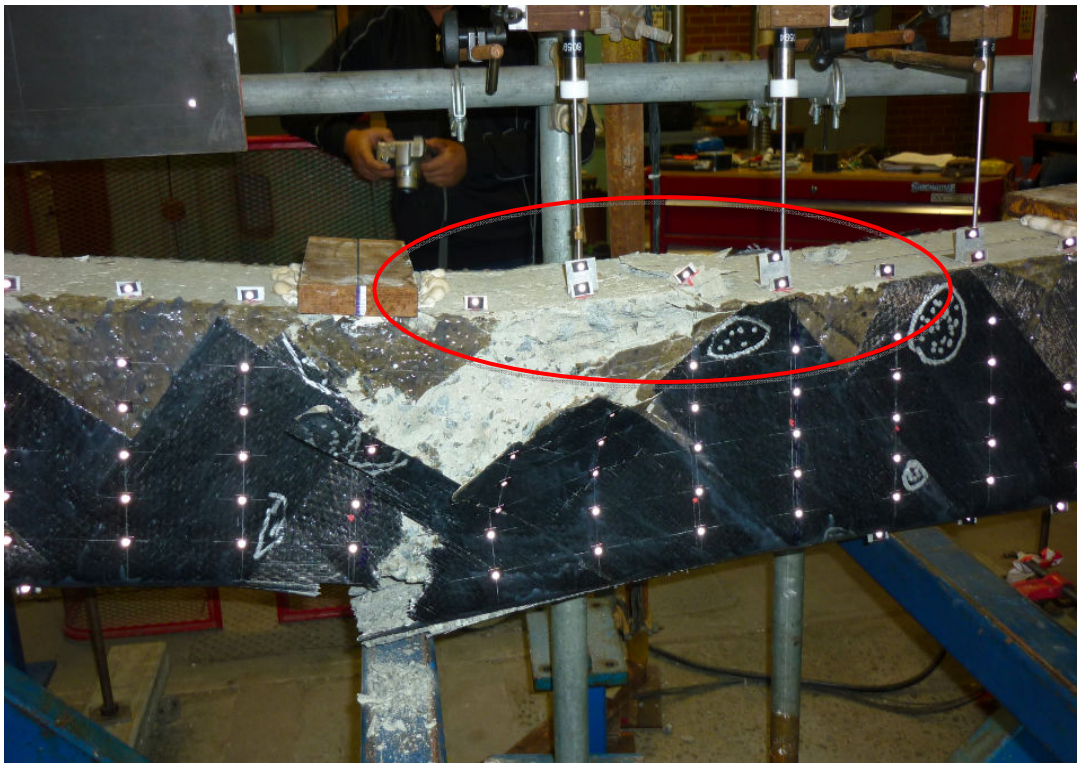

Figure 5.69: Compression failure of Specimen J1

5.4 Flexural Strength Gain

Table 5.3 summarises the flexural strength gain of the FRP-strengthened concrete beams compared with the lower control beam (H6) and the upper control beam (H2). All FRP-strengthened concrete beams showed significant gain in flexural strength with at least twice the load capacity. The longitudinal FRP sheet was the major contributor to this gain as it provided additional tensile capacity for the concrete beams. Simultaneously, the end anchorages played a role in resisting the debonding of the longitudinal FRP from the surface of the concrete beams.

Table 5.3: Flexural bending results for all specimens

Beam	Beam description	Experimental ultimate load (kN)	Load capacity gained compared with lower control beam	Load capacity gained compared with upper control beam
H6	Lower control	31	1.0	0.5
H2	Upper control	67	2.2	1.0
J4		84	2.7	1.3
H4		82	2.6	1.2
H7		78	2.5	1.2
H5		64	2.1	1.0
H3		64	2.1	1.0
H1		80	2.6	1.2
J3		67	2.2	1.0
J2		74	2.4	1.1
J5		79	2.5	1.2
J1		78	2.5	1.2
		Mean	2.4 ± 0.2	1.1 ± 0.2

5.5 Ductility Measurements

The ductility measurement for each beam was calculated by dividing the deflection ultimate by the deflection yield for each specimen. An illustration on how to determine the values for specimen H6 is shown in Figure 5.70. A sample calculation on how to determine the yielding moment is shown in Appendix G. Table 5.3 summarises the ductility measures for all beams. According to Dr Ian Chandler, as a rule of thumb, a ductility index of less than 2.0 indicates a non-ductile manner and above 5.0 indicates an excellent ductile manner[1]. Specimens H1 and H2 were not especially ductile; Beam H2 exhibited a concrete crushing failure and the entire beam buckled during the test, as shown in Figure 5.9. Beam H3, with a ductility index of 3.4, exhibited the most ductility of all the beams. This shows that the hybridisation technique indeed worked, improving the ductility of the beam compared with the other strengthened beams and the lower control beam, H6. Although this research does not establish a benchmark, it does indicate that future studies of hybridisation techniques may produce clear cut results. This research also showed that CFRP-strengthened beams are not as ductile as GFRP-strengthened beams. As shown in Table 5.4, beams J1, J2, J3 and J5, which were CFRP-strengthened beams, exhibited a ductility index of less than 3.0, whereas the GFRP-strengthened beams exhibited higher ductility indexes of 3.1 in average. This indicates the physical properties of CFRP and GFRP: GFRP has better elongation than does CFRP.

[1] Personal communication with Dr Ian Chandler on 14 April 2011.

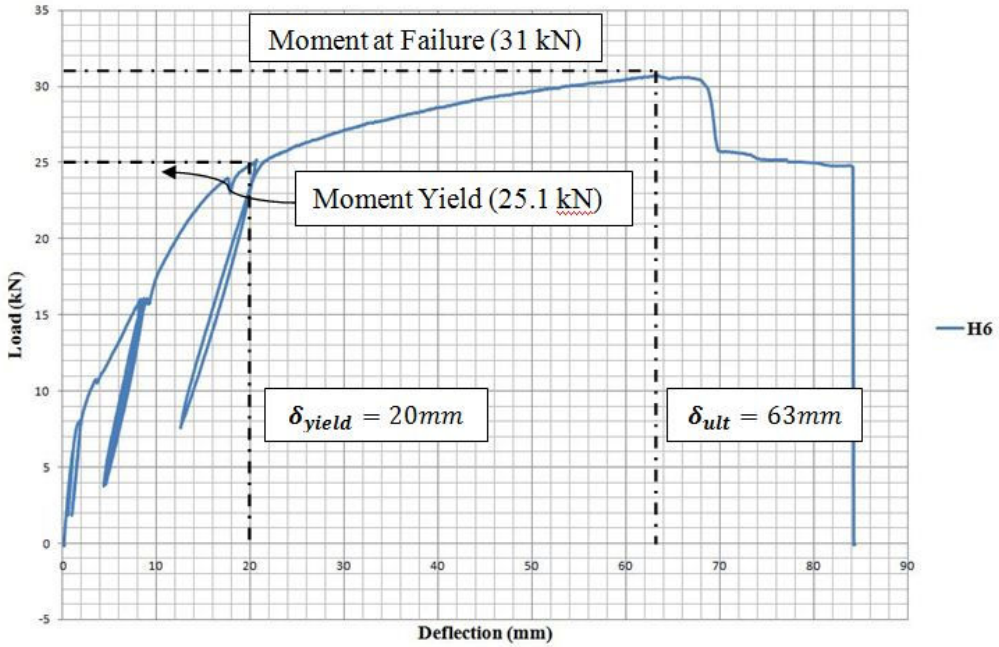

Figure 5.70: Determination of deflection yield and deflection ultimate

The formula used to measure the ductility of beams was:

$$\text{Ductility} = \frac{\delta_{ult}}{\delta_{yield}} \qquad \text{(Equation 2)}$$

where δ_{ult} = deflection ultimate, δ_{yield} = deflection yield.

Table 5.4: Ductility measurements for all specimens

Specimen	Theoretical moment at yield (kN)	Experimental moment at failure (kN)	Deflection yield (mm)	Deflection at failure (mm)	Ductility measure
H6	25.1	31	20	63	3.2
H2	66	67	22	24	1.1
J4	43.8	84	16	50	3.1
H4	41.8	82	16	50	3.1
H7	41.7	78	15	44	2.9
H5	33.8	64	15	45	3.0
H3	33.9	64	14	48	3.4
H1	69.9	80	21	36	1.7
J3	43.0	67	18	40	2.2
J2	43.0	74	18	46	2.6
J5	43.0	79	16	46	2.9
J1	43.0	78	16	41	2.6

5.6 Deflection profile and bending stiffness of specimens

The deflection profiles of the specimens were plotted from the photogrammetry data collected during the flexural testing. As mentioned in Chapter 3 (Section 3.5.2), images were taken of the reflective dots placed on each beam, and these images were analysed to determine the movement of the beam. The two supervisors, Dr Natalie Lloyd and Dr Ian Chandler, mentioned that the deflection profile of each specimen was related to the specimen's bending stiffness. Aside from that, specimens strengthened with the same quantity of FRP should have the same stiffness at the same load magnitude[2]. Hence, the deflection profile for each specimen, followed by the bending stiffness of that specimen, is shown in Figures 5.70–5.80 and Table 5.5. The formula for calculating the bending stiffness is:

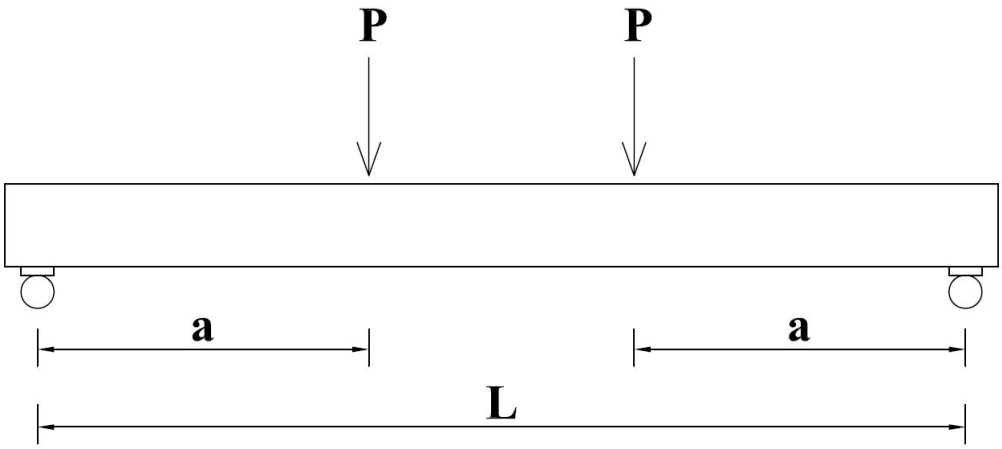

$$\delta = \frac{PL^3}{6EI}\left[\frac{3a}{4L} - \left(\frac{a}{L}\right)^3\right]$$

Hence,

$$EI = \frac{PL^3}{6\delta}\left[\frac{3a}{4L} - \left(\frac{a}{L}\right)^3\right] \qquad \text{(Equation 3)}$$

Where EI = bending stiffness (Nmm^2), δ = deflection (mm)

a = 1000 mm, L = 2800 mm

[2] Personal communication with Dr Natalie Lloyd and Dr Ian Chandler, 14 April 2011.

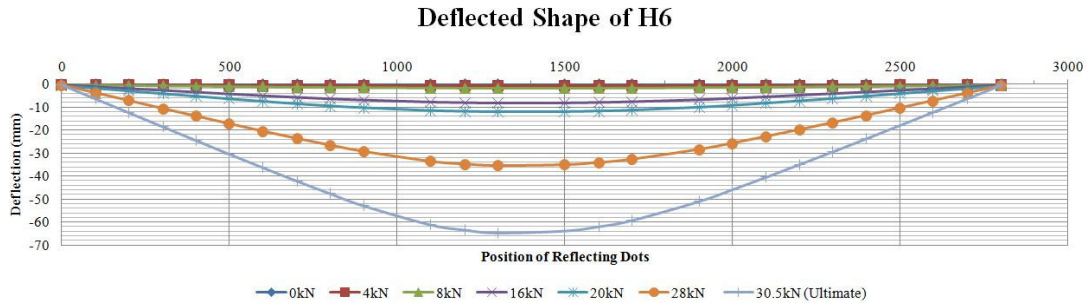

a (mm)	L (mm)	Load, P (kN)	Deflection at load P, δ (mm)	Bending stiffness, *EI* (Nmm^2)
1000	2800	16	8	1.62667×10^{12}
1000	2800	20	12	1.35556×10^{12}
1000	2800	28	35	6.50667×10^{11}
1000	2800	31	63	4.00212×10^{11}

Figure 5.71: Deflection profile and bending stiffness of Specimen H6

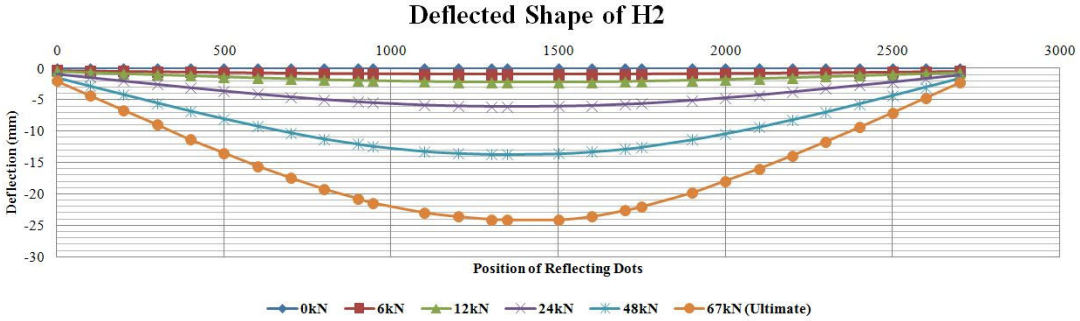

a (mm)	L (mm)	Load, P (kN)	Deflection at Load P, δ (mm)	Bending stiffness, *EI* (Nmm^2)
1000	2800	12	3	3.25333×10^{12}
1000	2800	24	6	3.25333×10^{12}
1000	2800	48	14	2.78857×10^{12}
1000	2800	67	24	2.27056×10^{12}

Figure 5.72: Deflection profile and bending stiffness of Specimen H2

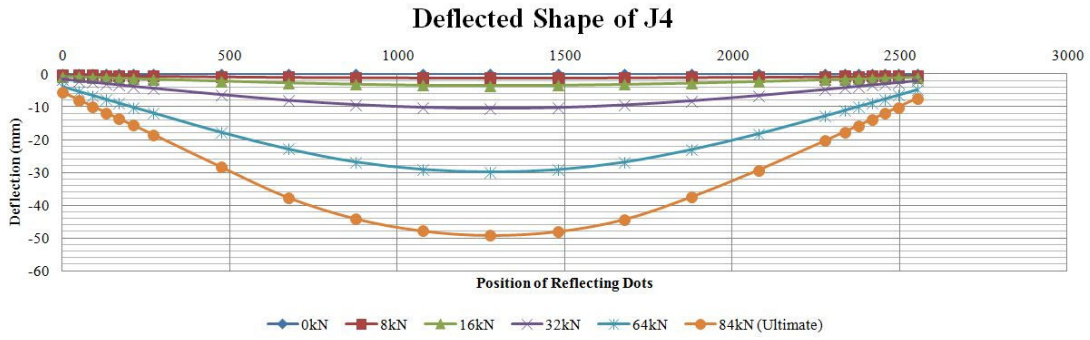

a (mm)	L (mm)	Load, P (kN)	Deflection at Load P, δ (mm)	Bending stiffness, *EI* (Nmm^2)
1000	2800	16	3.5	3.7181×10^{12}
1000	2800	32	10.0	2.60267×10^{12}
1000	2800	64	29.0	1.79494×10^{12}
1000	2800	84	50.0	1.3664×10^{12}

Figure 5.73: Deflection profile and bending stiffness of specimen J4

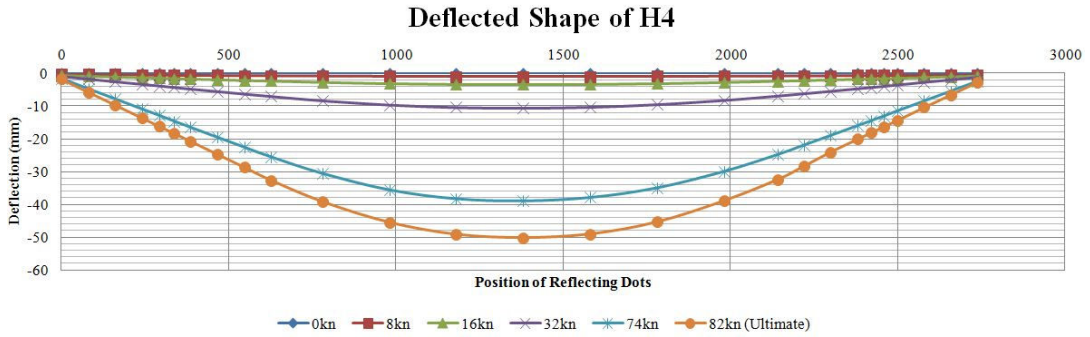

a (mm)	L (mm)	Load, P (kN)	Deflection at Load P, δ (mm)	Bending stiffness, *EI* (Nmm^2)
1000	2800	16	3.5	3.7181×10^{12}
1000	2800	32	10.0	2.60267×10^{12}
1000	2800	74	38.5	1.56329×10^{12}
1000	2800	82	50.0	1.33387×10^{12}

Figure 5.74: Deflection profile and bending stiffness of Specimen H4

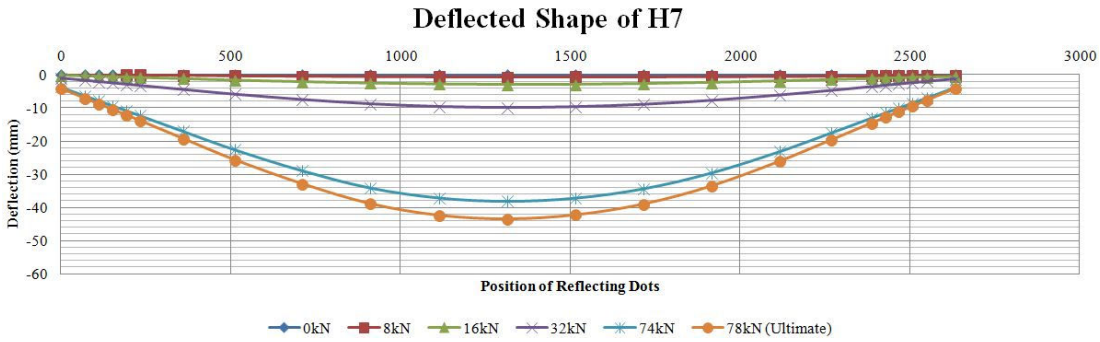

a (mm)	L (mm)	Load, P (kN)	Deflection at Load P, δ (mm)	Bending Stiffness, *EI* (Nmm^2)
1000	2800	16	3.5	3.7181×10^{12}
1000	2800	32	10.0	2.60267×10^{12}
1000	2800	74	38.0	1.58386×10^{12}
1000	2800	78	44.0	1.44182×10^{12}

Figure 5.75: Deflection profile and bending stiffness of specimen H7

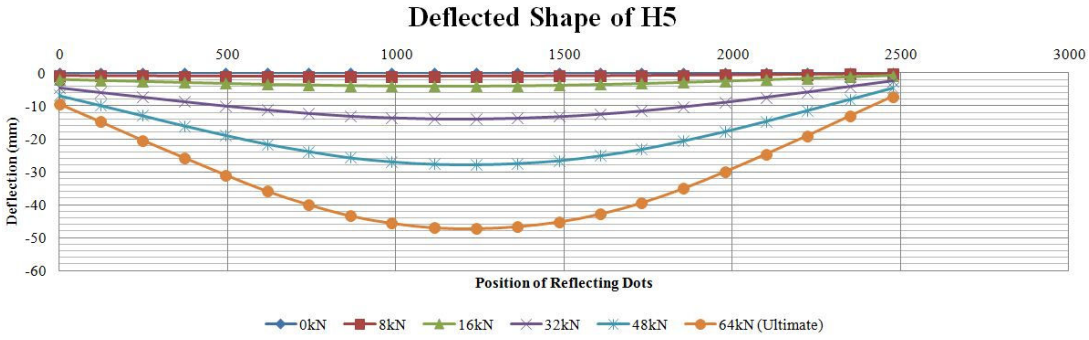

a (mm)	L (mm)	Load, P (kN)	Deflection at Load P, δ (mm)	Bending Stiffness, *EI* (Nmm^2)
1000	2800	16	4	3.25333×10^{12}
1000	2800	32	14	1.85905×10^{12}
1000	2800	48	27	1.44593×10^{12}

Figure 5.76: Deflection profile and bending stiffness of Specimen H5

Due to technical problems with the photogrammetry setup during the flexural testing for Specimen H3, it was not possible to plot the deflection profile of Specimen H3. Hence, the deflection data used in Table 5.5 was extracted from the load versus deflection graph of LVDT.

Table 5.5: Bending stiffness of Specimen H3

a (mm)	L (mm)	Load, P (kN)	Deflection at load P, δ (mm)	Bending stiffness, *EI* (Nmm^2)
1000	2800	16	4	3.25333 x 10^{12}
1000	2800	32	14	1.85905 x 10^{12}
1000	2800	48	26	1.50154 x 10^{12}
1000	2800	64	48	1.08444 x 10^{12}

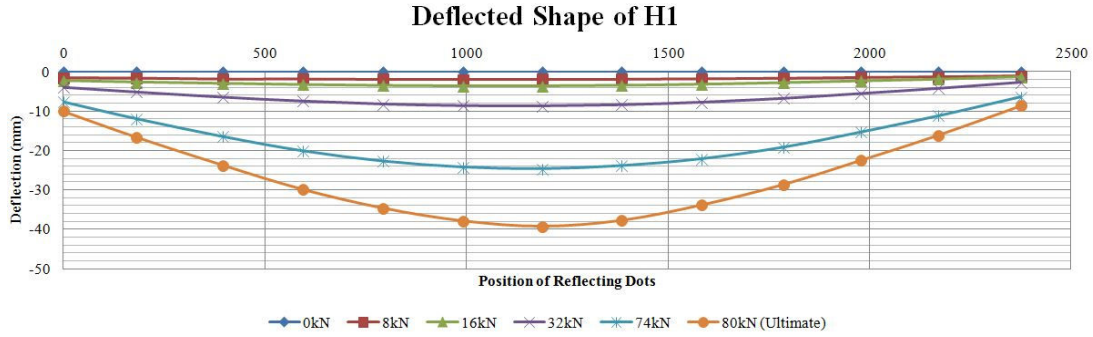

a (mm)	L (mm)	Load, P (kN)	Deflection at load P, δ (mm)	Bending stiffness, *EI* (Nmm^2)
1000	2800	16	3	4.33778 x 10^{12}
1000	2800	32	8	3.25333 x 10^{12}
1000	2800	74	23	2.61681 x 10^{12}
1000	2800	80	36	1.80741 x 10^{12}

Figure 5.77: Deflection profile and bending stiffness of Specimen H1

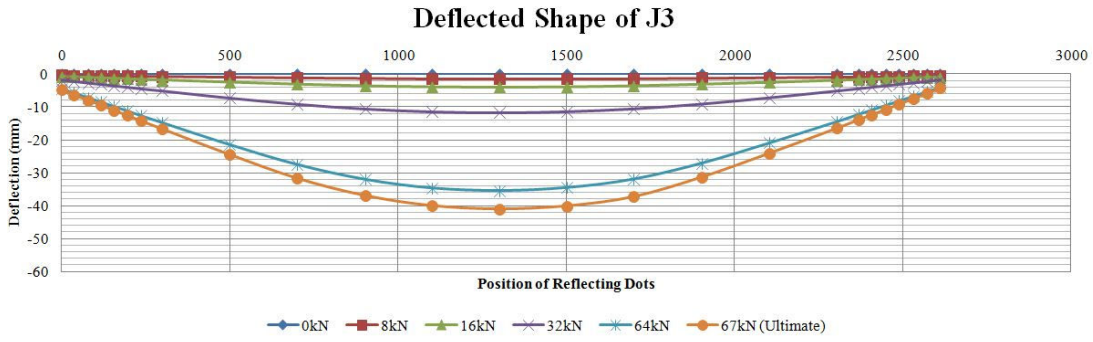

a (mm)	L (mm)	Load, P (kN)	Deflection at load P, δ (mm)	Bending stiffness, *EI* (Nmm^2)
1000	2800	16	4	3.25333 x 10^{12}
1000	2800	32	12	2.16889 x 10^{12}
1000	2800	64	36	1.44593 x 10^{12}
1000	2800	67	40	1.36233 x 10^{12}

Figure 5.78: Deflection profile and bending stiffness of Specimen J3

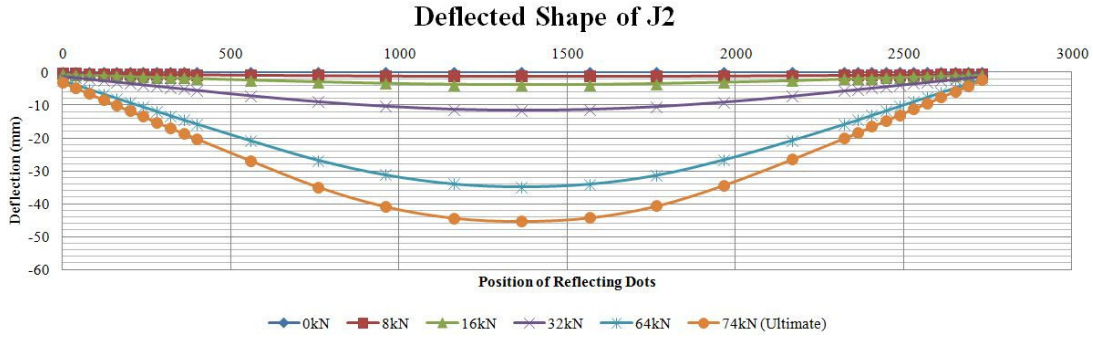

a (mm)	L (mm)	Load, P (kN)	Deflection at load P, δ (mm)	Bending stiffness, *EI* (Nmm^2)
1000	2800	16	4	3.25333×10^{12}
1000	2800	32	12	2.16889×10^{12}
1000	2800	64	35	1.48724×10^{12}
1000	2800	74	46	1.30841×10^{12}

Figure 5.79: Deflection profile and bending stiffness of specimen J2

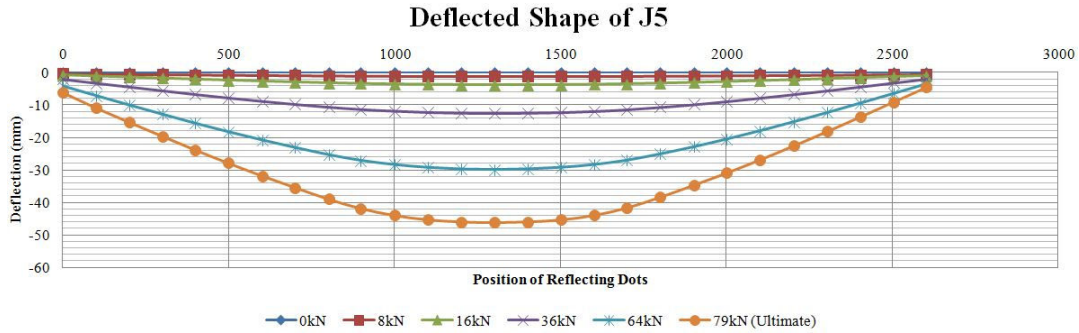

a (mm)	L (mm)	Load, P (kN)	Deflection at load P, δ (mm)	Bending stiffness, *EI* (Nmm^2)
1000	2800	16	4	3.2533×10^{12}
1000	2800	36	12	2.44×10^{12}
1000	2800	64	30	1.73511×10^{12}
1000	2800	79	46	1.39681×10^{12}

Figure 5.80: Deflection profile and bending stiffness of Specimen J5

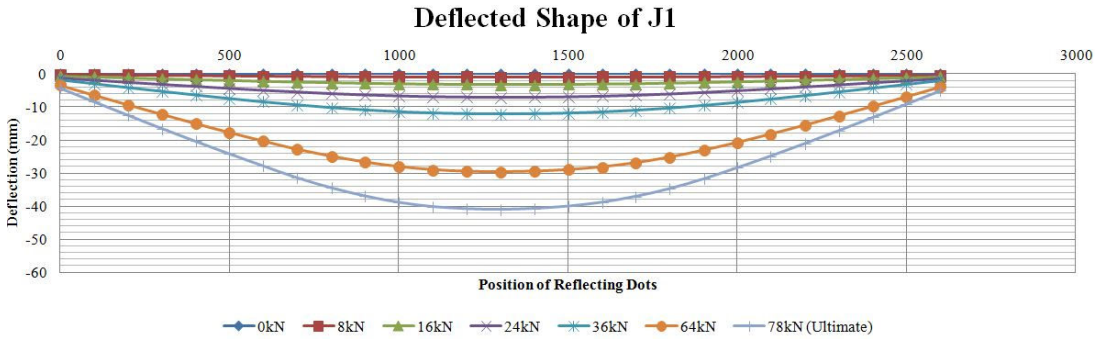

a (mm)	L (mm)	Load, P (kN)	Deflection at load P, δ (mm)	Bending stiffness, *EI* (Nmm^2)
1000	2800	16	4	3.25333 x 10^{12}
1000	2800	36	12	2.44 x 10^{12}
1000	2800	64	30	1.73511 x 10^{12}
1000	2800	78	41	1.54732 x 10^{12}

Figure 5.81: Deflection profile and bending stiffness of Specimen J1

The data above indicates that Specimen H6 showed the least stiffness among all specimens, which was indeed the case as the lower control beam (H6) was not strengthened with any FRP materials. The deflection profiles of Specimens J4, H4 and H7 indicate that all three specimens had the same amount of deflection at the same load magnitudes of 16 kN and 32 kN; therefore, all three had the same bending stiffness (3.7181 x 10^{12} Nmm^2 at 16 kN and 2.60267 x 10^{12} Nmm^2 at 32 kN) as shown in Figures 5.72, 5.73 and 5.74. This indicates that the three specimens strengthened with the same amount of GFRP had the same stiffness. However, due to different anchorage designs, the three beams failed at different load magnitudes.

This was the same for Specimens H5 and H3. Both beams were strengthened with an inner layer of CFRP and an outer layer of GFRP; Specimen H5 was not strengthened with any anchorages, whereas Specimen H3 had V-shaped anchorages at both ends. As shown in Figure 5.75 and Table 5.4, both beams indicated the same bending stiffness (3.25333 x 10^{12} Nmm^2 at 16 kN and 1.85905 x 10^{12} Nmm^2 at 32 kN). However, at 48 kN load, Specimen H5 had an extra 1 mm deflection than did Specimen H3, which shows that Beam H5 had four per cent less stiffness than did Beam H3. Although both beams failed at the same load magnitude of 64 kN, Beam H3 exhibited more deflection due to the anchorages.

This was the same for Specimens J3 and J2. Both beams were strengthened with three layers of CFRP but had different anchorage designs. Both specimens showed the same stiffness at 16 kN and 32 kN (3.25333 x 10^{12} Nmm^2 at 16 kN and 2.16889 x 10^{12} Nmm^2 at 32 kN), as shown in Figures 5.77 and 5.78. At load 64 kN, Specimen J3 showed three per cent less stiffness than did Specimen J2.

Lastly, Specimens J5 and J1, which were strengthened with the same amount of CFRP and fully wrapped with anchorages on the entire length, indicated the same bending stiffness at loads 16 kN, 36 kN and 64 kN (3.25333 x 10^{12} Nmm^2 at 16 kN, 2.44 x 10^{12} Nmm^2 at 36 kN and 1.73511 x 10^{12} Nmm^2 at 64 kN), as shown in Figures 5.79 and 5.80. An overall view of the results indicates that the GFRP-strengthened beams, J4, H4 and H7, had greater stiffness than did the CFRP-strengthened beams, J3 and J2. The GFRP-strengthened beams were 14 per cent stiffer than the CFRP-strengthened beams at load 16 kN. Further, by comparing Beam J4 with Beam J3, where both beams had the same amount of FRP and the same U-shaped anchorage design but J4 was strengthened with GFRP and J3 was strengthened with CFRP, Specimen J4 exhibited a 24 per cent higher level of stiffness than did Specimen J3.

5.7 Summary

Among all 12 specimens, the most noticeable flexural strength gain achieved occurred with Specimen J4, which was a GFRP-strengthened beam with U-shaped end anchorages. It had an unprecedented strength of 84 kN, which is 170 per cent higher than an unstrengthened beam. However, when comparing Specimen J4 with Specimen H4, Specimen H4 showed similar performance but had better ductility. This demonstrates that V-shaped end anchorages are more effective than U-shaped end anchorages, as V-shaped anchorages provide both longitudinal and transverse resistance. This is also in accordance with the results of the flexural bending tests of Specimen J3 and Specimen J2 conducted by Domazetoski. The longitudinal CFRP tore the U-shaped end anchorage of Specimen J3 during the flexural test, as the U-shaped anchorage failed to resist the shear forces. Hence, the V-shaped anchorage in Specimen J2 provided more moment capacity. Therefore, it can be concluded that V-shaped anchorages are superior to U-shaped anchorages.

Comparing Specimens H4 and J2, which had the same configuration and dimensions but different strengthening material, Specimen H4 performed better than Specimen J2. This was expected, as the results of the FRP fabric tensile test (see Chapter 4, Section 4.4) suggest that GFRP has a higher tensile capacity than does CFRP. Specimen H4 was more ductile than Specimen J2, as the failure mode of the latter was extremely brittle.

When comparing the two fully wrapped Specimens J1 and J5 with Specimen J2, a slight 3 to 5 kN increase in flexural strength was gained, but this small improvement does not warrant the expense of fully wrapping the entire length of the beam in CFRP. In the case of the mechanically strengthened Specimen H7, better installation of the steel plate would be beneficial, such as using mechanical fasteners rather than epoxy to form a stronger connection between the steel plate and the concrete surface.

As discussed, hybridisation techniques can improve the ductility of concrete structures. Specimen H3 had the highest ductility index among all of the specimens. The results from this research indicate that further investigation with the aim of improving hybridisation techniques for future applications would be worthwhile.

Chapter 6: Conclusions

This research has investigated and compared the performance of FRP-strengthened beams with different end anchorages. Twelve reinforced concrete beams were constructed for this research. Two beams were tested as control beams and the remaining ten beams were strengthened with FRP with different anchorage configurations. The beams were examined by flexural testing, and the results of the testing demonstrate the efficiency of strengthening with FRP composites when EBR is applied. In those beams strengthened with FRP–EBR systems, the average increase in flexural strength was 140 per cent.

The failure mode of most FRP-reinforced beams was concrete crushing and tensile rupture of the FRP composites. Beams strengthened with EBR systems and anchorage systems either delayed or avoided the debonding of longitudinal FRP laminates.

V-shaped anchorages performed better than U-shaped anchorages, as the inclined component was able to resist both horizontal and vertical forces. Further, it was found that surface preparation before the installation of the FRP was extremely important, affecting the performance of the FRP–EBR systems.

Ductility of the FRP-strengthened beams was reduced due to the brittle failure, constituting a tensile rupture, of the FRP. However, hybridisation techniques with the addition of anchorages were effective at improving the ductility of the beams. GFRP-strengthened beams also indicated better ductility in contrast with CFRP-strengthened beams, as GFRP has better elongation properties than CFRP.

Overall, this research showed that concrete compression failure is fully utilised when the concrete beam is reinforced with FRP fabric. This research has demonstrated that an externally bonded reinforcement system of FRP improves the overall flexural capacity and stiffness of beams.

Chapter 7: Recommendations

This research has shown that strengthening a concrete beam with FRP can increase the beam's flexural capacity. An adequate amount of FRP anchorage can also solve debonding issues. It is recommended that anchorage arrangements be doubly wrapped and inclined (V-shaped), as this enhances the efficiency of the anchorages. Proper preparation and surface roughening can help ensure that the FRP and epoxy resin bond properly, increasing the reliability of the FRP anchorages by helping to prevent secondary failures of the anchorages, such as tensile and shear rupture. However, a major issue with FRP-strengthened concrete beams is ductility, as most FRP-strengthened beams exhibit a non-ductile manner. Hence this research also aimed to solve the ductility issues by introducing the hybridisation method. In this research, the concrete beams were strengthened with a layer of CFRP followed by a layer of GFRP. This research has demonstrated that this method improves the ductility of concrete beams, with very little sacrifice of flexural capacity. Although not creating a benchmark, this aspect of the research does indicate that further investigation may show significant improvements in the area. Therefore, it is recommended that future research and detailed assessments be conducted on the capacity of hybridisation techniques to improve the ductility behaviour of FRP-strengthened concrete beams, as brittle failure in concrete structures is undesirable.

References

Acintha, M., G. Guan and C. Burgoyne. 2010. 'Debonding of FRP Plates'. University of Cambridge. Accessed 5 July. <http://www-civ.eng.cam.ac.uk/cjb/frpdebond/index.html>.

Au, C. 2006. 'Moisture degradation in FRP bonded concrete systems: an interface fracture approach'. PhD Thesis, Department of Civil and Environmental Engineering, Massachusetts Institute of Technology, Cambridge, MA.

Blaschko M. 'Anchorage Device for FRP Strips'. 2001. In *Proceedings of the Fifth Conference on Non-Metallic Reinforcement for Concrete Structures*, *FRPRCS-5, Cambridge, 16–18 July 2001, volume 2*, edited by C. J. Burgoyne, UK, 1255–64. London: Thomas Telford.

Büyüköztürk, O., J. Park, and C. Au. 2003. 'A novel approach to non-destructive evaluation of FRP-confined concrete using microwaves'. In *Proceedings of International Symposium on Non-Destructive Testing in Civil Engineering*, September 16-19, Berlin, Germany.

Büyüköztürk, O., O. Gunes and E. Karaca. 2002. 'Characterization and Modeling of Debonding in RC Beams Strengthened with FRP Composites'. Paper presented at the 15th ASCE Engineering Mechanics Conference, Columbia University, New York, NY, 2–5 June. Accessed 8 August 2011. Ceroni, F. 2010. 'Experimental Performances of RC Beams Strengthened with FRP Materials'. *Construction and Building Materials* 24 (9): 1547–59.

Büyüköztürk, O., O. Gunes, and E. Karaca. 2004. 'Progress on understanding debonding problems in reinforced concrete and steel members strengthened using FRP composites'. Construction and Building Materials, Vol. 18, pp.919.

Büyüköztürk, O. and T.Y. Yu. 2006. 'Understanding and Assessment of Debonding Failures in FRP-Concrete Systems'. Paper presented at the Seventh International Congress on Advances in Civil Engineering, Yildiz Technical University, Istanbul, Turkey, 11–13 October.

Ceroni F. and M. Pecce. 2005. 'Strength and Ductility of RC Beams Strengthened with FRP Sheets under Monotonic and Cyclic Loads'. In *Keep Concrete Attractive: Proceedings of the fib Symposium, Budapest, Hungary, 23 to 25*

May 2005, edited by G. L. Balázs and A. Borosnyoi, 418–23. Budapest: Budapest University of Technology and Economics.

Ceroni F., M. Pecce, S. Matthys and L. Taerwe. 2008. 'Debonding Strength and Anchorage Devices for Reinforced Concrete Elements Strengthened with FRP Sheets'. *Composites Part B: Engineering* 39 (3): 429–41.

Chajes, M. J., T. A. Thomson. Jr, T. F. Januszka and W. W. Finch Jr. 1994. 'Flexural Strengthening of Concrete Beams using Externally Bonded Composite Materials'. *Construction and Building Materials* 8 (3): 191–201.

Chen, J. F. and J. G. Teng. 2001. 'Anchorage Strength Models for FRP and Steel Plates Bonded to Concrete'. *Journal of Structural Engineering* 127 (7): 784–91.

fib 2001. 'Externally Bonded Reinforcement of RC Structures.' Technical Report. fib Bulletin No. 14. Lausanne, Switzerland: Federation International du Beton.

Gunes, O. 2004. 'A Fracture-Based Approach to Understanding Debonding in FRP Bonded Structural Members'. PhD thesis, Department of Civil and Environmental Engineering, Massachusetts Institute of Technology, Cambridge, MA.

Hall J. D., H. R. Schuman and H. R. Hamilton III. 2002. 'Ductile Anchorage for Connecting FRP Strengthening of Under Reinforced Masonry Building'. *ASCE Journal of Composites for Construction* 6 (1): 3–10.

Hashemi, S. H., A. A. Maghsoudi and R. Rahgozar. 2008. 'Flexural Ductility of Reinforced HSC Beams Strengthened with CFRP Sheets'. *Structural Engineering and Mechanics* 30 (4): 403–13.

Jansze, W. 1997. 'Strengthening of Reinforced Concrete Members in Bending by Externally Bonded Steel Plates'. PhD diss., TU Delft.

Jinno Y., H. Tsukagoshi and Y. Yabe. 2001. 'RC Beams with Slabs Strengthened by CF Sheets and Bundles of CF Strands'. In *Proceedings of the 5th International Conference on Fibre-Reinforced Plastics for Reinforced Concrete Structures, FRPRCS-5, Cambridge, 16–18 July 2001*, edited by C. J. Burgoyne, 981–7. London: Thomas Telford.

Karantzikis M., C. G. Papanicolaou, C. P. Antonopoulos and T. C. Triantafillou. 2005. 'Experimental Investigation of Nonconventional Confinement for Concrete using FRP'. *ASCE Journal of Composites for Construction* 9 (6):

480–7.

Koayshi K., S. Fujii, Y. Yabe, H. Tukagoshi and T. Sugiyama. 2001. 'Advanced Wrapping System with CF-Anchor: Stress Transfer Mechanism of CF-Anchor'. In *Proceedings of the 5th International Conference on Fibre-Reinforced Plastics for Reinforced Concrete Structures, FRPRCS-5, Cambridge, 16–18 July 2001*, edited by C. J. Burgoyne, London: Thomas Telford.

Leung, C.K.Y. 2001. 'Delamination failure in concrete beams retrofitted with a bonded plate'. *Journal of Materials in Civil Engineering*, Vol. 13, No. 2, pp.106-113.

Mukhopadhyaya P., N. Swamy and C. Lynsdale. 1998. 'Optimizing Structural Response of Beams Strengthened with GFRP Plates'. *Journal of Composites for Construction* 2 (2): 87–95.

Oehlers, D. J., I. S. T. Liu, R. Seracino and M. S. Mohamed Ali. 2004. 'Prestress Model for Shear Deformation Debonding of FRP- and Steel-Plated RC Beams'. *Magazine of Concrete Research* 56 (8): 475–86.

<http://www.quakewrap.com/frp%20papers/Characterization-And-Modeling-Of-Debonding-In-RC-Beams-Strengthened-With-FRP-Composites.pdf>.

Smith, S.T. and J.G. Teng. 2001. 'Interfacial stresses in plated beams'. *Engineering Structures*, Vol. 23, No. 7, pp.857-871.

Standards Australia. 2009. 'AS 3600-2009'. *Concrete Structures*.

Teng, J. G. and J. Yao. 2007. 'Plate End Debonding in FRP-Plated RC Beams—II: Strength Model.' *Engineering Structures* 29 (10): 2472–86.

Toutanji, H., and G. Ortiz, T. 2001. 'The Effect of Surface Preparation on the Bond Interface between FRP Sheets and Concrete Members.' *Composite Structures* 53 (4): 457–62.

Yao J. and J. G. Teng. 2007. 'Plate End Debonding in FRP-Plated RC Beams—I: Experiments'. *Engineering Structures* 29 (10): 2457–71.

Appendix A: GFRP Technical Data Sheet

Construction

Product Data Sheet
Edition 0507 / 1
SikaWrap®-430G

SikaWrap®-430G

Woven glass fiber fabric for structural strengthening

Product Description

SikaWrap®-430G is a unidirectional woven glass fiber fabric for the dry application process.

Uses

Strengthening of reinforced concrete structures, brickwork and timber to increase flexural and shear load capacity. Reasons:

- Prevention of defects caused by seismic action
- Blast mitigation (accidents or terrorism)
- Improved seismic performance of masonry walls
- Electrical environments that ask for non-conductive material
- Strength and ductility of columns

Characteristics / Advantages

- Manufactured with weft fibers to keep the fabric stable (heat-set process)
- Multifunctional use for every kind of strengthening requirement
- Flexibility of surface geometry (beams, columns, chimneys, piles, walls, silos)
- Approvals available in several countries
- Economical compared to traditional techniques
- Excellent cost performance
- Non conductive

Product Data

Form

Fiber Type

E-glass fibers

Fabric Construction

- Fiber orientation 0° (unidirectional)
- Warp — white glass fibers (99% of total areal weight)
- Weft — white thermoplastic heat-set fibers (1% of total areal weight)

Packaging

	Fabric length / roll	Fabric width
1 roll in cardboard box	≥ 50 m	600 mm

Storage

Storage Conditions / Shelf Life

2 years from the date of production if stored properly in original, unopened and undamaged sealed packaging in dry conditions at temperatures between +5°C and +35°C. Protect from direct sunlight.

Technical Data

Areal Weight	445 ± 22 g/m²
Fabric Design Thickness	0.172 mm (based on total area of glass fibers)
Fiber Density	2.56 g/cm³

Mechanical /Physical Properties

Dry Fiber Properties

Tensile Strength	3,400 N/mm² (measured on virgin filament) 2,300 N/mm² (measured on roving)
Tensile E-Modulus	76,000 N/mm² (nominal)
Elongation at Break	2.8% (measured on roving)

Laminate Properties

Laminate Thickness	0.8 mm/layer (impregnated with Sikadur®-330)
Ultimate Load	270 kN/m width per layer (at typical laminate thickness of 0.8 mm)
Tensile E-modulus	19.0 kN/mm² (based on typical laminate thickness of 0.8 mm)

Note:

The above values are typical and indicative only. The achievable laminate properties obtained from tensile test are dependant on the impregnating /laminating resin used, sample preparation and the type of tensile testing procedure. A loss of 30% for the measured actual strength compared to the theoretical values is possible. Apply material reduction factors according to the relevant design standard.

Design

Design strain:

This value is dependent on the type of loading and must be adapted according to the relevant design standards.

System Information

System Structure

The system configuration as described must be fully complied with and may not be changed.

Concrete primer	Sikadur®-330
Impregnating /laminating resin	Sikadur®-330
Structural strengthening fabric	SikaWrap®-430G

For detailed resin properties, fabric application details and general information, please refer to Sikadur®-330 Product Data Sheet.

Application Details Sikadur®-330

Consumption

Depending on the roughness of the substrate.

First layer including primer	~ 0.8 – 1.4 kg/m²
Following layers	~ 0.6 kg/m²

Substrate Quality

The substrate must be sound and of sufficient tensile strength to provide a minimum pull-off strength of 1.0 N/mm² or as per the requirements of the design specification.

The surface must be dry and free of all contaminants such as oil, grease, coatings and surface treatments, etc.

The surface to be bonded must be level (max. deviation 2 mm per 0.3 m length), with steps and formwork marks not greater than 0.5 mm. High spots can be removed by abrasive blasting or grinding.

Wrapped corners must be rounded to a minimum radius of 20 mm or as per the design specification. This can be achieved by grinding edges or by building up with Sikadur® Mortars.

Substrate Preparation	Concrete and masonry substrates must be prepared mechanically using abrasive blast cleaning or grinding equipment, to remove cement laitance, loose and friable material to achieve a profiled open textured surface. Timber substrates must be planed or sanded. All dust, loose and friable material must be completely removed from all surfaces before application of the Sikadur®-330 preferably by brush and industrial vacuum cleaner. Weak concrete/masonry must be removed and surface defects such as honeycombed areas, blowholes and voids must be fully exposed. Repairs to substrate, filling of blowholes/voids and surface levelling must be carried out using Sikadur®-41 LP or a mixture of Sikadur®-30 and Sikadur®-501 quartz sand (mix ratio 1 : 1 max parts by weight). Bond tests must be carried out to ensure substrate preparation is adequate. Inject cracks wider than 0.25 mm with Sikadur®-52 MY or other suitable Sikadur® injection resin.

Application Instructions

Application Method / Tools	The fabric can be cut with special scissors or a very sharp knife. Never fold the fabric! *Resin Application* Apply the Sikadur®-330 to the prepared substrate using a trowel, roller or brush. *Fabric Placement and Laminating* Place the SikaWrap®-430G fabric in the required direction onto the Sikadur®-330. Carefully work the fabric into the resin with the Sika plastic impregnation roller parallel to the fiber direction until the resin is squeezed out between and through the fiber strands and distributed evenly over the whole fabric surface. Avoid excessive force when laminating to prevent folding or creasing of the SikaWrap®-430G fabric. *Additional Fabric Layers* For additional layers of SikaWrap® -430G fabric, apply Sikadur®-330 to previous applied layer wet on wet within 60 minutes (at +23°C) after application of the previous layer and repeat laminating procedure. If it is not possible to apply within 60 minutes, a waiting time of at least 12 hours must be observed before application of next layer. *Overlays* If a cementitious overlay is to be applied over SikaWrap®-430G fabric an additional Sikadur-330 resin layer must be applied over final layer at a max. 0.5 kg/m^2. Broadcast with quartz sand while wet which will serve as a key for the overlay. If a coloured coating is to be applied, the wet Sikadur®-330 surfaces can be smoothed with a brush. *Overlaps – Fiber Direction* Overlapping of the SikaWrap®-430G fabric must be at least 100 mm or as specified in the strengthening design.
Notes on Application / Limitations	This product may only be used by experienced professionals. The strengthening application is inherently structural and great care must be taken when choosing suitably experienced contractors. Grinding edges or building up with Sikadur® Mortars may be necessary. For side-by-side application, no overlapping length in the weft direction is required. Overlaps of additional layers must be distributed over the column circumference. The SikaWrap®-430G fabric is coated to ensure maximum bond and durability with the Sikadur® Impregnating / laminating resins. To maintain system compatibility do not interchange system parts. The SikaWrap®-430G may be / must be coated with a cementitious overlay or coatings for aesthetic and / or protective purposes. Selection will be dependent on exposure requirements. For basic UV protection use Sikagard®-550W Elastic, Sikagard® ElastoColor-675W or Sikagard®-680S.

Value Base

All technical data stated in this Product Data Sheet are based on laboratory tests. Actual measured data may vary due to circumstances beyond our control.

Construction

Health and Safety Information

For information and advice on the safe handling, storage and disposal of chemical products, users should refer to the most recent Material Safety Data Sheet (available upon request) containing physical, ecological, toxicological and other safety-related data.

Legal Note

The information, and, in particular, the recommendations relating to the application and end-use of Sika products, are given in good faith based on Sika's current knowledge and experience of the products when properly stored, handled and applied under normal conditions in accordance with Sika's recommendations. In practice, the differences in materials, substrates and actual site conditions are such that no warranty in respect of merchantability or of fitness for a particular purpose, nor any liability arising out of any legal relationship whatsoever, can be inferred either from this information, or from any written recommendations, or from any other advice offered. The user of the product must test the product's suitability for the intended application and purpose. Sika reserves the right to change the properties of its products. The proprietary rights of third parties must be observed. All orders are accepted subject to our current terms of sale and delivery. Users must always refer to the most recent issue of the local Product Data Sheet for the product concerned, copies of which will be supplied on request.

Sika Kimia Sdn Bhd
Lot 689 Nilai Industrial Estate
71800 Nilai, Negeri Sembilan DK
MALAYSIA

Phone: +6 06 799 1762
Fax: +6 06 799 1980
e-mail: info@my.sika.com
www.sika.com.my

Construction

Sika Wrap® (Dry)

Carbon fibre fabric strengthening system

Description	Sika Wrap (Dry) is an externally applied carbon fibre strengthening system for reinforced concrete, masonry or timber. It consists of two components, Sikadur-330 epoxy based impregnating resin and Sika Wrap-230C carbon fibre fabric.
Uses	Sika Wrap (Dry) can be used to strengthen reinforced concrete structures, brickwork and timber for flexural and shear loads due to: • Loading increases. • Damage to structural parts. • Changes in structural system. • Design or construction defects. • Earthquake/seismic requirements. Sika Wrap (Dry) can also be used in reprofiling and confinement work on columns, beams and walls as part of a repair and restoration system.
Advantages	• Multifunctional, can be used in bending and in shear. • Low in weight. • Available in any length. • Flexible, fits around any given structural element. • Excellent chemical and weathering resistance. • Low overall thickness. • Economic application. • Easy to use solvent free impregnating resin.
Storage and Shelf Life	When not exposed to direct sunlight, Sika Wrap-230C has unlimited shelf life. Sikadur-330, when stored in the original sealed containers within the temperature range of +5°C to +25°C, this product will keep for a minimum of eighteen (18) months.
Instructions for Use	
Surface Preparation	The substrate should be prepared by sandblasting or grinding. Any dust, loose particles and laitance should be removed using an industrial vacuum cleaner. The substrate should be free of grease and oil and have a maximum moisture content of 4%. The surface to be bonded must be level. Steps and formwork marks should be no greater than 0.5mm. Structural corners should be rounded to a radius of at least 10mm. This can be achieved using a diamond grinding disk.
Mixing	Sikadur-330 is supplied in factory proportioned units comprising the correct quantities of Park A and Part B. Thoroughly stir both components separately using a slow running drill/stirrer with a helical paste mixer (max. speed 600rpm).
Application	If any necessary patching work needs to be done on the surface, this must be done with Sikadur-41, on the day preceding the actual bonding operations. Application of the Sika Wrap (Dry) system can be broken up into 4 steps. 1. Apply the well mixed Sikadur-330 to the prepared substrate by lamb skin roller. This seals the substrate and promotes adhesion. 2. Place Sika Wrap-230C onto the resin coating in the required direction. Carefully work the fabric into the resin with a plastic roller until the resin is squeezed out between the rovings. 3. Application of more than one layer of fabric – apply more resin, as in step1. This must be done within 1 hour (at 20°C) after the application of the previous layer. If this is not possible, a waiting time of at least 12 hours must be observed before the next layer is applied. Apply the next layer as in step 2. 4. The system can be coated using Sikadur or Sikagard coating for protective or aesthetic purposes.

Construction

Cleaning	Clean all tools immediately after use with Sika Colma Cleaner. Wash hands and skin thoroughly in warm soapy water. Cured material can only be removed mechanically.
Technical Data (Typical)	
Sika Wrap-230C	**Carbon Fibre Fabric**
Form	High strength carbon fibres
Colour	Black
Weight	225g/m²
Thickness	0.13mm (based on total area of carbon fibres)
Tensile strength	3500 MPa
Tensile Elastic Modulus	230 000 MPa
Elongation at Break	1.5%
Packaging	Supplied in 500 mm width Length 100 m 300 mm and 600 mm widths available on request
Sikadur-330	**Impregnation**
Appearance	Part A: White Part B: Grey Part A + B: Light Grey when mixed
Mix Ratio	A : B = 4 : 1 by weight
Density	1.31 kg / litre (A+B)
Pot Life	90 minutes (at 15°C) 30 minutes (at 35°C)
Open Time	30 minutes (at 35°C)
Viscosity	Paste like
Adhesive Strength	>1.5 MPa (concrete failure)
Tensile Strength	30 MPa (cured 7 days at 23°C)
Flexural E-Modulus	3800 MPa (cured 7 days at 23°C)
Application Temperature	5°C to 35°C (ambient and substrate)
Packaging	5 kg tins Part A = 4 kg Part B = 1 kg
Consumption Rates	• Applying Sikadur-330 to prepared substrate 0.7 to 1.2kg/m². • Applying Sikadur-330 to applied fabric 0.5kg/m².
Design	• Design calculations must be made and certified by an independent consulting structural engineer. • For design details refer to Sika's Structural Strengthening Engineering Guidelines.
Important Notes	• If required on site, the fabric can be cut by sharp scissors or knife. Never fold the material. • When overlapping, the fabric must extend at least 100mm over the applied fabric (in the fibre direction). • Overlapping is not necessary when placing several fabric webs side by side. • At low temperatures and/or high humidity, the surface of the epoxy and the fabric may become sticky. Before a further coat of adhesive or layer of fabric is applied, the stickiness must be removed with a water soaked sponge, followed by rinsing with plenty of water. • Prevent exposure of the carbon fabric to constant U.V. light. • Ambient temperature during application must be at least 3°C above dew point. • Constant exposure to service temperatures >50°C may affect the performance of the product.

Construction

Handling Precautions	• Avoid contact with the skin, eyes and avoid breathing it's vapour. • Wear protective gloves when mixing or using. • If poisoning occurs, contact a doctor or the Poisons Information Centre. • If swallowed, do NOT induce vomiting. Give a glass of water. • If skin contact occurs, remove contaminated clothing and wash skin thoroughly. • If in eyes, hold eyes open, flood with water for at least 15 minutes and see a doctor.
Important Notification	The information, and, in particular, the recommendations relating to the application and end-use of Sika's products, are given in good faith based on Sika's current knowledge and experience of the products when properly stored, handled and applied under normal conditions. . In practice, the differences in materials, substrates and actual site conditions are such that no warranty in respect of merchantability or of fitness for a particular purpose, nor any liability arising out of any legal relationship whatsoever, can be inferred either from this information, or from any written recommendations, or from any other advice offered. The proprietary rights of third parties must be observed. All orders are accepted subject of our terms and conditions of sale. Users should always refer to the most recent issue of the Technical Data Sheet for the product concerned, copies of which will be supplied on request. PLEASE CONSULT OUR TECHNICAL DEPARTMENT FOR FURTHER INFORMATION.

Appendix B: GFRP Material Safety Data Sheet

Material Safety Data Sheet

1 . Identification of the material and supplier

Names

Product name	:	SikaWrap (all types)

Supplier

Supplier/Manufacturer	:	Sika Australia Pty. Ltd. 55 Elizabeth Street (Locked Bag 482 BDC) Wetherill Park, NSW 2164 Australia
Telephone no.	:	+61 2 9725 11 45
Fax no.	:	+61 2 9725 33 30
Emergency telephone number	:	+61 1800 033 111
Use of the substance/preparation		Chemical product for construction and industry

2 . Hazards identification

Classification	:	Not regulated.
Risk phrases	:	Not classified.
Statement of hazardous/dangerous nature	:	NON-HAZARDOUS SUBSTANCE. NON-DANGEROUS GOODS.

3 . Composition/information on ingredients

Mixture	:	Yes.

Other ingredients, determined not to be hazardous according to NOHSC criteria, and not dangerous according to the ADG Code, make up the product concentration to 100%.

There are no ingredients present which, within the current knowledge of the supplier and in the concentrations applicable, are classified as hazardous to health or the environment and hence require reporting in this section.

4 . First aid measures

First aid measures

Inhalation	:	Move exposed person to fresh air. Keep person warm and at rest. If not breathing, if breathing is irregular or if respiratory arrest occurs, provide artificial respiration or oxygen by trained personnel. Get medical attention if symptoms occur.
Ingestion	:	Wash out mouth with water. Move exposed person to fresh air. Keep person warm and at rest. If material has been swallowed and the exposed person is conscious, give small quantities of water to drink. Do not induce vomiting unless directed to do so by medical personnel. Get medical attention if symptoms occur.
Skin contact	:	Flush contaminated skin with plenty of water. Remove contaminated clothing and shoes. Get medical attention if symptoms occur.
Eye contact	:	Immediately flush eyes with plenty of water, occasionally lifting the upper and lower eyelids. Check for and remove any contact lenses. Continue to rinse for at least 10 minutes. Get medical attention if irritation occurs.
Protection of first-aiders	:	No action shall be taken involving any personal risk or without suitable training.
Notes to physician	:	No specific treatment. Treat symptomatically. Contact poison treatment specialist immediately if large quantities have been ingested or inhaled.

5 . Fire-fighting measures

Extinguishing media

Suitable	:	Use an extinguishing agent suitable for the surrounding fire.
Not suitable	:	None known.
Special exposure hazards	:	Promptly isolate the scene by removing all persons from the vicinity of the incident if there is a fire. No action shall be taken involving any personal risk or without suitable training.

5 . Fire-fighting measures

No specific fire or explosion hazard.

Special protective equipment for fire-fighters : Fire-fighters should wear appropriate protective equipment and self-contained breathing apparatus (SCBA) with a full face-piece operated in positive pressure mode.

Hazardous combustion products : No specific data.

Special protective equipment for fire-fighters : Fire-fighters should wear appropriate protective equipment and self-contained breathing apparatus (SCBA) with a full face-piece operated in positive pressure mode.

6 . Accidental release measures

Personal precautions : No action shall be taken involving any personal risk or without suitable training. Evacuate surrounding areas. Keep unnecessary and unprotected personnel from entering. Do not touch or walk through spilled material. Put on appropriate personal protective equipment (see section 8).

Environmental precautions : Avoid dispersal of spilled material and runoff and contact with soil, waterways, drains and sewers. Inform the relevant authorities if the product has caused environmental pollution (sewers, waterways, soil or air).

Large spill : Move containers from spill area. Prevent entry into sewers, water courses, basements or confined areas. Vacuum or sweep up material and place in a designated, labeled waste container. Dispose of via a licensed waste disposal contractor. Note: see section 1 for emergency contact information and section 13 for waste disposal.

Small spill : Move containers from spill area. Vacuum or sweep up material and place in a designated, labeled waste container. Dispose of via a licensed waste disposal contractor.

7 . Handling and storage

Handling : Put on appropriate personal protective equipment (see section 8). Eating, drinking and smoking should be prohibited in areas where this material is handled, stored and processed. Workers should wash hands and face before eating, drinking and smoking.

Storage : Store in accordance with local regulations. Store in original container protected from direct sunlight in a dry, cool and well-ventilated area, away from incompatible materials (see section 10) and food and drink. Keep container tightly closed and sealed until ready for use. Containers that have been opened must be carefully resealed and kept upright to prevent leakage. Do not store in unlabeled containers. Use appropriate containment to avoid environmental contamination.

8 . Exposure controls/personal protection

Occupational exposure limits : **No exposure standard allocated.**

Recommended monitoring procedures : If this product contains ingredients with exposure limits, personal, workplace atmosphere or biological monitoring may be required to determine the effectiveness of the ventilation or other control measures and/or the necessity to use respiratory protective equipment.

Exposure controls

Engineering measures : No special ventilation requirements. Good general ventilation should be sufficient to control worker exposure to airborne contaminants. If this product contains ingredients with exposure limits, use process enclosures, local exhaust ventilation or other engineering controls to keep worker exposure below any recommended or statutory limits.

Hygiene measures : Wash hands, forearms and face thoroughly after handling chemical products, before eating, smoking and using the lavatory and at the end of the working period. Appropriate techniques should be used to remove potentially contaminated clothing. Wash contaminated clothing before reusing. Ensure that eyewash stations and safety showers are close to the workstation location.

Eyes : Safety eyewear complying with an approved standard should be used when a risk assessment indicates this is necessary to avoid exposure to liquid splashes, mists or dusts.

8 . Exposure controls/personal protection

Hands : Chemical-resistant, impervious gloves complying with an approved standard should be worn at all times when handling chemical products if a risk assessment indicates this is necessary.

Respiratory : Use a properly fitted, air-purifying or air-fed respirator complying with an approved standard if a risk assessment indicates this is necessary. Respirator selection must be based on known or anticipated exposure levels, the hazards of the product and the safe working limits of the selected respirator.

Skin : Personal protective equipment for the body should be selected based on the task being performed and the risks involved and should be approved by a specialist before handling this product.

Environmental exposure controls : Emissions from ventilation or work process equipment should be checked to ensure they comply with the requirements of environmental protection legislation. In some cases, fume scrubbers, filters or engineering modifications to the process equipment will be necessary to reduce emissions to acceptable levels.

9 . Physical and chemical properties

Physical state : Solid. [Fibrous solid.]

Color : Various

Odor : Odorless.

Density : 1.4 to 2.6 g/cm^3 [20°C (68°F)]

Flash point : Closed cup: Not applicable.

Solubility : Insoluble in the following materials: cold water.

10 . Stability and reactivity

Stability : The product is stable.

Conditions to avoid : No specific data.

Materials to avoid : No specific data.

Hazardous decomposition products : Under normal conditions of storage and use, hazardous decomposition products should not be produced.

11 . Toxicological information

Potential acute health effects

Inhalation : No known significant effects or critical hazards.

Ingestion : No known significant effects or critical hazards.

Skin contact : No known significant effects or critical hazards.

Eye contact : No known significant effects or critical hazards.

Acute toxicity

Conclusion/Summary : Not available.

Potential chronic health effects

Chronic toxicity

Conclusion/Summary : Not available.

Carcinogenicity

Conclusion/Summary : Not available.

Mutagenicity

Conclusion/Summary : Not available.

Teratogenicity

Conclusion/Summary : Not available.

Reproductive toxicity

Conclusion/Summary : Not available.

Chronic effects : No known significant effects or critical hazards.

Carcinogenicity : No known significant effects or critical hazards.

Mutagenicity : No known significant effects or critical hazards.

Teratogenicity : No known significant effects or critical hazards.

Developmental effects : No known significant effects or critical hazards.

Fertility effects : No known significant effects or critical hazards.

11 . Toxicological information

Over-exposure signs/symptoms

Inhalation : No specific data.

Ingestion : No specific data.

Skin : No specific data.

Eyes : No specific data.

12 . Ecological information

Environmental effects : No known significant effects or critical hazards.

Aquatic ecotoxicity

Conclusion/Summary : Not available.

Other ecological information

Biodegradability

Conclusion/Summary : Not available.

Other adverse effects : No known significant effects or critical hazards.

13 . Disposal considerations

Methods of disposal : The generation of waste should be avoided or minimized wherever possible. Empty containers or liners may retain some product residues. This material and its container must be disposed of in a safe way. Dispose of surplus and non-recyclable products via a licensed waste disposal contractor. Disposal of this product, solutions and any by-products should at all times comply with the requirements of environmental protection and waste disposal legislation and any regional local authority requirements. Avoid dispersal of spilled material and runoff and contact with soil, waterways, drains and sewers.

14 . Transport information

ADG

Not regulated.

ADG Class : -

Label No. :

ADR

Not regulated.

IMDG

Not regulated.

Marine pollutant : No.

IATA

Not regulated.

15 . Regulatory information

Standard for the Uniform Scheduling of Drugs and Poisons

Not regulated.

Control of Scheduled Carcinogenic Substances

Ingredient name	Schedule
No listed substance	

Australia inventory (AICS) : All components are listed or exempted.

EU Classification : Not classified.

16 . Other information

Person who prepared the MSDS : Validated by Englert on 09.02.2009.

Date of previous issue : **No previous validation.**

Indicates information that has changed from previously issued version.

Disclaimer

Material Safety Data Sheets are updated frequently. Please ensure that you have a current copy. MSDS may be obtained from the following website: www.sika.com.au

The information contained in this Safety Data Sheet corresponds to our level of knowledge at the time of publication. All warranties are excluded. Our most current General Sales Conditions shall apply. Please consult the Technical Data Sheet prior to any use and processing.

Appendix C: Tensile Test Report of Steel Reinforcement

Melbourne Testing Services

Unit 1/15 Pickering Road
Mulgrave Vic 3170
Telephone: 9560 2759
Mobile: 0419 116 733

Tensile Test Report

Report No:	MT-10/515-N10	**Client:**	Curtin University
Report Date:	13-Sep-10		Department of Civil Engineering
Specimen I.D.	N10		GPO Box U1987
Testing Machine:	TE Machine		PERTH WA 6845

TEST DETAILS				
Test Date/Number:	***11/09/2010***		1	2
Curtin Sample I.D.			1	7
Extensometer Gauge Length:	L_e	(mm)	50.00	50.00
SPECIMEN DETAILS				
Nominal Diameter:	d	(mm)	10.00	10.00
Nominal Area:	S_o	(mm^2)	78.54	78.54
TENSILE PROPERTIES				
Tensile Strength:	R_m	(MPa)	677	670
Proof Stress:	$R_{p0.2}$	(MPa)	567	551
Ratio:	$R_m / R_{p0.2}$	(MPa)	1.19	1.22
Uniform Elongation:	A_{gt}	(%)	7.7	10.0
Uniform Elongation:	$A_{gt0.5\ drop}$	(%)	8.4	11.3

Test Comments:
Tested in accordance with
AS 1391-2007.

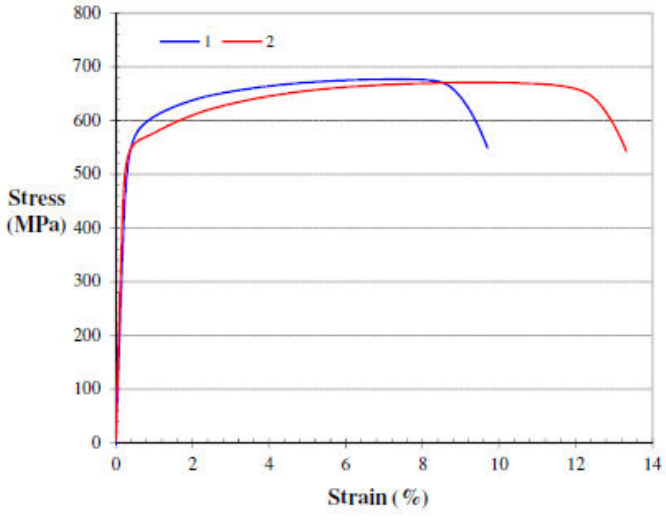

Rodney Wilkie
Authorised Signatory

Melbourne Testing Services

Unit 1/15 Pickering Road
Mulgrave Vic 3170
Telephone: 9560 2759
Mobile: 0419 116 733

Tensile Test Report

Report No: MT-10/515-N12
Report Date: 13-Sep-10
Specimen I.D. N12
Testing Machine: TE Machine

Client: Curtin University
Department of Civil Engineering
GPO Box U1987
PERTH WA 6845

TEST DETAILS

			1	2	3	4	5	6	7	8
Test Date/Number:	*11/09/2010*									
Curtin Sample I.D.			2	3	6	12	I1815	H	13	15
Extensometer Gauge Length:	L_e	(mm)	50							

SPECIMEN DETAILS

Nominal Diameter:	d	(mm)	10							
Nominal Area:	S_o	(mm^2)	113							

TENSILE PROPERTIES

Tensile Strength:	R_m	(MPa)	689	700	698	699	688	648	710	693
Proof Stress:	$R_{p0.2}$	(MPa)	531	537	535	535	574	538	637	644
Ratio:	$R_m / R_{p0.2}$	(MPa)	1.30	1.30	1.31	1.31	1.20	1.21	1.12	1.08
Uniform Elongation:	A_{gt}	(%)	12.5	12.5	13.4	13.5	7.7	7.5	8.3	6.7
Uniform Elongation:	$A_{gt0.5\ drop}$	(%)	14.2	15.0	14.7	15.0	8.5	8.1	9.0	7.2

Test Comments:
Tested in accordance with
AS 1391-2007.

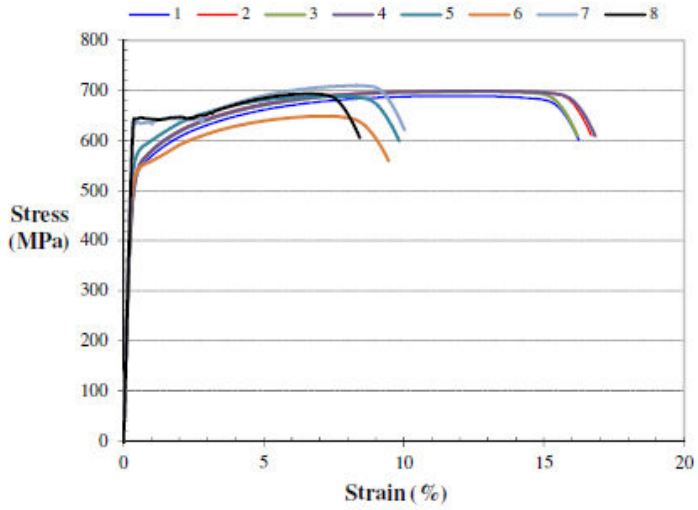

Rodney Wilkie
Authorised Signatory

Melbourne Testing Services
ABN: 71353261540

Melbourne Testing Services

Unit 1/15 Pickering Road
Mulgrave Vic 3170
Telephone: 9560 2759
Mobile: 0419 116 733

Tensile Test Report

Report No: MT-10/515-N20
Report Date: 13-Sep-10
Specimen I.D. N20
Testing Machine: TE Machine

Client: Curtin University
Department of Civil Engineering
GPO Box U1987
PERTH WA 6845

TEST DETAILS

Test Date/Number:			***11/09/2010***	1	2	3	4	5
Curtin Sample I.D.				2	4	4	5	6
Extensometer Gauge Length:	L_e	(mm)	50					
SPECIMEN DETAILS								
Nominal Diameter:	d	(mm)	20					
Nominal Area:	S_o	(mm^2)	314					
TENSILE PROPERTIES								
Tensile Strength:	R_m	(MPa)	658	666	657	660	666	
Proof Stress:	$R_{p0.2}$	(MPa)	568	579	562	563	577	
Ratio:	$R_m / R_{p0.2}$	(MPa)	1.16	1.15	1.17	1.17	1.15	
Uniform Elongation:	A_{gt}	(%)	11.6	11.9	14.2	13.6	12.9	
Uniform Elongation:	$A_{gt0.5\,drop}$	(%)	13.8	13.3	15.2	15.1	14.2	

Test Comments:
Tested in accordance with
AS 1391-2007.

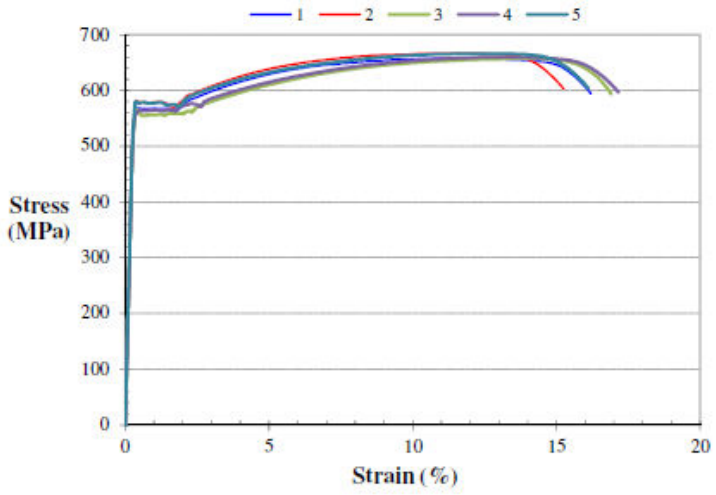

Rodney Wilkie
Authorised Signatory

Melbourne Testing Services
ABN: 71353261540

Appendix D: Sample Calculation of Flexural Capacity (Initial Design)

Flexural Capacity Sample Calculation (Initial Design)

H6 (Lower Control Beam)

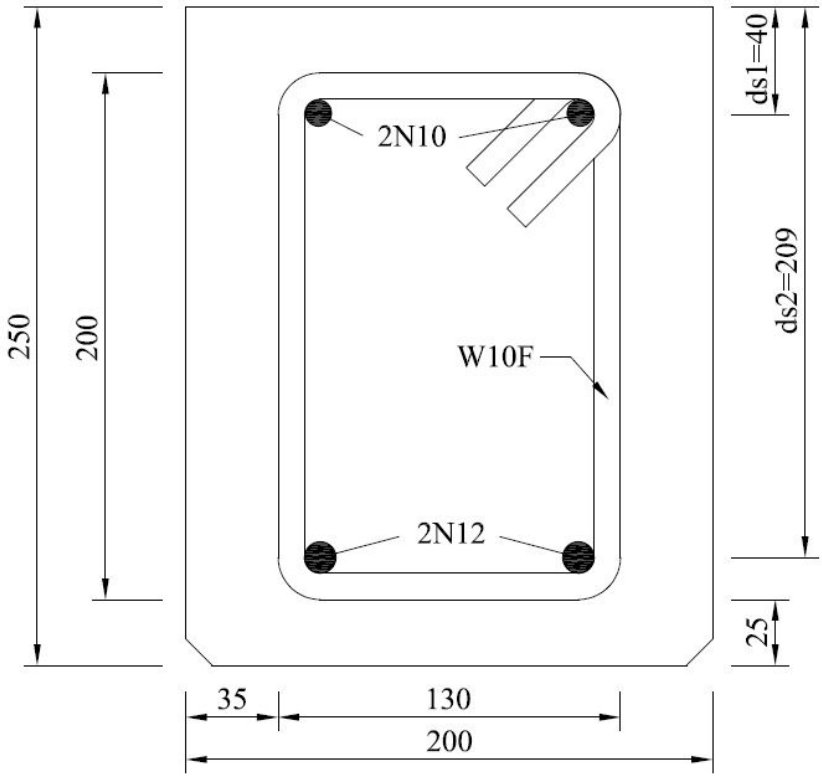

Steel

Area of steel, 2N10, A_{s1} = 157 mm^2

Area of steel, 2N12, A_{s2} = 226 mm^2

Elastic modulus of steel = 200000 MPa (nominal)

Yield strength of steel, f_{yv} = 550 MPa (nominal)

Concrete

Cover = 25mm (nominal), Side= 35mm (nominal)

Compressive strength of concrete, f'_{cm} = 40 MPa (nominal)

d_{s1} = 40mm

d_{s2} = 209mm

Compressive flange width, B = 200mm

Rectangular stress block < 8.1.2.2 >

$\gamma = 0.85 - 0.007(f'_{cm} - 28) = 0.766$

Assumption:

Top steel in tension and not at yield.

Bottom steel in tension and has yielded.

Tension of bottom steel,

$T_{s2} = A_{s2} \times f_{yv}$

$T_{s2} = 226 \times 550$

$T_{s2} = 124300\ N$

Concrete compression force,

$C_c = 0.85 \times f'_c \times B \times \gamma \times d_n$

$C_c = 0.85 \times 40 \times 200 \times 0.766 \times d_n$

$C_c = 5208.8 d_n$

Tension of top steel,

$T_{s1} = A_{s1} \times \sigma_{sc}$

$T_{s1} = A_{s1} \times \varepsilon_{s1} \times E_s$

$T_{s1} = 0.003 \times \left(\frac{d_{s1} - d_n}{d_n}\right) \times E_s \times A_{s1}$

$T_{s1} = 0.003 \times \left(\frac{d_{s1} - d_n}{d_n}\right) \times 200000 \times 157$

$T_{s1} = 94200 \times \left(\frac{40 - d_n}{d_n}\right)$

Determining d_n

$T_{s2} + T_{s1} = C_c$

$124300 + 94200\left(\frac{40 - d_n}{d_n}\right) = 5208.8 d_n$

$5208.8 {d_n}^2 - 30100 d_n - 3768000 = 0$

$d_n = 29.9mm$

Hence, $k_u = \frac{29.9}{250} = 0.12 < 0.4 \quad \therefore Ductile$

Check steel yielding

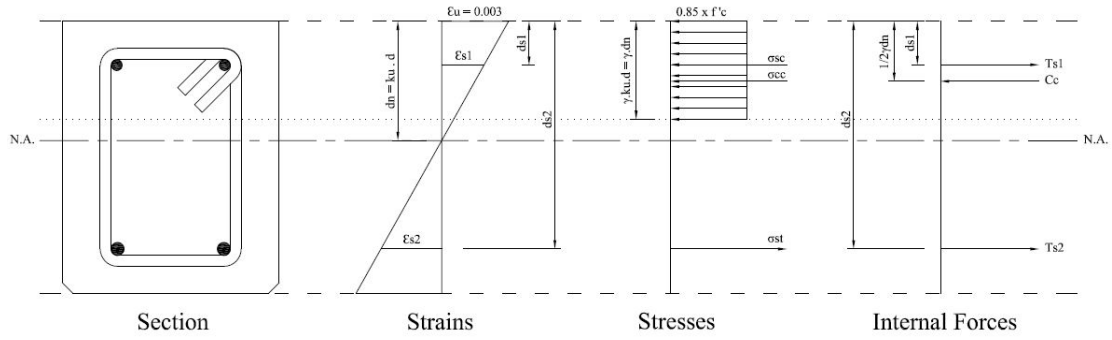

$$\varepsilon_{yield} = \frac{550}{200000} = 0.00275$$

$$\varepsilon_{s1} = 0.003 \times \left(\frac{d_{s1} - d_n}{d_n}\right) = 0.00101 < 0.00275 \quad \therefore OK, not\ yield.$$

$$\varepsilon_{s2} = 0.003 \times \left(\frac{d_{s2} - d_n}{d_n}\right) = 0.018 > 0.00275 \quad \therefore OK, yield.$$

Moment capacity

$$M_u = T_{s2} \times d_{s2} + T_{s1} \times d_{s1} - C_c \times \frac{\gamma d_n}{2}$$

$$M_u = 124300 \times 209 + 94200 \times \left(\frac{d_{s1} - d_n}{d_n}\right) \times d_{s1} - 5740.6 \times \frac{0.766{d_n}^2}{2}$$

$$M_u = 124300 \times 209 + 94200 \times \left(\frac{40 - 29.9}{29.9}\right) \times 40 - 5208.8 \times \frac{0.766 \times 29.9^2}{2}$$

$$M_u = \ 25467979 \text{ Nmm}$$

$$M_u = \ 25.5 \text{ kNm}$$

Design shear load

$M_u = P_u = Load\ in\ one\ jack = 25.5\ kN$

Hence, the shear capacity has to be above the design shear load.

Shear capacity > 1.5 x 25.5 = 38.25 kN

Flexural Capacity Sample Calculation (Initial Design)

H2 (Upper Control Beam)

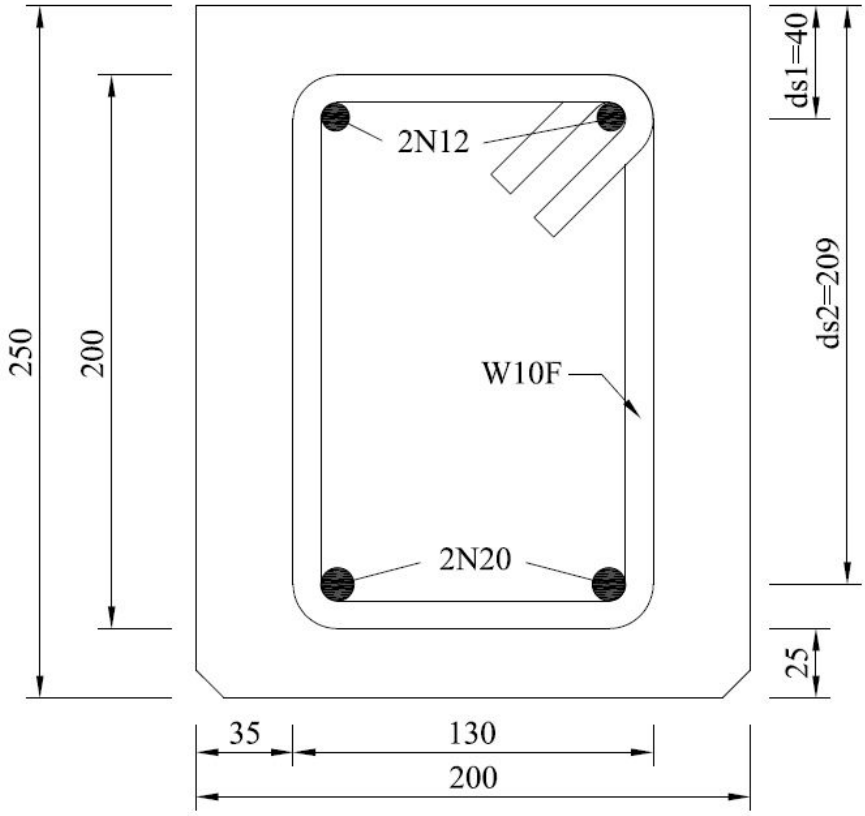

Steel

Area of steel, 2N10, A_{s1} = 226 mm^2

Area of steel, 2N12, A_{s2} = 628 mm^2

Elastic modulus of steel = 200000 MPa (nominal)

Yield strength of steel, f_{yv} = 550 MPa (nominal)

Concrete

Cover = 25mm (nominal), Side= 35mm (nominal)

Compressive strength of concrete, f'_{cm} = 40 MPa (nominal)

d_{s1} = 41mm

d_{s2} = 205mm

Compressive flange width, B = 200mm

Rectangular stress block < 8.1.2.2 >

$\gamma = 0.85 - 0.007(f'_{cm} - 28) = 0.766$

Assumption:

Top steel in compression and not at yield.

Bottom steel in tension and has yielded.

Tension of bottom steel,

$T_{s2} = A_{s2} \times f_{yv}$

$T_{s2} = 628 \times 550$

$T_{s2} = 345400\ N$

Concrete compression force,

$C_c = 0.85 \times f'_c \times B \times \gamma \times d_n$

$C_c = 0.85 \times 40 \times 200 \times 0.766 \times d_n$

$C_c = 5208.8 d_n$

Compression of top steel,

$C_{s1} = A_{s1} \times \sigma_{sc}$

$C_{s1} = A_{s1} \times \varepsilon_{s1} \times E_s$

$C_{s1} = 0.003 \times \left(\frac{d_n - d_{s1}}{d_n}\right) \times E_s \times A_{s1}$

$C_{s1} = 0.003 \times \left(\frac{d_n - d_{s1}}{d_n}\right) \times 200000 \times 226$

$C_{s1} = 135600 \times \left(\frac{d_n - 41}{d_n}\right)$

Determining d_n

$T_{s2} = C_{s1} + C_c$

$345400 = 135600\left(\frac{41 - d_n}{d_n}\right) + 5208.8 d_n$

$5208.8 {d_n}^2 - 481000 d_n + 5559600 = 0$

$d_n = 78.8\ mm$

Hence, $k_u = \frac{78.8}{250} = 0.32 < 0.4 \quad \therefore Ductile$

Check steel yielding

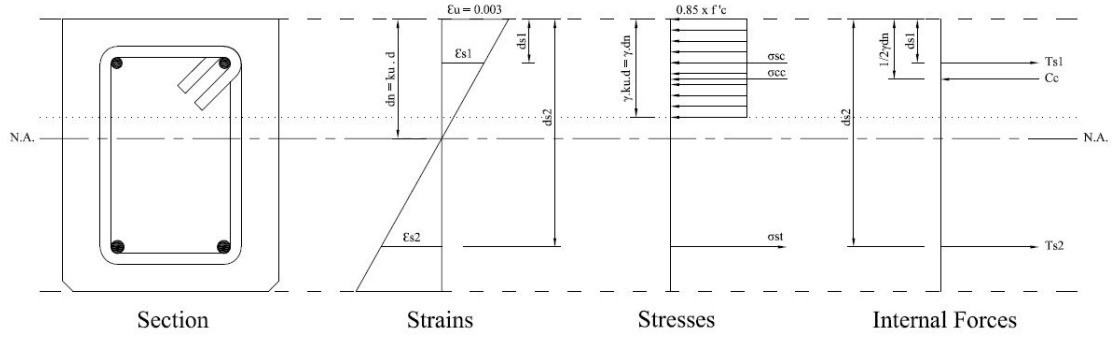

$$\varepsilon_{yield} = \frac{550}{200000} = 0.00275$$

$$\varepsilon_{s1} = 0.003 \times \left(\frac{d_n - d_{s1}}{d_n}\right) = 0.00144 < 0.00275 \qquad \therefore OK, not\ yield.$$

$$\varepsilon_{s2} = 0.003 \times \left(\frac{d_{s2} - d_n}{d_n}\right) = 0.0048 > 0.00275 \qquad \therefore OK, yield.$$

Moment capacity

$$M_u = T_{s2} \times d_{s2} - C_{s1} \times d_{s1} - C_c \times \frac{\gamma d_n}{2}$$

$$M_u = 345400 \times 205 - 135600 \times \left(\frac{d_n - d_{s1}}{d_n}\right) \times d_{s1} - 5208.8 \times \frac{0.766{d_n}^2}{2}$$

$$M_u = 345400 \times 205 + 135600 \times \left(\frac{78.8 - 41}{78.8}\right) \times 41 - 5208.8 \times \frac{0.766 \times 78.8^2}{2}$$

$$M_u = 61086266 \text{ Nmm}$$

$$M_u = 61.1 \text{ kNm}$$

Design shear load

$$M_u = P_u = Load\ in\ one\ jack = 61.1\ kN$$

Hence, the shear capacity has to be above the design shear load.

Shear capacity > 1.5 x 61.1 = 91.65 kN

Flexural Capacity Sample Calculation (Initial Design)

J4 (U-shaped GFRP-strengthened Beam)

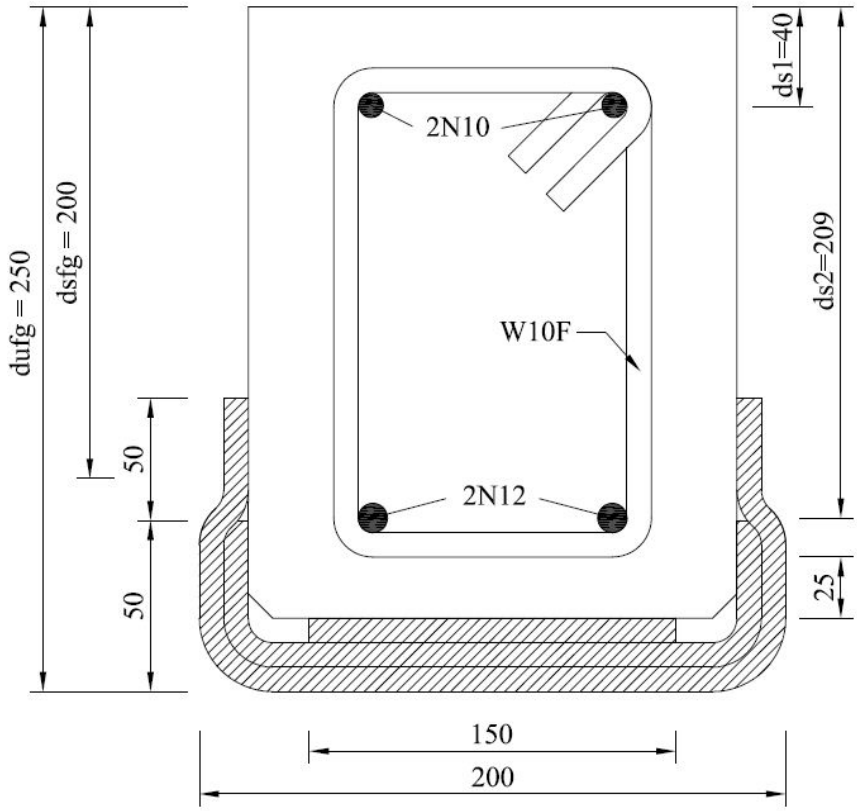

Steel

Area of steel, 2N10, A_{s1} = 157 mm^2

Area of steel, 2N12, A_{s2} = 226 mm^2

Elastic modulus of steel = 200000 MPa (nominal)

Yield strength of steel, f_{yv} = 550 MPa (nominal)

Concrete

Cover = 25mm (nominal), Side= 35mm (nominal)

Compressive strength of concrete, f'_{cm} = 40 MPa (nominal)

d_{s1} = 40mm

d_{s2} = 209mm

Compressive flange width, B = 200mm

Elastic modulus of concrete, $E_{conc} = 33000\ MPa$

Rectangular stress block < 8.1.2.2 >

$\gamma = 0.85 - 0.007(f'_{cm} - 28) = 0.766$

GFRP

Area of side face GFRP, $A_{sfg} = 129mm^2$ $(both\ sides)$

Area of under face GFRP, $A_{ufg} = 236.5mm^2$

Elastic modulus of GFRP, $E_{glass} = 76000\ MPa$

Tensile strength of GFRP, $f_{uglass} = 935\ MPa$

Assumption

Top steel in compression and not at yield.

Bottom steel in tension and has yielded.

Side face GFRP in tension and not at yield.

Under face GFRP in tension and has yielded.

Tension of bottom steel,

$T_{s2} = A_{s2} \times f_{yv}$

$T_{s2} = 226 \times 550$

$T_{s2} = 124300\ N$

Concrete compression force,

$C_c = 0.85 \times f'_c \times B \times \gamma \times d_n$

$C_c = 0.85 \times 40 \times 200 \times 0.766 \times d_n$

$C_c = 5208.8 d_n$

Compression of top steel,

$C_{s1} = A_{s1} \times \sigma_{sc}$

$C_{s1} = A_{s1} \times \varepsilon_{s1} \times E_s$

$C_{s1} = 0.003 \times \left(\frac{d_n - d_{s1}}{d_n}\right) \times E_s \times A_{s1}$

$C_{s1} = 0.003 \times \left(\frac{d_n - d_{s1}}{d_n}\right) \times 200000 \times 157$

$C_{s1} = 94200 \times \left(\frac{d_n - 40}{d_n}\right)$

Tension of side face GFRP,

$T_{sfg} = \sigma_{sfg} \times A_{sfg}$

$T_{sfg} = \varepsilon_{sfg} \times E_{glass} \times A_{sfg}$

Tension of under face GFRP,

$T_{ufg} = A_{sfg} \times f_{uglass}$

$T_{ufg} = 236.5 \times 935$

$T_{sfg} = 0.003 \times \left(\frac{d_{sfg}-d_n}{d_n}\right) \times 76000 \times 129$ $\quad T_{ufg} = 221127.5\ N$

$T_{sfg} = 29412\left(\frac{200-d_n}{d_n}\right)$

Determining d_n

$T_{s2} + T_{sfg} + T_{ufg} = C_{s1} + C_c$

$124300 + 29412\left(\frac{200-d_n}{d_n}\right) + 221127.5 = 94200\left(\frac{d_n-40}{d_n}\right) 5208.8d_n$

$5208.8{d_n}^2 - 221815.5d_n - 9650400 = 0$

$d_n = 69.3\ mm$

Hence, $k_u = \frac{69.3}{250} = 0.28 < 0.4 \quad \therefore Ductile$

Check for yield

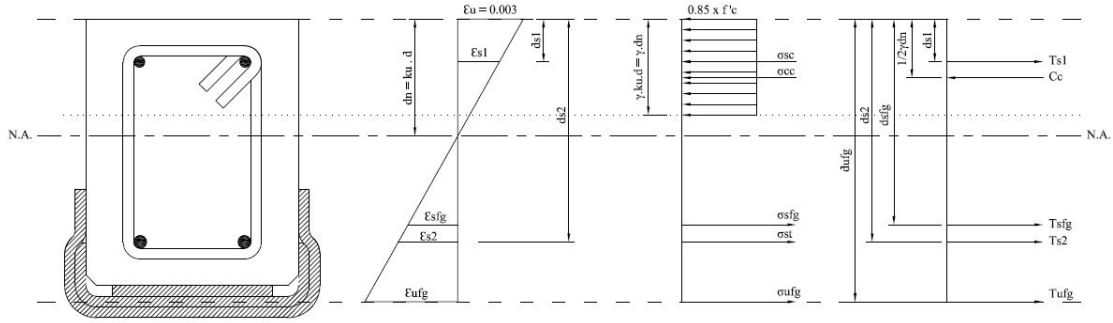

$\varepsilon_{yield\ steel} = \frac{550}{200000} = 0.00275$

$\varepsilon_{yield\ glass} = \frac{935}{76000} = 0.0123$

$\varepsilon_{s1} = 0.003 \times \left(\frac{d_n-d_{s1}}{d_n}\right) = 0.00127 < 0.00275 \quad \therefore OK.$

$\varepsilon_{s2} = 0.003 \times \left(\frac{d_{s2}-d_n}{d_n}\right) = 0.006 > 0.00275 \quad \therefore OK.$

$\varepsilon_{sfg} = 0.003 \times \left(\frac{d_{sfg}-d_n}{d_n}\right) = 0.0057 < 0.0123 \quad \therefore OK.$

$\varepsilon_{ufg} = 0.003 \times \left(\frac{d_{ufg}-d_n}{d_n}\right) = 0.0078 < 0.0123 \quad \therefore OK.$

Moment capacity

$$M_u = T_{s2} \times d_{s2} + T_{sfg} \times d_{sfg} + T_{ufg} \times d_{ufg} - C_{s1} \times d_{s1} - C_c \times \frac{\gamma d_n}{2}$$

$$M_u = 124300 \times 209 + 29412 \times \left(\frac{200 - 69.3}{69.3}\right) \times 200 + 221127.5 \times 250 - 94200 \times \left(\frac{69.3 - 40}{69.3}\right) \times 40 - 5208.8 \times \frac{0.766 {d_n}^2}{2}$$

$$M_u = 124300 \times 209 + 29412 \times 1.89 \times 200 + 221127.5 \times 250 - 94200 \times 0.423 \times 40 - 5208.8 \times \frac{0.766 \times 69.3^2}{2}$$

$$M_u = 81203622 \text{ Nmm}$$

$$M_u = 81.2 \text{ kNm}$$

Design shear load

$M_u = P_u = Load\ in\ one\ jack = 81.2\ kN$

Hence, the shear capacity has to be above the design shear load.

Shear capacity > 1.5 x 81.2 = 121.8 kN

Appendix E: Sample Calculation of Shear Capacity

Shear Capacity Sample Calculation (Initial Design)

H6 (Lower Control Beam)

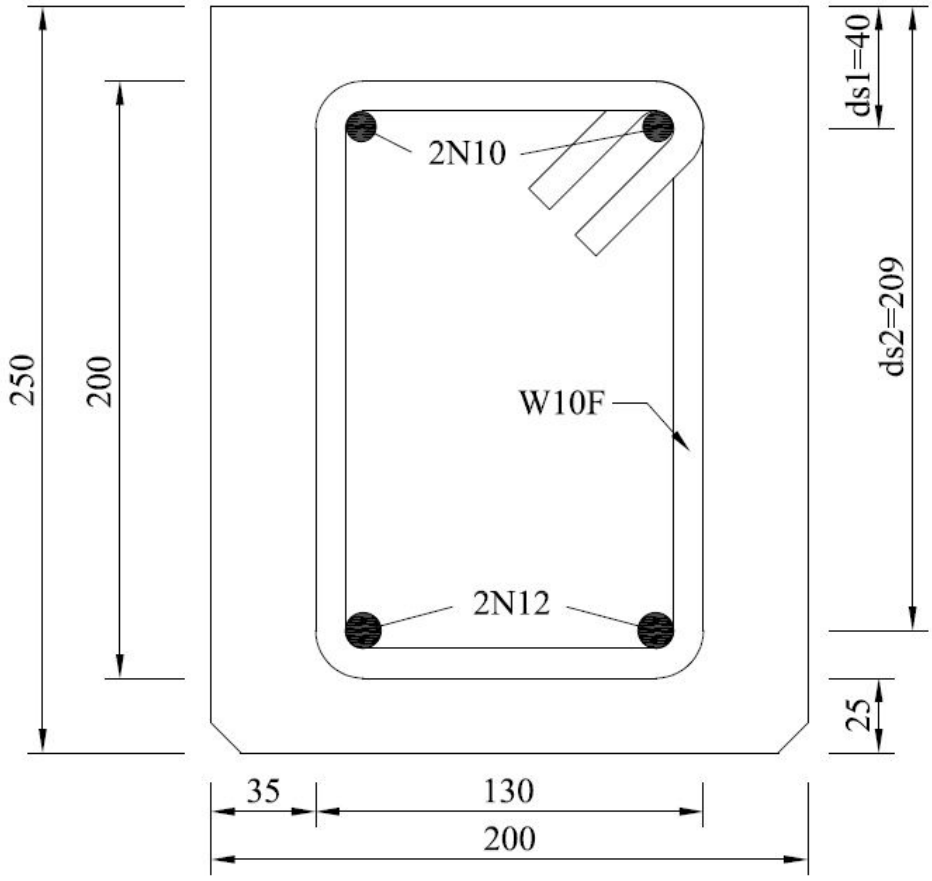

Steel

Area of steel, 2N10, A_{s1} = 157 mm^2

Area of steel, 2N12, A_{s2} = 226 mm^2

Area of fitment, W10F, 2φligs = 78.5 mm^2 A_{sv} = 157 mm^2

Spacing of fitment, s = 125 mm

Elastic modulus of steel = 200000 MPa (nominal)

Yield strength of steel, f_{yv} = 550 MPa (nominal)

Concrete

Cover = 25mm (nominal), Side= 35mm (nominal)

Compressive strength of concrete, f'_{cm} = 40 MPa (nominal)

d_0 = 209mm

Compressive flange width, b_v = 200mm

The design shear load from flexural calculation, V* = 33 kN

Contribution by concrete and tensile reinforcement,

$V_{uc} = \beta_1\beta_2\beta_3 b_v d_0 \left(\frac{A_{st}\times f'_c}{b_v d_0}\right)^{1/3}$ where $\beta_1 = 1.1 \times \left(1.6 - \frac{d_0}{1000}\right)$

$V_{uc} = 1.53 \times 1.0 \times 1.0 \times 200 \times 209 \left(\frac{226\times 40}{200\times 209}\right)^{1/3}$ $\beta_1 = 1.1 \times \left(1.6 - \frac{209}{1000}\right) = 1.53$

$V_{uc} = 38388.3\ N$ $\beta_2 = 1.0$

$V_{uc} = 38.4\ kN$ $\beta_3 = 1.0$

$0.5\emptyset V_{uc} = 0.5 \times 0.7 \times 38.4 = 13.44\ kN < V^*\ (33kN)$ where $\emptyset = 0.7$

$V_{umin} = V_{uc} + 0.6 b_v d_0$

$V_{umin} = 38388.3 + 0.6 \times 200 \times 209$

$V_{umin} = 63468.3\ N$

$V_{umin} = 63.5\ kN$

$\emptyset V_{umin} = 0.7 \times 63.5$

$\emptyset V_{umin} = 44.5\ kN\ > V^*\ (33\ kN)$ $\therefore Minimum\ steel\ is\ not\ sufficient.$

Hence, clause <AS 3600–C8.2.10> contribution to shear strength by shear reinforcement is required.

Contribution by fitment

$V_{us} = \frac{A_{sv} \times f_{syf} \times d_0}{s}\ cot\theta = \frac{157 \times 550 \times 209}{125} \times 1 = 144.4\ kN$

$V_{uc} + V_{us} > V^*\ (40\ kN)$

$38.4 + 144.4 = 182.8 > V^*\ (40\ kN)$

$\therefore Shear\ capacity\ is\ sufficient.$

Shear Capacity Sample Calculation (Initial Design)

H6 (Upper Control Beam)

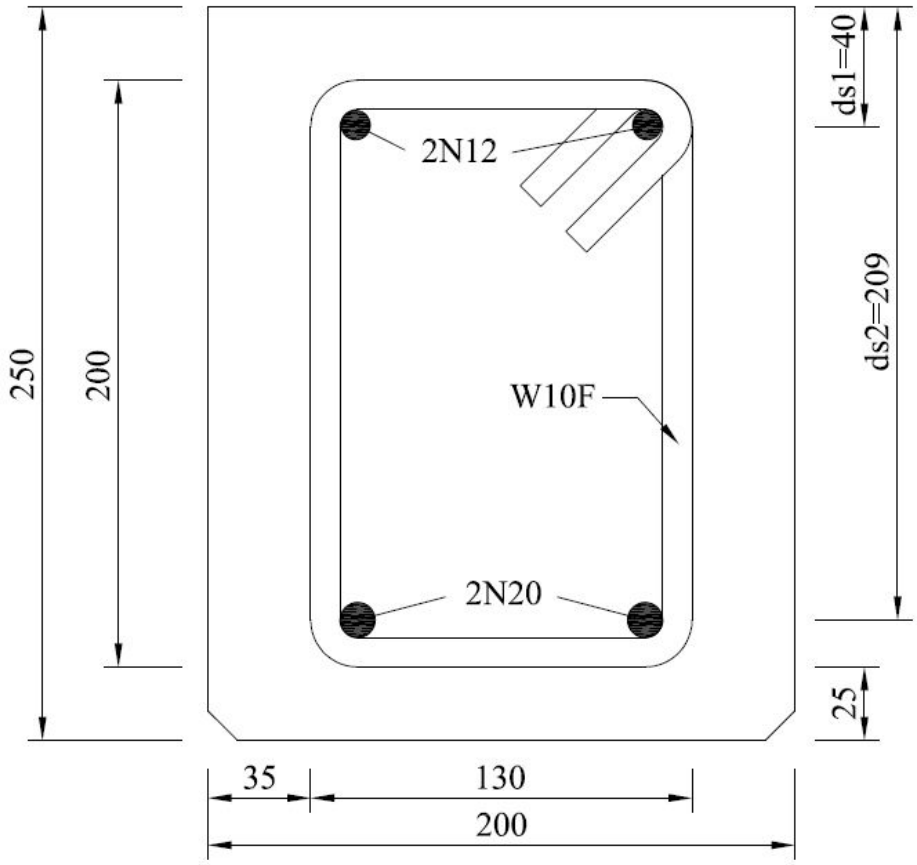

Steel

Area of steel, 2N12, A_{s1} = 226 mm^2

Area of steel, 2N20, A_{s2} = 628 mm^2

Area of fitment, W10F, 2φligs = 78.5 mm^2 A_{sv} = 157 mm^2

Spacing of fitment, s = 125 mm

Elastic modulus of steel = 200000 MPa (nominal)

Yield strength of steel, f_{yv} = 550 MPa (nominal)

Concrete

Cover = 25mm (nominal), Side= 35mm (nominal)

Compressive strength of concrete, f'_{cm} = 40 MPa (nominal)

d_0 = 205 mm

Compressive flange width, b_v = 200mm

The design shear load from flexural calculation, V* = 78 kN

Contribution by concrete and tensile reinforcement,

$V_{uc} = \beta_1\beta_2\beta_3 b_v d_0 \left(\frac{A_{st} \times f'_c}{b_v d_0}\right)^{1/3}$ where $\beta_1 = 1.1 \times \left(1.6 - \frac{d_0}{1000}\right)$

$V_{uc} = 1.53 \times 1.0 \times 1.0 \times 200 \times 205 \left(\frac{628 \times 40}{200 \times 205}\right)^{1/3}$ $\beta_1 = 1.1 \times \left(1.6 - \frac{205}{1000}\right) = 1.53$

$V_{uc} = 53278.7\ N$ $\beta_2 = 1.0$

$V_{uc} = 53.3\ kN$ $\beta_3 = 1.0$

$0.5\emptyset V_{uc} = 0.5 \times 0.7 \times 53.3 = 18.67\ kN < V^*\ (78\ kN)$ where $\emptyset = 0.7$

$V_{umin} = V_{uc} + 0.6 b_v d_0$

$V_{umin} = 53278.7 + 0.6 \times 200 \times 205$

$V_{umin} = 77878.7\ N$

$V_{umin} = 78\ kN$

$\emptyset V_{umin} = 0.7 \times 78$

$\emptyset V_{umin} = 54.6\ kN\ < V^*\ (78\ kN)$ $\therefore Minimum\ steel\ is\ not\ sufficient.$

Hence, clause <AS 3600–C8.2.10> contribution to shear strength by shear reinforcement is required.

Contribution by fitment

$V_{us} = \frac{A_{sv} \times f_{syf} \times d_0}{s}\ cot\theta = \frac{157 \times 550 \times 205}{125} \times 1 = 141.6\ kN$

$V_{uc} + V_{us} > V^*\ (40\ kN)$

$53.3 + 141.6 = 194.9 > V^*\ (78\ kN)$

$\therefore Shear\ capacity\ is\ sufficient.$

Appendix F: Sample Calculation of Flexural Capacity (As Constructed)

Flexural Capacity Moment Calculation (As Constructed)

H6 (Lower Control Beam)

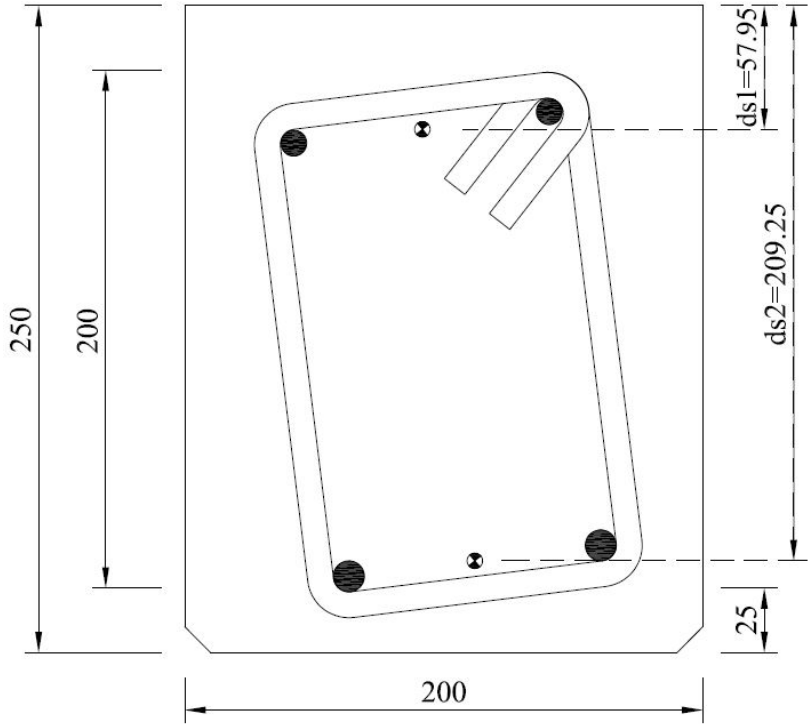

Steel

Area of steel, 2N10, A_{s1} = 157mm^2

Area of steel, 2N12, A_{s2} = 226mm^2

Elastic modulus of steel = 200000 MPa (nominal)

Yield strength of top steel, f_{yv} = 567 MPa (actual)

Yield strength of bottom steel, f_{yv} = 535 MPa (actual)

Concrete

Compressive strength of concrete, f'_{cm} = 46.9 MPa (actual)

d_{s1} = 57.95mm

d_{s2} = 209.25mm

$\gamma = 1.05 - 0.007f'_{cm} = 0.72$

Assumption:

Top steel in tension and not at yield.

Bottom steel in tension and at yield.

Tension of bottom steel,

$T_{s2} = A_{s2} \times f_{yv}$

$T_{s2} = 226 \times 535$

$T_{s2} = 120910\ N$

Concrete compression force,

$C_c = 0.85 \times f'_c \times B \times \gamma \times d_n$

$C_c = 0.85 \times 46.9 \times 200 \times 0.72 \times d_n$

$C_c = 5740.6 d_n$

Tension of top steel

$T_{s1} = A_{s1} \times \sigma_{sc}$

$T_{s1} = A_{s1} \times \varepsilon_{s1} \times E_s$

$T_{s1} = \frac{567}{200000} \times \left(\frac{d_{s1} - d_n}{d_n}\right) \times E_s \times A_{s1}$

$T_{s1} = \frac{567}{200000} \times \left(\frac{d_{s1} - d_n}{d_n}\right) \times 200000 \times 157$

$T_{s1} = 89019 \times \left(\frac{57.95 - d_n}{d_n}\right)$

Determining d_n

$T_{s2} + T_{s1} = C_c$

$120910 + 89010\left(\frac{57.95 - d_n}{d_n}\right) = 5740.6 d_n$

$5740.6 {d_n}^2 - 31891 d_n - 5158651.1 = 0$

$d_n = 32.9mm$

Hence, $k_u = \frac{32.9}{250} = 0.13 < 0.4 \quad \therefore Ductile$

Check steel yielding

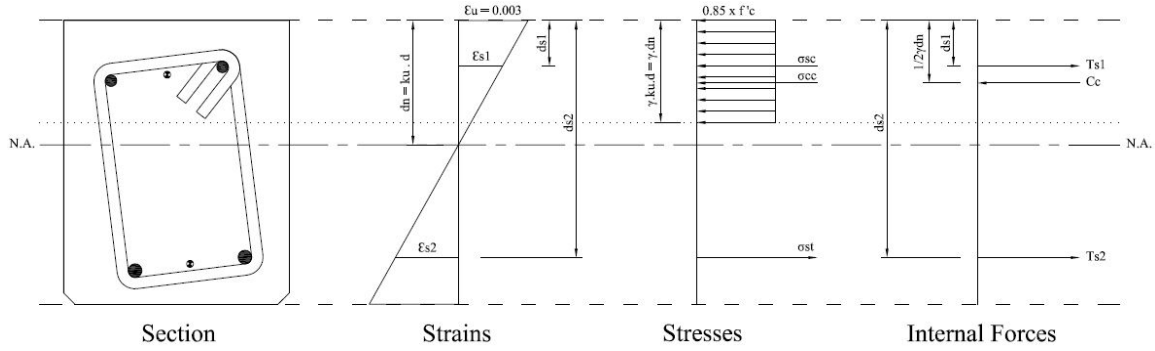

$$\varepsilon_{yield} = \frac{535}{200000} = 0.0027$$

$$\varepsilon_{s1} = 0.0027 \times \left(\frac{d_{s1} - d_n}{d_n}\right) = 0.0021 < 0.0027 \quad \therefore OK, not\ yield.$$

$$\varepsilon_{s2} = 0.0027 \times \left(\frac{d_{s2} - d_n}{d_n}\right) = 0.014 > 0.0027 \quad \therefore OK, yield.$$

Moment capacity

$$M_u = T_{s2} \times d_{s2} + T_{s1} \times d_{s1} - C_c \times \frac{\gamma d_n}{2}$$

$$M_u = 120910 \times 209.25 + 89019 \times \left(\frac{d_{s1} - d_n}{d_n}\right) \times d_{s1} - 5740.6 \times \frac{0.72{d_n}^2}{2}$$

$$M_u = 120910 \times 209.25 + 89019 \times \left(\frac{57.95 - 32.9}{32.9}\right) \times 57.95 - 5740.6 \times \frac{0.72 \times 32.9^2}{2}$$

$$M_u = 26991279 \text{ Nmm}$$

$$M_u = 27 \text{ kNm}$$

Flexural Capacity Moment Calculation (As Constructed)

J4 (U-shaped GFRP-strengthened beam)

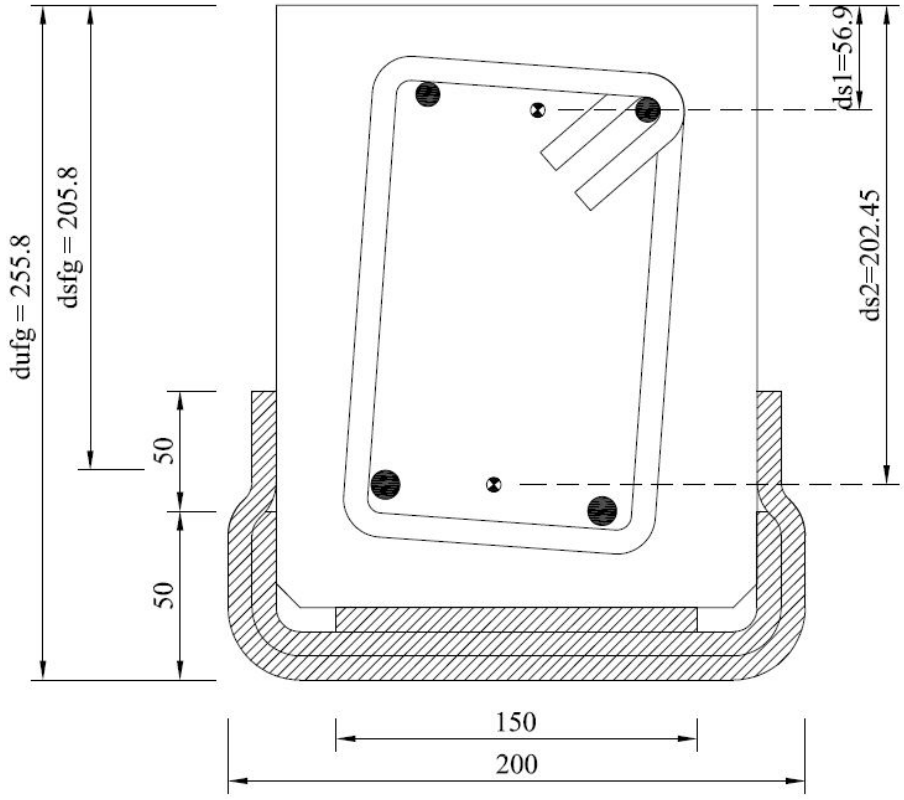

Steel

Area of steel, 2N10, A_{s1} = 157 mm^2

Area of steel, 2N12, A_{s2} = 226 mm^2

Elastic modulus of steel = 200000 MPa (nominal)

Tensile strength of top steel, f_{yv} = 567 MPa (actual)

Tensile strength of bottom steel, f_{yv} = 535 MPa (actual)

GFRP

Area of side face GFRP, A_{sfg} = 129 mm^2

Area of under face GFRP, A_{ufg} = 236.5 mm^2

Elastic modulus of GFRP = 76000 MPa (nominal)

Tensile strength of GFRP, f_{uglass} = 935 MPa (actual)

Concrete

Compressive strength of concrete, f'_{cm} = 46.9 MPa (actual)

d_{s1} = 56.9mm

d_{s2} = 202.45mm

d_{sfg} = 205.8mm

d_{ufg} = 255.8mm

$\gamma = 1.05 - 0.007f'_{cm} = 0.72$

Assumption:

Top steel in compression and not at yield.

Bottom steel in tension and at yield.

Side face GFRP in tension and not yield.

Under face GFRP in tension and yield.

Tension of side face GFRP, GFRP,

$T_{sfg} = A_{sfg} \times \sigma_{sfg}$

$T_{sfg} = A_{sfg} \times \varepsilon_{sfg} \times E_{glass}$

$T_{sfg} = \frac{535}{200000} \times \left(\frac{d_{sfg}-d_n}{d_n}\right) \times E_{glass} \times A_{sfg}$

$T_{sfg} = \frac{535}{200000} \times \left(\frac{205.8-d_n}{d_n}\right) \times 76000 \times 129$

$T_{sfg} = 26225.7 \times \left(\frac{205.8-d_n}{d_n}\right)$

Tension of under face

$T_{ufg} = A_{ufg} \times f_{uglass}$

$T_{ufg} = 236.5 \times 935$

$T_{ufg} = 221127.5\ N$

Tension of bottom steel,

$T_{s2} = A_{s2} \times f_{yv}$

$T_{s2} = 226 \times 535$

$T_{s2} = 120910\ N$

Concrete compression force,

$C_c = 0.85 \times f'_c \times B \times \gamma \times d_n$

$C_c = 0.85 \times 46.9 \times 200 \times 0.72 \times d_n$

$C_c = 5740.6 d_n$

Compression of top steel

$$C_{s1} = A_{s1} \times \sigma_{sc}$$

$$C_{s1} = A_{s1} \times \varepsilon_{s1} \times E_s$$

$$C_{s1} = \frac{567}{200000} \times \left(\frac{d_n - d_{s1}}{d_n}\right) \times E_s \times A_{s1}$$

$$C_{s1} = \frac{567}{200000} \times \left(\frac{d_n - d_{s1}}{d_n}\right) \times 200000 \times 157$$

$$C_{s1} = 89019 \times \left(\frac{d_n - 56.9}{d_n}\right)$$

Determining d_n

$$T_{s2} + T_{sfg} + T_{ufg} = C_{s1} + C_c$$

$$120910 + 26225.7\left(\frac{205.8 - d_n}{d_n}\right) + 221127.5 = 89019\left(\frac{d_n - 56.9}{d_n}\right) + 5740.6d_n$$

$$5740.6{d_n}^2 - 226792.8d_n - 10462430 = 0$$

$$d_n = 66.8mm$$

Hence, $k_u = \frac{66.8}{250} = 0.27 < 0.4 \quad \therefore Ductile$

Check steel yielding

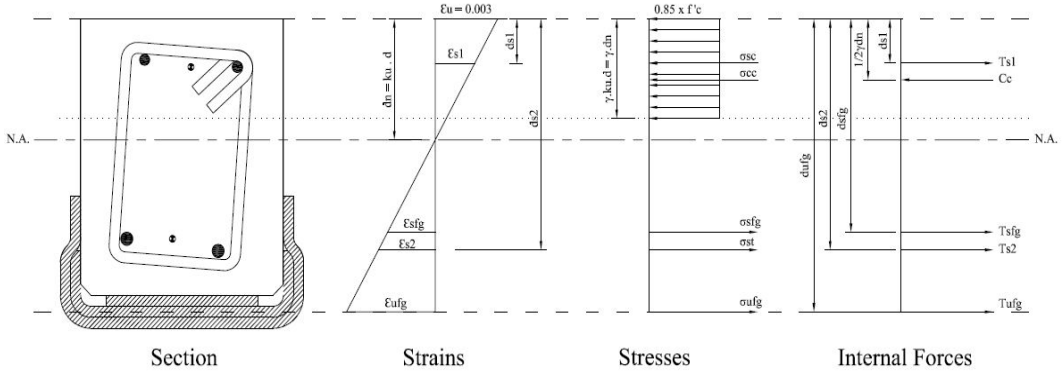

$$\varepsilon_{yield\ steel} = \frac{535}{200000} = 0.0027$$

$$\varepsilon_{yield\ glass} = \frac{935}{76000} = 0.0123$$

$$\varepsilon_{s1} = 0.0027 \times \left(\frac{d_n - d_{s1}}{d_n}\right) = 0.0004 < 0.0027 \quad \therefore OK$$

$$\varepsilon_{s2} = 0.0027 \times \left(\frac{d_{s2} - d_n}{d_n}\right) = 0.0054 > 0.0027 \quad \therefore OK$$

$$\varepsilon_{sfg} = 0.0027 \times \left(\frac{d_{sfg} - d_n}{d_n}\right) = 0.0056 < 0.0123 \quad \therefore OK$$

$$\varepsilon_{ufg} = 0.0027 \times \left(\frac{d_{ufg} - d_n}{d_n}\right) = 0.0076 < 0.0123 \quad \therefore OK$$

Moment capacity

$$M_u = T_{s2} \times d_{s2} + T_{sfg} \times d_{sfg} + T_{ufg} \times d_{ufg} - C_{s1} \times d_{s1} - C_c \times \frac{\gamma d_n}{2}$$

$$M_u = 120910 \times 202.45 + 26225.7 \times \left(\frac{205.8 - d_n}{d_n}\right) \times 205.8 + 221127.5 \times 255.8 - 89019 \times \left(\frac{d_n - d_{s1}}{d_n}\right) \times d_{s1} - 5740.6 \times \frac{0.72 {d_n}^2}{2}$$

$$M_u = 120910 \times 202.45 + 26225.7 \times \left(\frac{205.8 - 66.8}{66.8}\right) \times 205.8 + 221127.5 \times 255.8 - 89019 \times \left(\frac{66.8 - 56.9}{66.8}\right) \times 56.9 - 5740.6 \times \frac{0.72 \times 66.8^2}{2}$$

$$M_u = 82301032 \text{ Nmm}$$

$$M_u = 82.3 \text{ kNm}$$

Appendix G: Sample Calculation of Yielding Moment

Moment Yield Sample Calculation

H6 (Lower Control Beam)

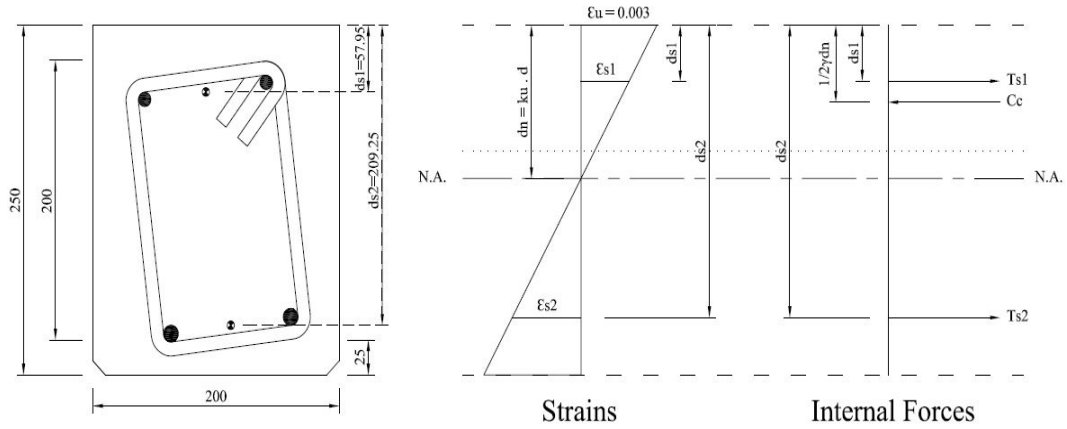

Area of steel, 2N10, A_{s1} = 157mm^2 (nominal)

Area of steel, 2N12, A_{s2} = 226mm^2 (nominal)

Elastic modulus of steel = 200000 MPa (nominal)

Yield strength of top steel = 567 MPa (actual)

Yield strength of bottom steel = 535 MPa (actual)

Compressive strength of concrete, f'_{cm} = 46.9 MPa (actual)

d_{s1} = 57.95mm (actual)

d_{s2} = 209.25mm (actual)

$\gamma = 1.05 - 0.007 f'_{cm} = 0.72$ Rectangular stress block < 8.1.2.2 >

$\alpha_2 = 1 - 0.003\, f'_{cm} = 0.86$ Rectangular stress block < 8.1.2.2 >

$\varepsilon_{sc} = 0.003$

$$\varepsilon_{s1} = \frac{f_{yield}}{E_{steel}} = \frac{567}{200000}$$

$$\varepsilon_{s2} = \frac{f_{yield}}{E_{steel}} = \frac{535}{200000}$$

Assumption

Top steel in tension and not at yield.

Bottom steel in tension and has yielded.

Using similar triangle,

$$\frac{\varepsilon_{s2}}{d_{s2}-d_n}=\frac{\varepsilon_{s1}}{d_{s1}-d_n}$$

$$\varepsilon_{s1}=\varepsilon_{s2}\frac{(d_{s1}-d_n)}{(d_{s2}-d_n)}=\frac{535}{200000}\times\frac{(57.95-d_n)}{(209.25-d_n)}$$

$$T_{s2}=E_s\times\varepsilon_{s2}\times A_{s2}$$

$$T_{s2}=200000\times\frac{535}{200000}\times 226$$

$$T_{s2}=120910\,N$$

$$T_{s1}=E_s\times\varepsilon_{s1}\times A_{s1}$$

$$T_{s1}=200000\times\frac{535}{200000}\times\frac{(57.95-d_n)}{(209.25-d_n)}\times 157$$

$$T_{s1}=83995\,\frac{(57.95-d_n)}{(209.25-d_n)}$$

$$C_c=\alpha_2 f'_c B\gamma d_n$$

$$C_c=0.86\times 46.9\times 200\times 0.72 d_n$$

$$C_c=5808.1 d_n$$

$$TENSION=COMPRESSION$$

$$T_{s2}+T_{s1}=C_c$$

$$120910+83995\,\frac{(57.95-d_n)}{(209.25-d_n)}=5808.1 d_n$$

$$5808.1 d_n{}^2-1420250 d_n+30167928=0$$

Solving equation graphically…

$d_n=23.5\,mm$

Bottom steel tension force,

$T_{s2} = 120910\ N$

Top steel tension force,

$$T_{s1} = 83995\ \frac{(\ 57.95 - 23.5)}{(209.25 -\ 23.5)}$$

$T_{s1} =\ 15578\ N$

Concrete Compression force,

$C_c = 5808.1 d_n$

$C_c = 136490\ N$

Ultimate Capacity

$T_{s2} \times d_{s2} = 120910 \times 209.25 = 25300417.5\ Nmm$

$T_{s1} \times d_{s1} =\ 15578 \times 57.95 =\ 902745\ Nmm$

$C_c \times \frac{1}{2}\gamma d_n = 136490 \times \frac{1}{2} \times 0.72 \times 23.5 = 1154705.4\ Nmm$

Moment yield $= 25300417.5 + 902745 -\ 1154705.4$

Moment yield $= 25048457.1$ Nmm $= 25.1$ kNm

Moment Yield Sample Calculation

J4 (U-shape Glass Fibre Strengthened RC Beam)

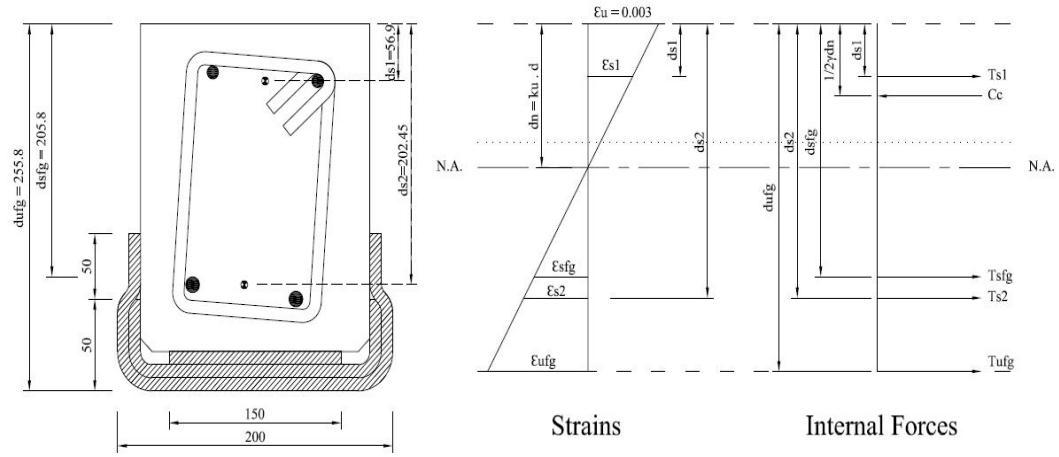

Area of steel, 2N10, A_{s1} = 157mm^2 (nominal)

Area of steel, 2N12, A_{s2} = 226mm^2 (nominal)

Elastic modulus of steel = 200000 MPa (nominal)

Yield strength of top steel = 567 MPa (actual)

Yield strength of bottom steel = 535 MPa (actual)

Compressive strength of concrete, f'_{cm} = 46.9 MPa (actual)

d_{s1} = 56.9mm (actual) d_{sfg} = 205.8mm (actual)

d_{s2} = 202.45mm (actual) d_{ufg} = 255.8mm (actual)

$\gamma = 1.05 - 0.007f'_{cm} = 0.72$ Rectangular stress block < 8.1.2.2 >

$\alpha_2 = 1 - 0.003\, f'_{cm} = 0.86$ Rectangular stress block < 8.1.2.2 >

$\varepsilon_{sc} = 0.003$

$$\varepsilon_{s1} = \frac{f_{yield}}{E_{steel}} = \frac{567}{200000}$$

$$\varepsilon_{s2} = \frac{f_{yield}}{E_{steel}} = \frac{535}{200000}$$

Assumption

Top steel in tension and not at yield.

Bottom steel in tension and has yielded.

Side face glass in tension and has yielded.

Bottom face glass in tension and has yielded.

Using similar triangle,

$$\frac{\varepsilon_{s2}}{d_{s2}-d_n}=\frac{\varepsilon_{s1}}{d_n-d_{s1}}$$

$$\varepsilon_{s1}=\varepsilon_{s2}\frac{(d_{s1}-d_n)}{(d_{s2}-d_n)}=\frac{535}{200000}\times\frac{(56.9-d_n)}{(202.45-d_n)}$$

$$\frac{\varepsilon_{s2}}{d_{s2}-d_n}=\frac{\varepsilon_{sfg}}{d_{sfg}-d_n}$$

$$\varepsilon_{sfg}=\varepsilon_{s2}\frac{(d_{sfg}-d_n)}{(d_{s2}-d_n)}=\frac{535}{200000}\times\frac{(205.8-d_n)}{(202.45-d_n)}$$

$$\frac{\varepsilon_{s2}}{d_{s2}-d_n}=\frac{\varepsilon_{ufg}}{d_{ufg}-d_n}$$

$$\varepsilon_{ufg}=\varepsilon_{s2}\frac{(d_{ufg}-d_n)}{(d_{s2}-d_n)}=\frac{535}{200000}\times\frac{(255.8-d_n)}{(202.45-d_n)}$$

$$T_{s2}=E_s\times\varepsilon_{s2}\times A_{s2}$$

$$T_{s2}=200000\times\frac{535}{200000}\times 226$$

$$T_{s2}=120910\,N$$

$$T_{s1}=E_s\times\varepsilon_{s1}\times A_{s1}$$

$$T_{s1}=200000\times\frac{535}{200000}\times\frac{(56.9-d_n)}{(202.45-d_n)}\times 157$$

$$T_{s1}=83995\,\frac{(56.9-d_n)}{(202.45-d_n)}$$

$$T_{sfg} = E_{glass} \times \varepsilon_{sfg} \times A_{sfg}$$

$$T_{sfg} = 76000 \times \frac{535}{200000} \times \frac{(205.8 - d_n)}{(202.45 - d_n)} \times 129 = 26225.7 \frac{(205.8 - d_n)}{(202.45 - d_n)}$$

$$T_{ufg} = E_{glass} \times \varepsilon_{ufg} \times A_{ufg}$$

$$T_{ufg} = 76000 \times \frac{535}{200000} \times \frac{(255.8 - d_n)}{(202.45 - d_n)} \times 236.5 = 48080.5 \frac{(255.8 - d_n)}{(202.45 - d_n)}$$

$$C_c = \alpha_2 f'_c B \gamma d_n$$

$$C_c = 0.86 \times 46.9 \times 200 \times 0.72 d_n$$

$$C_c = 5808.1 d_n$$

$$TENSION = COMPRESSION$$

$$T_{s2} + T_{sfg} + T_{ufg} + T_{s1} = C_c$$

$$120910 + 26225.7 \frac{(205.8 - d_n)}{(202.45 - d_n)} + 48080.5 \frac{(255.8 - d_n)}{(202.45 - d_n)} + 83995 \frac{(56.9 - d_n)}{(202.45 - d_n)} = 5808.1 d_n$$

$$5808.1 {d_n}^2 - 1455061 d_n + 46113836 = 0$$

Solving equation graphically…

$d_n = 37.2\ mm$

Bottom steel tension force,

$T_{s2} = 120910\ N$

Under face glass fibre tension force,

$$T_{ufg} = 48080.5 \frac{(255.8 - d_n)}{(202.45 - d_n)} = 63603\ N$$

Side face glass fibre tension force,

$$T_{sfg} = 26225.7 \frac{(205.8 - d_n)}{(202.45 - d_n)} = 26757\ N$$

Top steel tension force,

$$T_{s1} = 83995\ \frac{(56.9 - d_n)}{(202.45 - d_n)}$$

$$T_{s1} = 10013\ N$$

Concrete Compression force,

$$C_c = 5808.1 d_n$$

$$C_c = 216061\ N$$

Ultimate Capacity

$$T_{s2} \times d_{s2} = 120910 \times 202.45 = 24478229.5\ Nmm$$

$$T_{ufg} \times d_{ufg} = 63603 \times 255.8 = 16269647\ Nmm$$

$$T_{sfg} \times d_{sfg} = 26757 \times 205.8 = 5506591\ Nmm$$

$$T_{s1} \times d_{s1} = 10013 \times 56.9 = 569739.7\ Nmm$$

$$C_c \times \frac{1}{2}\gamma d_n = 216061 \times \frac{1}{2} \times 0.72 \times 37.2 = 2893489\ Nmm$$

$$\text{Moment yield} = 24478229.5 + 16269647 + 5506591 + 569739.7 - 2893489$$

$$\text{Moment yield} = 43930718 = 43.9\ \text{kNm}$$